CONFORMATIONS AND STRUCTURE TRANSITIONS OF ϕX174 BACTERIOPHAGE CIRCULAR DOUBLE-STRANDED DNA

by

Douglas J. Jolly B.Sc.

July, 1972

Institute of Biochemistry,
University of Glasgow,
Glasgow,
Scotland.

ACKNOWLEDGEMENTS

I would like to express my gratitude to a number of people for their help in this work.

to Professors J.N.Davidson and R.M.S.Smellie for the provision of facilities, encouragement and support throughout the course of this work.

to my supervisor, Dr.A.M.Campbell for her constant help in all ways, encouragement, and discussion.

to Dr. K. Sargeant of the Microbiological Research Establishment at Porton, Wiltshire, for the provision of bacteriophage infected cells.

to all the residents of D floor in the Glasgow University Department of Biochemistry for help, both mental and physical, on occasions.

to the Medical Research Council for providing a research scholarship from 1969-72.

to Miss Pam Todd for typing this thesis.

to Mr. Robert Brown for help in production of this thesis

to my wife Jeanette for her unfailing help and understanding during this work.

LIST OF ABBREVIATIONS

All abbreviations are as in Biochem.J. (1972) 126, 1-19, with the following additions.

EB: ethidium bromide.

PI: propidium iodide.

PF: proflavine (hemisulphate).

RNase: ribonuclease.

ϕX174-RF: replicative double-stranded intracellular form of bacteriophage ϕX174 DNA.

(form) I: double-stranded intact circular DNA.

(form) II: double-stranded relaxed circular DNA, with at least one single-stranded break.

CT: calf thymus.

SV40: simian virus 40.

O.R.D.: optical rotatory dispersion.

C.D.: circular dichroism.

dn/dc: refractive index increment.

Pθ: particle scattering factor in light scattering.

r.m.s.; root-mean-square.

Rg: r.m.s. radius.

B: second virial coefficient.

σ: superhelix density.

α: topographical winding number.

τ: super-helix winding number.

β: duplex winding number.

CONTENTS

LIST OF FIGURES

Fig. page

LIST OF TABLES

SUMMARY

Initially general aspects of DNA structure, particularly tertiary, and its investigation are discussed together with the difficulties encountered; this leads to the choice of ϕX174-RF DNA, investigated mainly by light scattering as the experimental system for investigating DNA structure. As ϕX174-RF DNA is circular and exists in two forms, RFI which is supercoiled and RFII which is an open circle, the implication of this and the significance of the experimental work undertaken are discussed in the light of previous workers' findings.

The following experiments were performed: (1) light scattering on ϕX174-RFI DNA at 25°C; (2) light scattering on ϕX174-RFI DNA at temperatures from 14.9°- 74.5°C; (3) light scattering on ϕX174-RFI DNA at different mol bound proflavine/mol equiv. nucleotide from 0 to 0.06; (4) light scattering on ϕX174-RFII at 25°C. All experiments were in buffer, pH 6.8 and I = 0.2.

From all experiments the value of the mol. wt. was $3.22 \pm 0.05 \times 10^6$ (S.D. of 20 experiments), which is somewhat less than the accepted value of 3.4×10^6. This downward re-evaluation of the mol. wt. is in line with the recent re-evaluation for a number of widely-used phage DNA molecules. In experiment (1), the experimental r.m.s.radius, contour length and number of superhelical turns determined by EB titration, were used to define exactly the dimensions of various models for a superhelix: the straight interwound, the Y interwound and the toroidal models. The PΘ for these was calculated from the formula $P\Theta = \frac{1}{N^2} \times \sum_{n}^{N} \sum_{m}^{N} \frac{\sin hr_{nm}}{hr_{nm}}$ where N is the no. of scattering segments, r_{nm} the distance between the nth and mth segments and h a constant dependent on the scattering angle, Θ, by computer summation. These results indicated that at $\gamma = -12$ a Y shape was the best model, though

no exact fit was found.

In experiments (2) and (3) the superhelix density (σ) was varied by temperature variation and by proflavine intercalation. These experiments indicated, both from the r.m.s. radius and general appearance of the $P\theta^{-1}$ curves, that from $\sigma = -0.027$ ($\gamma = -12.5$) to $\sigma = -0.021$ ($\gamma = -10$) the molecular conformation was as in experiment (1), a Y shape; as $|\sigma|$ decreased further to 0.017 approx., the molecule became very compact (r.m.s. radius = 60 - 70nm) before expanding slowly to an open circular conformation at $\sigma = 0$ (r.m.s.radius = 120nm with 0.06 mol dye bound/mol equiv. nucleotide. From experiments (1) - (3) the r.m.s. radius of the Y type structure of ϕX174-RFI at 25°C was 97.4 ± 8nm (S.D. of 5 experiments). Predicting $P\theta^{-1}$ curves on the lines of experiment (1) indicated that compact conformation was a toroid-type structure.

Some small variation of the second virial coefficient from zero, was found, which was tentatively attributed to increased exposure of hydrophobic bases due to torsional strain in the superhelix. Simple thermodynamic calculations on the energy requirements of the various models indicates that the above structures and transitions were quite possible and reasonable.

In experiment (4), RFII was found to have a second virial coefficient of zero and a r.m.s. radius of 109.4 ± 15nm. A theoretical $P\theta$ function was calculated for a circular worm-like coil at different values of the persistence length from the above formula for $P\theta$, using polymer distribution functions. One summation was performed analytically, the other by computer summation. From this experiment the persistence length was found to be 41 ± 3.5nm for DNA which is in good agreement with values from hydrodynamic experiments, in contrast to almost all other light scattering results; this is attributed to the correctness of the interpretation of the results by conventional methods, due to the small size and optical isotropy of ϕX174-RFII.

The persistence length of RFI titrated to an open circle with

proflavine was also found; this was 36 $\pm$ 3.0nm which indicates a drop in the persistence length on binding proflavine.

1. I TRO UCTION

1.1

DNA STRUCTURE AND CONFORMATION

Since the postulation of the double-stranded, base-paired structure for DNA by Watson & Crick (1953a,b) from X-ray diffraction evidence formed a basis for speculation, there have been many investigations of DNA structure.

DNA structure can be divided fairly clearly into three sections: (a) the primary structure, which is the sequence of bases in the strands of the double helix; (b) the secondary structure, which is the short-range ordered structure, i.e. the double helix, the pairing of bases, the pitch and position of bases with respect to the helix axis etc.; (c) the tertiary structure,which is the overall conformation of the whole molecule, normally the shape adopted by the linear thread of the duplex. The other parameter, which is related to (a) and (c), which describes DNA is the molecular weight, M.

The primary structure of DNA molecules has proved very resistant to elucidation because of the size of even the smallest naturally occurring molecules, bacterial plasmid DNA molecules, mol. wt. 9×10^5 approx., (Lee & Davidson, 1968; Riou & Delain, 1969) and because of the lack of specific endonucleases such as exist for RNA (Gilham, 1970). Progress so far, has been restricted to nearest neighbour (Subake-Sharpe et al., 1966) and pyrimidine run (Rajbhandary & Stuart, 1968) analyses, determination of G + C contents (Rendich, 1955) and special cases such as the sequence of the "sticky ends" of λ DNA (Wu & Taylor, 1971).

The secondary structures postulated for DNA have been based on the X-ray diffraction evidence (see Arnott, 1970 for a review) for molecular co-ordinates, which indicate three types of secondary structure designated A, B and C, in the fibres. Table 1.1 gives a summary of the major parameters related to these structures. These have been related to DNA solution structure experimentally by O.R.D., C.D., (Yang & Samejima, 1969; Tunis & Hearst, 1968; Tunis-Schneider & Maestre, 1970) X-ray scattering (Eisenberg & Cohen, 1968; Luzzati et al., 1964; Luzzati et al., 1967; Bram, 1971). Bram has obtained evidence that the secondary structure is

somewhat dependent on the primary. Thermal melting transitions monitored with U.V. spectroscopy (Hamaguchi & Geiduschek, 1962; Marmur & Doty, 1962) or with O.R.D. and C.D. (Samejima & Yang, 1965; Gennis & Cantor, 1972) have also indicated this and have shown that the secondary structure is dependent on temperature and ionic environment. Recently tritium exchange (MacConnel & von Hippel, 1970; Englander & von Hippel, 1972), reaction with formaldehyde (Utiyama & Doty, 1971) and n.m.r. (MacDonald et al., 1964; Lubas & Wilkzok, 1970) have been developed as probes of secondary structure.

The consensus of opinion is that the normal structure of DNA around room temperature, neutral pH, and ionic strength 0.1 to 2 is equivalent approximately to the B structure (Tunis-Schneider & Maestre, 1970) observed in fibres. In high salt ($>$ 4M), particularly Li^+, the C structure is thought to exist (Tunis-Schneider & Maestre, 1970: Tunis & Hearst, 1968). In 80% ethanol, O.R.D. spectra resembling those obtained from double-stranded RNA have been reported (Brahms & Mommaerts, 1964) which may indicate some type of A structure (Tunis-Schneider & Maestre, 1970). Although transitions, if any, between A, B, and C structures might be expected to be co-operative in nature, intermediate types seem to occur (Gennis & Cantor, 1972; Bram, 1971).

The tertiary structure of DNA has been examined experimentally by a number of techniques in recent years. These include electron microscopy (Lang et al., 1964; Lang, 1970), autoradiography (Rubinstein et al., 1961), sedimentation velocity (Studier, 1965; Rosenblum & Cox, 1966; Gray & Hearst, 1968), sedimentation equilibrium (Bancroft & Freifelder, 1970; Schmid & Hearst, 1969), viscosity (Douthart & Bloomfield, 1968; Crothers & Zimm, 1965; Hays & Zimm, 1970; Treiber et al., 1971), light scattering (Harpst et al., 1968; Cohen & Eisenberg, 1966; Krasna et al., 1970; Dawson & Harpst, 1971), optical mixing spectroscopy in conjunction with sedimentation velocity (Dubin et al., 1970), electro-optical scattering (Jennings & Plummer, 1970; Homick & Weill, 1971), electrical and flow

birefringence (Houssier, 1968; Weill et al., 1968; Harrington, 1970; Maestre & Kilkson, 1965), electrical and flow dichroism (Wada, 1964; Callis & Davidson, 1969), magnetic birefringence (Mekshenkov, 1964), fluorescence depolarisation in conjunction with dye binding (Hornick & Weill, 1971; Le Pecq & Paoletti, 1971) and n.m.r. (Lubas & Wilczock, 1971). In addition a number of theoretical predictions have been made for DNA examined by viscosity (Hearst et al., 1968a), sedimentation velocity (Hearst & Stockmayer, 1962; Gray et al., 1967) and light scattering (Sharp & Bloomfield, 1968b) in terms of the worm-like coil model. The majority of quantitive characterisations have been with these three techniques, and discussion has centred round them; however, agreement between different experiments is still not good (Schmid et al., 1971) and in fact conformity in molecular weight values is only beginning to appear (Freifelder, 1970). Values of other tertiary structure parameters such as the Kuhn statistical length and the excluded volume parameter (see section 1.4) are still in dispute.

Recently three main types of DNA have been used in secondary and tertiary structure investigation. These are: (a) calf thymus DNA, usually sonicated to low molecular weight about 500,000 (Cohen & Eisenberg, 1968; Litzler et al., 1964; Sponar et al., 1965; Weill & Hornick, 1968; Londos-Gagliardi et al., 1971); (b) synthetic deoxyribonucleotide polymers (Inman & Baldwin, 1962; de Gennes, 1968; Gennis & Cantor, 1972); (c) whole naturally occurring DNA molecules (Harpst et al., 1968; Crothers & Zimm, 1965; Freifelder, 1970; Gray & Hearst, 1968). This last type of DNA molecule has been most commonly used, as they are obviously more immediately relevant.

However, the only types which have been preparable in quantities large enough for use in most physico-chemical experiments have been bacterophage DNA molecules. These are normally very large (mol. wt. $> 24 \times 10^6$) and therefore difficult to handle for a number of reasons, in particular shear sensitivity. Also a number of methods are difficult to apply, with current techniques, to molecules of such a size. For example light scattering, a potentially very powerful tool for the elucidation of tertiary

structure in these molecules, has not been usable correctly with such molecules, because low enough scattering angles have not been examinable.

1.2

CHOICE OF EXPERIMENTAL SYSTEM

It was felt desirable to examine and characterise a DNA molecule, both to generally characterise DNA structure, and with a view to employing it in interaction experiments with other biological macromolecules. For ease of handling in general, and, in particular, to be able to use light scattering, a powerful tool for this type of investigation, it was necessary to use as small a DNA molecule as possible, which was preparable in large quantities. The replicative double-stranded form of bacteriaphage ϕ X174DNA (ϕ X174-RF DNA)(Kleinschmidt et al., 1963; Burton & Sinsheimer, 1963), mol. wt. 3.4×10^6 (Sinsheimer, 1959) fits these requirements. The other main possibility, PM2 phage DNA, mol. wt. 6×10^6 (Espejo et al., 1969) was, at the start of this project, hardly characterised and it is almost too large for light scattering experiments on conventional instruments. In addition, for projected interaction experiments, since this usually involves the determination of weight average molecular weights, the interactants should be as near one another with respect to M as possible; for DNA-protein type interactions, therefore, as small a DNA molecule as possible should again be used. ϕ X174-RF DNA accordingly was chosen for the project, which was the investigation of ϕ X174-RF DNA structure by physico-chemical methods, mainly light scattering. ϕ X174-RF DNA is circular and can be supercoiled. This leads to a number of interesting problems, the answers to which can be illuminating for DNA structure in general. This is discussed in the next section (section 1.3).

1.3

CIRCULAR DNA

1.3.1

ø X174 DNA

Double-stranded replicative form of ø X174 bacteriophage (ø X174-RF) exists in two forms, naturally: firstly the double stranded circular form with both strands of the DNA duplex intact, called form I, and secondly the double stranded circular form with at least one break in one of the strands of the DNA duplex, called form II. ø X174-RFI DNA has a number of tertiary turns imposed on the DNA duplex by topological constraints (Vinograd & Lebowitz, 1966), whereas the RFII DNA exists as an open circle with no topological constraints. This is represented diagrammatically in Fig. 1.1.

1.3.2

HISTORY AND CHARACTERISATION OF CIRCULAR DNA

The first suggestions of circular DNA molecules came from genetic recombination experiments (Jacob & Wollman, 1957). The first direct demonstrations of naturally occurring circular DNA molecules were for ø X174 mature phage DNA which is single stranded (Fiers & Sinsheimer, 1962) and the Escherichia coli chromosome (Cairns, 1963). These were followed by the demonstration that λDNA can be circularised by virtue of its "sticky ends" (Hershey et al., 1963) and that polyoma virus DNA existed in at least two forms one of which was a covalently closed circular duplex (Dulbecco & Vogt, 1963; Weil & Vinograd, 1963) with the two single strands topologically linked as catanenes in the sense of Wasserman (1960). At this stage it was thought that form I was a circular and form II a linear form of the same DNA molecule. ø X174-RF DNA which exists intracellularly (Sinsheimer et al., 1962) was shown to be analogous to polyoma DNA (Kleinschmidt et al., 1963; Burton & Sinsheimer, 1963). Also analogous were the DNA molecules from a number of mammaliam viruses: SV40 (Crawford & Black, 1964), rabbit papilloma (Crawford, 1964) and human papilloma (Crawford, 1965). λ phage was also shown to have a circular intracellular intermediate on infecting E. Coli (Young & Sinsheimer, 1964). However, it was apparent that the hypothesis of forms I and II, being

circular and linear respectively, did not explain properties such as the variation of sedimentation coefficient with pH and temperature of formaldehyde fixing (Crawford & Black, 1964; Powels & Janz, 1964; Vinograd et al., 1965). Furthermore Janz & Powels (1965) showed that I was converted to II by one single stranded nick by DNase.

Hence Vinograd and co-workers (Vinograd et al., 1965; Vinograd & Lebowitz, 1966) proposed that form I was supercoiled and form II was relaxed circular DNA. This hypothesis was substantiated experimentally, as in sedimentation-velocity monitored dye titration of form I to an open circular form (Crawford & Waring, 1967; Bauer & Vinograd, 1968), shown diagrammatically in Fig. 1.1.

A comprehensive review of these developments and other aspects of circular DNA has been given recently by Helinski & Clewell (1971).

1.3.3

SUPERCOILED DNA, FORM I

1.3.3.1

QUANTITATION OF SUPERCOILING

The degree of supercoiling and its relation to the duplex structure in a form I DNA molecule have been formulated quantitatively by Vinograd and co-workers (Bauer & Vinograd, 1968; Vinograd et al., 1968; Bauer & Vinograd, 1970a) and Wang (1969a,b). Three winding numbers are defined; the superhelix winding number, τ, defines the number of turns the duplex makes about the axis of the superhelix; the topographical winding number, α, is defined as the number of complete revolutions made by one strand about the duplex axis, when the axis is made to lie in a plane; the duplex winding, β, is the number of complete revolutions made by one strand about the duplex axis in the unconstrained molecule. The numbers are related by the equation

$$\tau = \alpha - \beta \qquad (1)$$

An analytical proof of this has been presented by Glaubiger & Hearst (1967). In addition, an intensive quantity, the superhelix density σ, is defined as

$$\sigma = \tau/\beta_o \qquad (2)$$

where β_o is one-tenth the number of base pairs in the molecule, and if the duplex is in the B structure is equal to β. Conventionally right-handed duplex turns are taken as positive. A number of possible supercoiled DNA structures are shown in Fig. 1.2. Because of the topology of the molecules, for the interwound models (a) and (c), left-handed superturns are positive, whereas for the non-interwound toroidal model, (b), right-handed superturns are positive.

Three basically different methods of determining τ have been described: (a) dye titration monitored by sedimentation velocity (Crawford & Waring, 1967; Bauer & Vinograd, 1968; Wang, 1969a,b), viscometry (Revet et al., 1971) or buoyant density (Bauer & Vinograd, 1968); (b) alkaline base titration monitored by buoyant density (Vinograd et al., 1968); (c) buoyant density difference of form I from form II due to their different affinities for dye molecules (Gray et al., 1971). Of these, dye titration, particularly, monitored by sedimentation-velocity, has been most commonly used (Crawford & Waring, 1967; Bauer & Vinograd, 1968; Radloff et al., 1967; Wang et al., 1967, Bujard, 1968; Ruttenberg et al., 1968; Wang, 1969a,b; Böttger & Kuhn, 1971). Because of this, because it has been used in work reported here and because it illustrates many important points concerning supercoiled DNA structure, the principles behind this method are presented in detail here. The mathematical relationships have been derived by Bauer & Vinograd (1968) and Wang (1969a).

From eqn (1), since for naturally occurring superhelical DNA, τ is negative and $\beta > \alpha$, if β decreases, so will $|\tau|$ until it reaches zero. At this point the closed circular form I DNA is in the shape of an open circle and very nearly equivalent in structure to form II. A decrease in $|\tau|$ to 0, accompanying a decrease in β can be followed by monitoring the change in sedimentation coefficient of the molecule until it has a sedimentation coefficient equivalent to that of form II. A further decrease in β then

leads to an increase in $|\tau|$, with τ assuming positive values and supercoils being formed in the opposite sense to the original. One method of decreasing β is by binding a drug such as EB (ethidium bromide, 2, 7-diamino-9-phenylphenanthridene-10-ethyl bromide) to the DNA molecule; the drug molecules intercalate between the base pairs, causing local unwinding of the double helix (Lerman, 1961, 1964) of 12^{0} per drug molecule bound, in the case of EB (Fuller & Waring, 1964).

For a closed cyclic DNA molecule with τ_o superhelical turns with no dye bound, when dye is bound

$$\tau = \tau_o + (\phi/2\pi)(20\beta_o)\cdot r \qquad (3)$$

where ϕ is the angle of unwinding in radians/bound dye molecule and r is the number of molecules of dye bound/molecule of nucleotide. Also,

$$\sigma = \sigma_o - (10\phi/\pi)\cdot r \qquad (4)$$

where σ_o is the superhelix density in the absence of dye. However, there is an additional effect to be accounted for; this is an allowance for any change in the angle θ, the average angle between two adjoining base pairs, due to stress associated with the superhelical turns. If $\theta = \theta_o$ when $\tau = \tau_o$ and $\theta = \theta_1$ at $\tau = \tau_1$, then

$$\tau_o + (10\beta_o/\pi)\theta_o = \tau_1 + \frac{10\beta_o}{2\pi}\theta_1 - \frac{\phi}{2\pi}20\beta_o r \qquad (5)$$

This is the general equation describing superhelical DNA in which the superturns are being titrated. At the critical binding ratio $r = r_c$, the superhelical turns disappear, $\tau = 0$ and

$$\tau_o = \frac{\phi}{2\pi}20\beta_o r_c + \frac{10\beta_o}{2\pi}(\theta_1 - \theta_2) \qquad (6)$$

In general θ_1 and θ_o will be slightly different. Thus dye titration measures $\tau_o + \frac{10\beta_o}{2\pi}(\theta_o - \theta_1) = \tau$. τ is called the number of superhelical turns and τ_o the number of physical superhelical turns. $\tau - \tau_o$ will generally be small (< 1) for DNA molecules of the size of ϕ X174-RFI unless the superhelix density is high, so that torsional strain due to supercoiling

is increased. The same, if any, alterations in θ will occur if the supercoils are unwound by other methods, e.g. alkaline base titration (Vinograd & Lebowitz, 1966; Vinograd et al., 1968; Powels et al., 1968), temperature increase (Wang, 1969a; Upholt et al., 1971) or ionic strength change (Gellert, 1967; Bode & MacHattie, 1968; Wang, 1969a; Upholt et al., 1971).

It should be noted that the exact molecular details of the intercalation process as outlined by Lerman (1961, 1964) have recently been questioned by Paoletti & Le Pecq (1971a,b), who have even suggested that intercalation winds rather than unwinds DNA. This hypothesis seems rather unlikely in view of the well-known alkali titration of supercoiled DNA, indicating this is achieved by unwinding the duplex and in view of O.R.D. results (Maestre & Wang, 1971; Campbell & Lochhead, 1971). However, the model of Paoletti & Le Pecq also allows unwinding and in this form there is considerable evidence for it (Saucier et al., 1971; Waring, 1970). Nevertheless, they also accept a value for the unwinding angle for EB of 12^{o} as is indicated by the agreement between the number of superhelical turns of the same DNA molecules as determined by dye titration and by buoyant density-alkaline base titration (Vinograd et al., 1968).

1.3.3.2

CONFORMATIONS OF SUPERCOILED DNA

Possible conformations of supercoiled DNA in solution are represented in Fig. 1.2. Other configurations such as H-shapes may also exist.

The earliest attempts to examine the conformation of circular DNA and, specifically what turned out to be supercoiled DNA, were by ultracentrifugation and electron microscopy (Kleinschmidt et al., 1963; Thomas & MacHattie, 1964; Janz & Powels, 1965; Vinograd et al., 1965; Weil & Vinograd, 1963; Chandler et al., 1964). These two techniques, along with viscosity (Revet et al., 1971; Saucier et al., 1971), have continued to be the tools used in the vast majority of investigations of supercoiled DNA structure ever since (Crawford & Waring, 1967; Follet & Crawford, 1967; Gellert, 1967; Bode & MacHattie, 1968; Bauer & Vinograd, 1968; Wang, 1969a;

Böttger & Kuhn, 1971; Upholt et al., 1971).

However, results from electron micrographs can produce artifactual results, especially where the results are taken as an indication of solution structure. Crawford & Waring (1967), Wang (1969a) and Vinograd et al. (1968) have all noted that the number of superhelical turns apparent in electron micrographs is very different from that calculated from sedimentation velocity-dye titration experiments for the same molecules. Possible reasons for this have been discussed by Vinograd et al. (1968) and Kleinschmidt et al. (1965)

It is possible to attempt to correlate the sedimentation coefficients of these molecules with molecular dimensions and some efforts have been made in this direction (Fukatsu & Kurata, 1966; Bloomfield, 1966; Gray, 1967). The theories of Bloomfield and Fukatsu & Kurata treat form I DNA as consisting of sub-rings linearly connected at fixed points by universal joints. Sedimentation coefficients predicted by these models are very much higher than experimentally observed values. This is probably because of at least three reasons: (a) the assumption that the strands of the molecules touch when crossing over; (b) the failure to consider more than one possible structure for supercoiled DNA; (c) in the case of Bloomfield, the assumption of equal loop size.

Gray (1967) has treated the molecule as rigid and used the Kirkwood-Riseman formulation (Kirkwood, 1954) to calculate sedimentation coefficients. He also considered two models, the toroid and the straight interwound (Fig.2.1a,b). He obtained sedimentation coefficients compatible with experimental results at different superhelix densities, by appropriate choice of pitch and superhelix radius, etc. However, in this approach a number of different dimensions for superhelical molecules predict the same sedimentation coefficients and the method becomes inaccurate at low superhelix densities when the molecules are obviously not rigid. As noted by Upholt et at. (1971), these theoretical difficulties are not surprising, given the nature of the problem. This is to describe these long chain molecules by

superposing some degree of order on the spacial disorder induced by thermal energy. In fact it now appears (Upholt et al., 1971) that the sedimentation coefficient is not a particularly sensitive measure of conformation change in these molecules. These workers have investigated the behaviour of the sedimentation coefficient of SV40 native viral DNA (mol. wt. 3×10^6) PM2 DNA (mol. wt. 6×10^6), over a large range of superhelix density and as a function of termperature, ionic strength and counter-ion. As indicated by Dean & Lebowitz (1971) and Wang (1969a) there appears to be more than one phase to the plot of sedimentation coefficient against superhelix density; in fact there appear to be at least 3 phases in going from $\sigma = -0.085$ to $\sigma = 0$ (Fig. 1.3). Because of the inadequacies, out-lined above, of the existing theories for calculating sedimentation coefficients, Upholt et al. were forced to rely on electron micrographs for correlation of sedimentation coefficients with molecular conformations. As discussed above correlation between electron micrographs and solution structure must be made cautiously. The attraction of electron microscopy and ultracentrifugation is the relatively small amounts of material necessary; otherwise, for examination of the molecular conformation of these molecules, other techniques seem better. In particular, light scattering offers a means of obtaining a mol. wt., a root-mean-square radius and a simple light interference pattern for these molecules (see, for example, Geiduschek & Holtzer, 1958). The last two results are direct measures of molecular conformation. It was obviously of interest, therefore, to perform light scattering experiments on ø X174-RFI DNA (mol. wt. 3.4×10^6) at various superhelix densities and deduce the structures that are implied.

1.3.4

RELAXED CIRCULAR DNA, FORM II

The results obtainable from a conformational analysis of ø X174-RFII DNA are important for two reasons. Firstly, circular DNA molecules are widely found (see section 1.3.5) where whole naturally occurring DNA molecules are examinable. It is obviously necessary to characterise these molecules with respect to their physical properties, in order to be better able to attempt

to investigate their biological significance, e.g. their modes of replication and transcription. Secondly, ϕ X174-RFII DNA is a very suitable molecule, by virtue of its size (mol. wt. 3.4×10^6) and its optical isotropy in solution, for investigation of the general conformational properties of all DNA molecules by light scattering, which, in theory, is a very powerful tool for this. A quantitative understanding of these properties is necessary for any thermodynamic calculations with respect to DNA packaging, speeds and modes of replication and transcription, as for instance attempted by Gray & Hearst (1968).

Recent theories of the solution behaviour of native DNA have treated it as a worm-like coil (Kratky & Porod, 1949) and have characterised it by the mol. wt., M, the excluded volume parameter ϵ (Bloomfield & Zimm, 1966; Peterlin, 1955), the persistence length $\frac{1}{2\lambda'}$ (Kratky & Porod, 1949; Flory 1968) or the Kuhn statistical length $1/\lambda'$(Kuhn, 1936, 1939), which are measures of the longitudinal stiffness of the DNA molecule, and the hydrodynamic diameter, d, of the double helix. The last three are assumed independent of the source of the DNA and to depend only on solution conditions.

Examination of results from sedimentation velocity and viscosity (Gray et al., 1967; Sharp & Bloomfield, 1968a,b; Ullman, 1968; Hearst et al., 1968a,b; Bloomfield, 1968; Hays et al., 1969; Triebel et al., 1971) shows that at room temperature, neutral pH and ionic strength about 0.2, the values $1/\lambda'$ = 90nm, ϵ = 0.11, d = 2.7nm seem fairly well accepted, for ordinary linear DNA. Also, Harrington (1970) has estimated $1/\lambda'$ = 93nm from flow birefringence.

The situation with regard to light scattering is less satisfactory. It has been understood for several years now that molecular weights for large DNA molecules ($M \geq 6 \times 10^6$), extrapolation from 30^o to 0^o would lead to values of M which were approximately half the actual value (Froelich et al., 1965; Harpst et al., 1968). However, despite experimental improvements, the results for the conformational parameters of DNA from light scattering still show little uniformity, in particular with respect to $1/\lambda'$. Estimates for this vary from 40nm to 350 nm (Geiduschek & Holtzer, 1958; Sharp &

Bloomfield, 1968b; Hays et al., 1969; Eisenberg, 1969; Jennings & Plummer, 1970). These results and the discrepancy with results from hydrodynamic experiments have been critically examined by Sharp & Bloomfield (1968b) and Schmid et al., (1971). The conclusions drawn were, firstly, that experiments with low angle instruments (down to 10^{o}) and large homogeneous DNA molecules such as T7 DNA (mol. wt. 25×10^{6})(Harpst et al., 1968) were inaccurate as they still entailed too large an extrapolation to zero angle; that is, experiments at still lower angles were necessary. Schmid et al. (1971) and Zimm (1948) have estimated that extrapolation to 0^{o} is satisfactory only from values of $P\theta^{-1} \leq 1.3$, or $P\theta^{-\frac{1}{2}} \leq 1.3$ for a Berry plot (Berry, 1966), where $P\theta$ is the particle scattering factor, equal to 1 at 0^{o}. Secondly, the use of DNA samples highly degraded by sonication (mol. wt. 500,000approx.) examined only at angles of 30^{o} and greater (Cohen & Eisenberg, 1966) has been criticised for ignoring anisotropy effects, which occur with small rod-like DNA molecules (Weill et al., 1968).

ϕ X174-RFII DNA is small and circular. It seems likely, therefore, that correct extrapolation to 0^{o} could be made and also that anisotropy would be negligible so that meaningful light scattering experiments could be performed. Comparison of the results with predicted scattering envelopes for various values of $1/\lambda'$ and ϵ should then give accurate values of these parameters from light scattering. This is more accurate than calculating $1/\lambda'$ from the root-mean-square radius, which has a moderate error when obtained from the initial slope of the Zimm plot (Zimm, 1948). There has been one examination of relaxed circular DNA by light scattering (Dawson & Harpst, 1971) using λ DNA, mol. wt. $31 - 33 \times 10^{6}$. This therefore suffers from some of the inaccuracies discussed above and also circular λ DNA is normally contaminated with linear and circularily aggregated forms. No attempt was made to estimate $1/\lambda'$ etc. Nevertheless it would be interesting to compare the results of light scattering from ϕ X174-RFII DNA with their results, and analyse these for $1/\lambda'$ and ϵ.

Therefore, in the experiments with ϕ X174-RFII DNA, the molecular weight, root-mean-square radius and behaviour of $P\theta^{-1}$ have been investigated. A theoretical $P\theta^{-1}$ curve for different scattering angles θ has been calculated, incorporating terms for $1/\lambda'$ and ϵ. This has been compared with the experi-

mental result for various values of $1/\lambda'$ and ϵ, to estimate values of these parameters.

1.3.5

OCCURRENCE, BIOLOGICAL AND BIOPHYSICAL SIGNIFICANCE OF CIRCULAR DNA

1.3.5.1

OCCURRENCE

Circular DNA molecules now seem extremely common and widely distributed in nature. In bacteria, the bacterial chromosome is apparently circular (Cairns, 1963; Jacob & Wollman, 1957); in addition, bacterial plasmid and episomal (Jacob & Wollman, 1961) DNA seems universally circular. Examples are coligenic factors (Bazaral & Helinski, 1968; Carlton & Helinski, 1969; Roth & Helinski, 1967; Lee & Davidson, 1968), sex factors (Friefelder, 1968a,b,c), R-factors (Rush et al., 1969; Cohen & Miller, 1969), defective phage genomes (Matsubara & Kaiser, 1968; Rush et al., 1969), trypanosomal kinetoplasts (Riou & Paolotti, 1967; Riou & Delain, 1969) and various examples with obscure functions (Cozzarelli et al., 1968). Also, for all bacteriophages where DNA intermediates have been sufficiently characterised, the genome appears to go through a circular stage (Helinski & Clewell, 1971; Thomas et al., 1968).

In eukaryotic systems, circular DNA is also widespread. A small DNA fragment from calf thymus DNA has been shown to have "sticky ends" like phage λ DNA (Thomas et al., 1970). Mitochondrial DNA seems universally circular (see Nass, 1969; Borst & Kroon, 1969 for reviews) and new instances are continually being demonstrated, e.g. in Neurospora crassa mitochondria (Clayton & Bramble, 1972). Chloroplast DNA, although not so well characterised, seems to be circular too (Kirk, 1971). Another instance of eukaryotic circular DNA is in boar sperm (Hotta & Bassel, 1965). A number of animal viruses have circular genomes including, as mentioned in Section 1.2, the oncogenic viruses polyoma, SV40, human and rabbit papilloma, and bovine papilloma (Lang et al., 1967), plus a large number of the adenovirus group (Smith, 1965).

A large number of the above-mentioned DNA molecules are known to exist in the supercoiled form I, and it seems likely that the rest do also.

1.3.5.2

BIOLOGICAL SIGNIFICANCE

It is evident that merely because of its ubiquity, circular DNA must be thoroughly characterised as part of the total explanation of its functions and modes of accomplishing these. However, circular DNA has also been heavily implicated in the crucial processes of transcription and replication in a number of systems. Observations with respect to transcription have been made on phage λ, where circularity has been shown to be necessary for transcription of both late (Herskowitz & Signer, 1970) and early (Pilarski & Egan, 1972) genes. In addition, it has been shown that the DNA duplex is transcribed asymmetrically, and presumably more specifically, by E. coli RNA polymerase in vitro, from the supercoiled form I of ϕ X174-RF DNA (Hayashi et al., 1964; Wamaar et al., 1969) and SV40 DNA (Westphal, 1970). In SV40 DNA, at least, this property of the DNA is apparently conferred only by the topology of the molecule as form II is not assymmetrically transcribed. Finally, in phage fd-RFI DNA, there appear to be three specific initiation sites for E. coli RNA polymerase (Sugiara et al., 1969).

As previously noted in Section 1.3.5.1 all bacteriophage genomes seem to be circularised at some stage of their replication cycle (Helinski & Clewell, 1971). This has been shown, for example, in detail for vegetative phage λ replication, where circularity is required (Tomizawa & Ogawa, 1968; Schnös & Inman, 1970). A major source of information on replication of circular DNA has been electron micrographs (and autoradiographs) of replicating DNA molecules. Two models seem acceptable for this process, the "swivel" model (Cairns, 1963) and the rolling circle model (Gilbert & Dressler, 1968). Electron micrographs and autoradiographs with branched structures suggesting both models have accumulated. The swivel mechanism seems to occur in replication of E. coli DNA (Cairns, 1963), mycoplasma DNA (Bode & Horowitz, 1967), early λ DNA (Schnös & Inman, 1970), polyoma DNA (Hirt, 1969), SV40 DNA (Levine et al., 1970), colicin factor E (Inselburg

& Fuke, 1970) and mitochondrial DNA (Kirschner et al., 1968). The rolling circle seems to occur with ϕ X174-RF DNA (Dresler & Wolfson, 1970), M13 DNA (Ray, 1969), late λ DNA (Kiger & Sinsheimer, 1971), phage PM2 DNA (Espejo et al., 1971), P2 DNA (Schnos & Inman, 1971), T4 DNA (Altman & Lerman, 1970), P22 DNA (Bolstein & Matz, 1970), and plasmid DNA of E. coli 15T⁻ (Lee & Davidson, 1970).

It is relevant to note here the w protein of Wang (1971) which induces a type of Cairns swivel into supercoiled λ DNA, reducing the number of supercoils, then reseals the presumably broken strand of DNA. This is obviously of interest in considering replication and transcription. A number of proteins similar in property to w have been isolated, though not all of them reseal the DNA molecule when removed from the DNA (Clewell & Helinski, 1970a,b; Helinski & Clewell, 1970; Kline & Helinski, 1971; Champoux & Dulbecco, 1972).

A detailed mechanism of initiation of DNA synthesis on the basis of genetic and other results has been proposed by Gross (1972). In this DNA replication is primed by a small specific amount of RNA synthesis with membrane bound, form I λ DNA as template. DNA synthesis then proceeds a short way along the parental molecule until the resulting untwisting of the DNA duplex has induced a number of tertiary supertwists which block further synthesis. DNA replication proper will not proceed until signalled by the arrival of a complex including a w-type untwisting protein. This model suggests a specific topological role for supercoiling in DNA and leads to a consideration of the D-loops found by Borst and co-workers in chick mitochondria supercoiled DNA (Ter Schegget & Borst, 1971a,b; Ter Schegget et al., 1971) and by Kasamatsu et al., (1971) in cultured mouse L cell mitochondria. These D-loops are sections of supercoiled DNA molecules (mol. wt. 10×10^6 approx.) where the duplex strands part and a small portion of single stranded DNA (mol. wt. 1.5×10^5 approx.) hydrogen bonds to one strand. This could conceivably be an intermediate in a replication initiation scheme, similar to that proposed by Gross for λ DNA.

Reviews of DNA replication (Goulian, 1971) and initiation of replication (Lark, 1969) are available.

Finally, supercoiled DNA (but not necessarily circular) has been invoked as a virus packaging method (Kilkson & Maestre, 1962) as structural (Pardon et al., 1967; Luzzati & Nicolaieff, 1963) and as functional (Crick, 1971; Sutton, 1972) units in terms of gene regulation methods (Britten & Davidson, 1969) in higher cells. Stahl (1962) has also proposed a chromosome model involving circular DNA units.

1.3.5.3

BIOPHYSICAL SIGNIFICANCE

Supercoiled DNA is of interest for other reasons apart from its direct biological significance. It reflects, because of the topological restraints exercised on it, effects on the secondary structure, in tertiary structure changes (see Section 1.3.1). This means that secondary structure changes with changes in environment can be followed using such well tried techniques as ultracentrifugation, viscosity and light scattering which are otherwise insensitive to secondary structure changes.

The most obvious example is that of intercalating dyes; these were originally used in conjunction with ultracentrifugation to estimate the degree of supertwisting in form I molecules (see Section 1.3.1). However, the reverse has also been done and the behaviour of supercoils in the presence of drug molecules used to determine if the drug molecules intercalate (Waring, 1970). Also, estimates of the effect of temperature, ionic strength on supercoiled DNA and hence on secondary structure in general have been made (Wang, 1969a; Upholt et al., 1971). It is notable that of the techniques used normally as secondary structure probes, only X-ray diffraction has been capable of this degree of quantitative resolution; however, this technique only examines discrete fibre forms, which are not in solution. X-ray scattering should in principle be able to give this type of information, but there have been problems in experimental practice and treatment of results (see, for example, Eisenberg & Cohen, 1968). C.D. or O.R.D., hydrogen exchange, n.m.r. and thermal melting do not give this type of experimental

result. Thus supercoiled DNA is a powerful means of examining aspects of DNA secondary structure.

Table 1.1

THE MAJOR STRUCTURAL PARAMETERS FOR DOUBLE-HELICAL NUCLEIC ACIDS

These parameters come from X-ray diffraction studies on nucleic acid fibres. The information is taken from Yang & Samejima (1969) and Arnott (1970). A, B, and C refer to the three major fibre structures for DNA known, and the helix pitch is given in nm.

Table 1.1

	A	B	C	DNA-RNA	RNA
helix pitch	2.82	3.37	3.10	2.80	3.05
residues/ turn	11	10	9.33	11	10-11
inclination of bases to horizontal (helix axis vertical)	20^{o}	2^{o}	6^{o}	20^{o}	15^{o}

Fig. 1.1

REPRESENTATION OF A SUPERCOILED DNA AND ITS UNWINDING

Here the single black line represents the DNA duplex. Initially all naturally occurring DNA molecules are supercoiled the one way, generally thought to be negative, as in the first structure. As the DNA duplex is unwound slowly, as in this case by intercalating dye molecules, the superturns also unwind as in the second structure until an open circular form is reached in the third structure. At any point in this process a single break in either of the duplex strands allows the molecule to relax immediately to a form equivalent to the third structure, disregarding the amount of dye bound.

Quantitation of these effects is dealt with in Section 1.3.3.1.

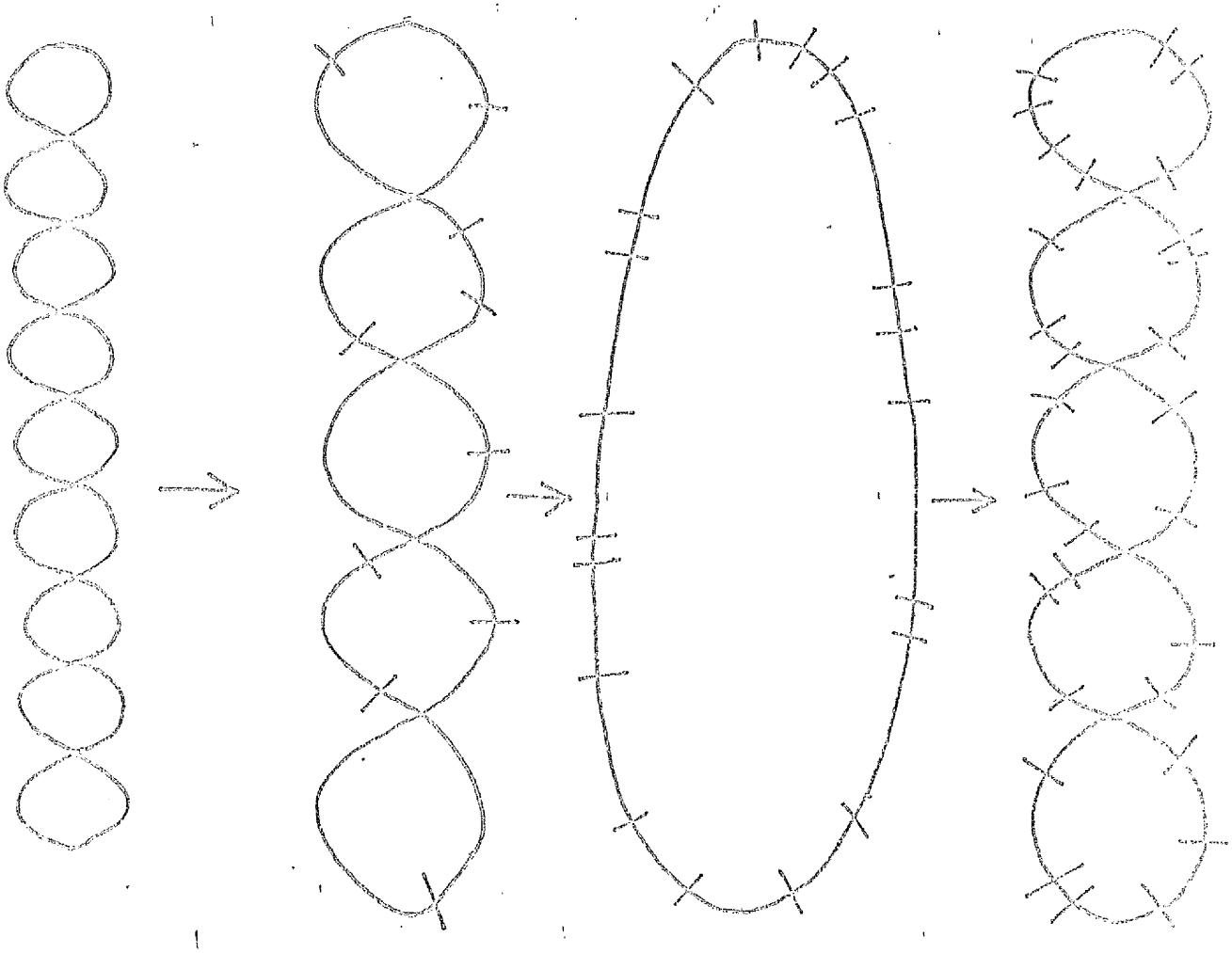
(a)
(b)
(c)
(d)

Fig. 1.2

HYPOTHETICAL STRUCTURES FOR VARIOUS FORMS OF SUPERCOILED DNA OF 12 SUPERHELICAL TURNS

(a) Rigid straight interwound superhelix;

(b) toroid;

(c) two forms of Y-shaped structure, one with all arms the same length and the other with arms of different lengths.

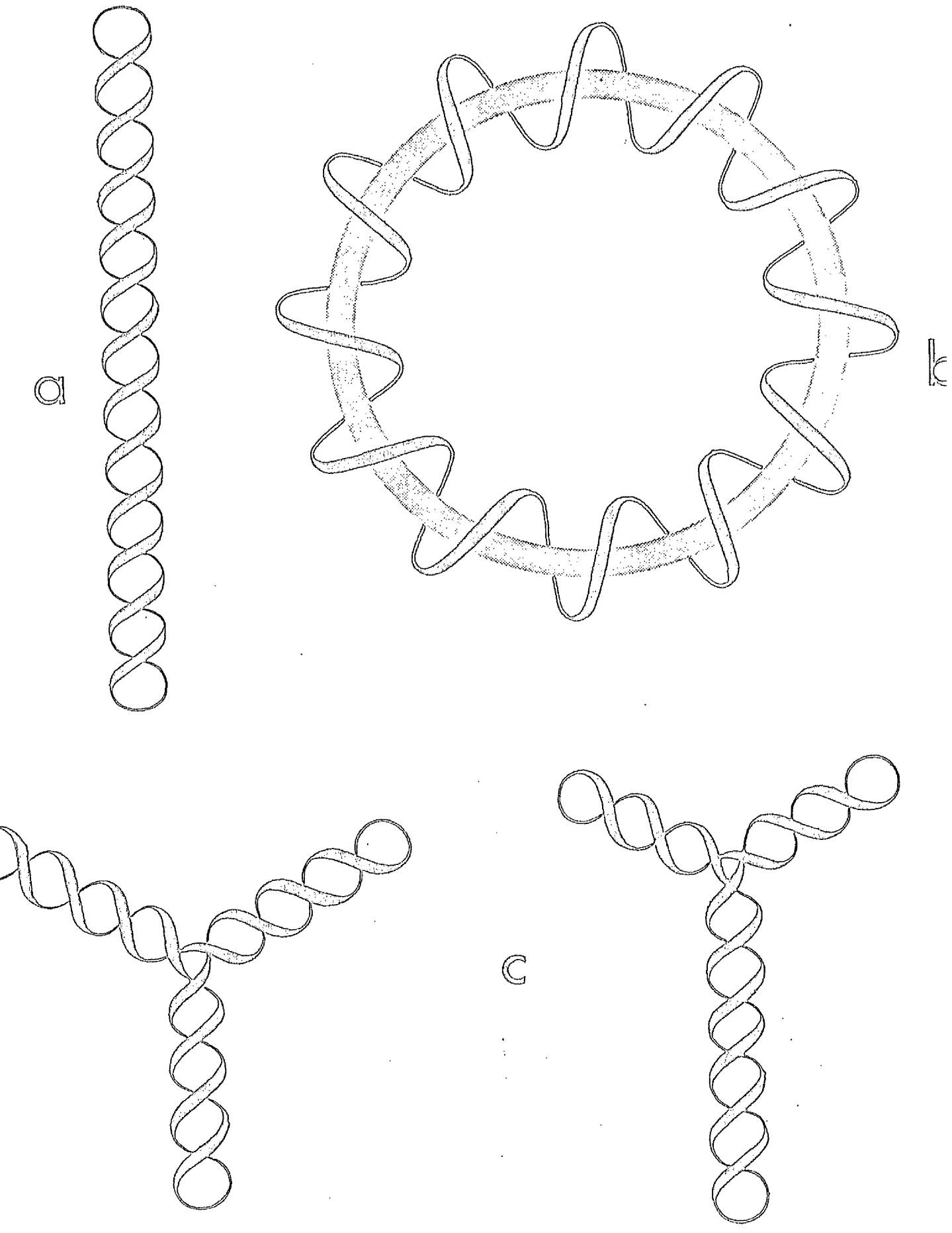
a
b
c

Fig. 1.3

SCHEME OF THE BEHAVIOUR OF THE SEDIMENTATION COEFFICIENT OF SUPERCOILED DNA AS A FUNCTION OF SUPERHELIX DENSITY, σ

This is based on the results of Upholt et al., (1971) for SV40 DNA (mol. wt. 3.1×10^6). Similar results were obtained for PM2 and λb2b5c DNA. The curve is at least triphasic, possibly quadrophasic. These phases are delineated approx. as follows:

I, below σ = -0.035

II from σ = -0.035 to -0.017

III A from σ = -0.017 to -0.005

III B from σ = -0.005 to 0.

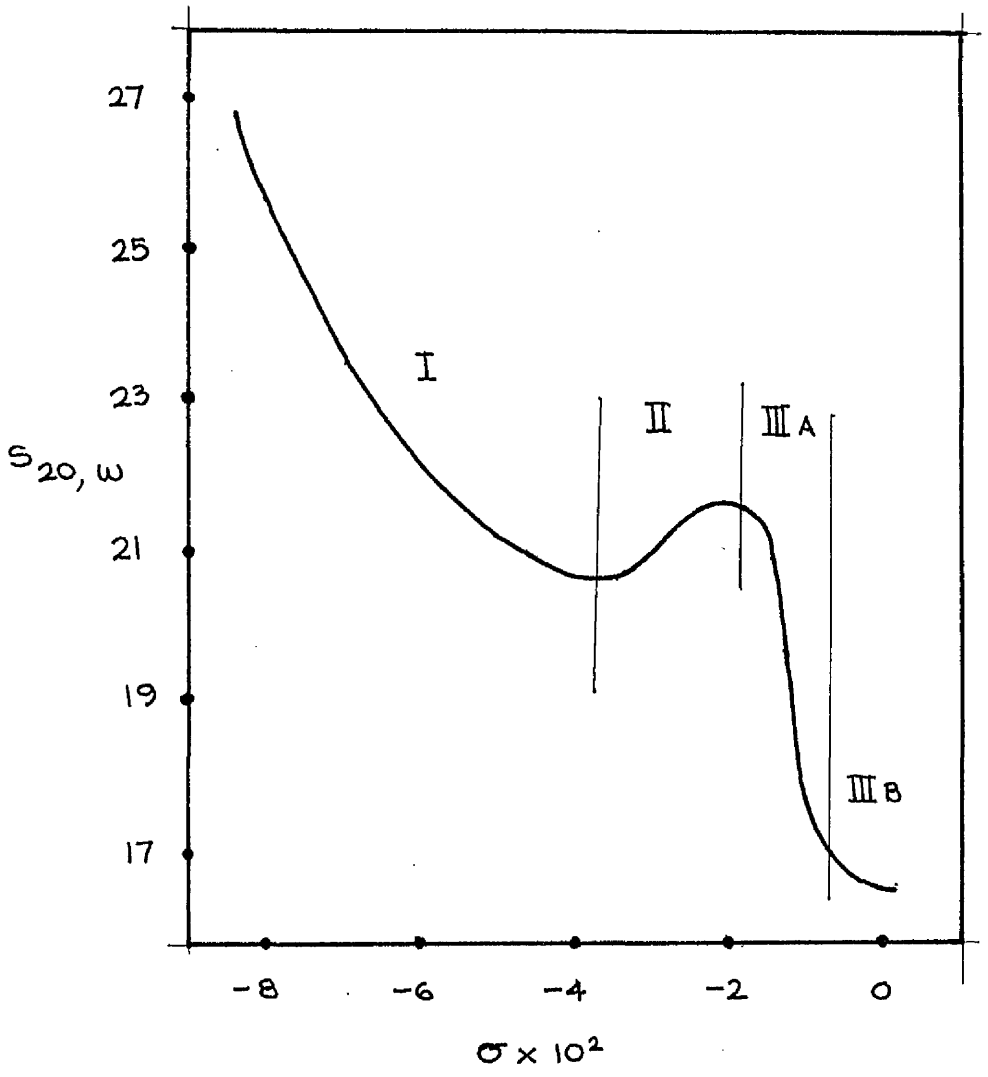
27
25
23
21
19
17
$S_{20,w}$
I
II
III A
III B
-8
-6
-4
-2
0
$\sigma \times 10^2$

2. MATERIALS & METHODS

2.1

MATERIALS

2.1.1

BIOLOGICAL

The double stranded replicative form of ϕ X174 bacteriophage DNA was obtained from infected E. coli C, grown at the Microbiological Research Establishment, Ministry of Defence, Porton, Salisbury, Wilts. 20 litre cultures of E. coli C in log phase with, typically, a viable bacteria count of 4.66×10^9 were infected with ϕ X174 bacteriophage. After two minutes 700 ml of chloramphenicol (D(-)-three-2,2-dichloro-N-(β-hydroxy-α-(hydroxymethyl)-p-nitrophenyl) acetamide) were added to the culture in a small volume, and the bacteria harvested after 45 min by cooling to $6^{\circ}C$ and centrifugation. This gave typically 280g, wet weight of bacteria per culture. The bacteria were stored frozen at $-80^{\circ}C$.

2.1.2

CHEMICAL

2.1.2.1

CHEMICALS AND BIOCHEMICALS

All chemicals unless otherwise stated were AnalaR grade reagents obtained from British Drug Houses Ltd., Poole, Dorset, England. Propidium iodide (PI), (3,8-diamino-5-diethylamino-propyl-6-phenyl phenanthridium di-iodide), A grade and ethidium bromide were obtained from Calbiochem, Los Angeles, California 90054, U.S.A. Caesium chloride for analytical centrifugation was optical grade obtained from the Harshaw Chemical Co., 6801 Cochran Road, Solon, Ohio 44139, U.S.A. Caesium chloride for preparative gradients was AnalaR grade obtained from Hopkin & Williams Ltd., Chadwell Heath, Essex, England. Dowex 50-w-X8 (Na) cation exchanger was obtained from British Drug Houses Ltd. Dialysis tubing was Visking, obtained from the Scientific Instrument Centre Ltd., 1 Leeke Street, London, W.C.1; before use, it was boiled for ten minutes successively in 2% (w/v) Na_2CO_3, 1% (w/v) Na_2EDTA and distilled water. Ludox colloidal silica suspension was a gift from E.I. Du Pont de Nemours & Co. inc., Wilmington, Delaware 19898, U.S.A.

Bovine pancreas RNase (E.C. 2.7.7.16) and calf thymus (CT) DNA were obtained from Sigma Chemical Co., St. Louis, Missouri 63118, U.S.A. Sephadex G-100 was obtained from Pharmacia Fine Chemicals, Uppsala, Sweden. Proflavine hemi-sulphate (PF), (3,6-diamino acridinium monohydrogen sulphate) was re-crystallised twice from distilled water before use.

2.1.2.2

SOLUTIONS AND BUFFERS

All solutions were made up using distilled water. BPES was 6mM-Na_2HPO_4—2mM-NaH_2PO_4—1mM-Na_2EDTA—0.179M-NaCl, pH 6.8 (Krasna & Harpst, 1964). 2 x SSC was 0.3M-NaCl—0.03M-Na_3 citrate, pH 7. EDTA/SDS was 15mM-Na_2EDTA—0.025%(w/v) Na dodecyl sulphate, pH 8. The buffers for calibration of the pH meter were as follows: pH 10, pH 7 Beckman standard buffers, obtained from Beckman Instruments Ltd., Glenrothes, Fife, Scotland; pH 12.63, 2 parts of a solution of 7.505g glycine, 5.85g NaCl per litre to 8 parts 0.1 N NaOH; pH 9.955, 6 parts to 4 parts respectively of the same solutions. The last two recipes were obtained from the International Critical Tables (1926a) and all pH values apply at 25°C. The bulk solution for analytical band sedimentation was 2.8M-CsCl—5mM-Na phosphate buffer —1mM-Na EDTA, pH 7.5.

2.2

METHODS

2.2.1

PREPARATION OF ϕ X174-RF DNA

This was prepared from infected E.coli C following the method of Rush et al. (1967). All solutions and materials were autoclaved, if possible, and all manipulations were kept as sterile as possible.

20g of bacteria were thawed in EDTA/SDS, 12 ml/g, and the pH raised to 12.4 by careful addition of IN-NaOH, with continuous stirring. The solution was kept at pH 12.4 for 3 min, then lowered to pH 7-8, still stirring continuously, with IN-HCl. The pH was monitored with a PHM526 digital pH meter, from Radiometer A/S, Emdrupvej 72, DK 2400, Copenhagen NV, Denmark, equipped with type G202B glass electrode and type K401 KCl electrode. The solution was centrifuged at 15000g (10,000 r.p.m.) in the 6 x 250 ml head of an MSE 18 centrifuge (MSE Ltd., London, England) for 10 min at $4^{o}C$, the precipitate discarded, the supernatant heated to $80^{o}C$ in a water bath, and a previously boiled solution of RNase, 1mg/ml in distilled water added to a concentration of 10μg/ml approx. The solution was recentrifuged at 15000g for 10 min and the supernatant reduced to about 200ml by flash evaporation at $30^{o}C$. The solution was then applied to a 5 x 90cm column of Sephadex G-100 and eluted with 2 x SSC at a flow rate of 0.5-1.0ml/min at $0^{o}C$. The void volume, containing only large DNA molecules, was collected. This was then run batchwise through a 2.5 x 40cm column of cellulose nitrate, which had been ground in a blender in ethanol: 2 x SSC . 1:1, and equilibrated with 2 x SSC. The eluent was collected and contained only ϕ X174-RF DNA. The percentage of RFI varied from 60% to 90%. From 20g of bacteria, the yield was usually 4-6mg of DNA. RFI and II were separated by equilibrium sedimentation in a self-forming caesium chloride - PI or EB gradient (Hudson et al., 1967) in 5/3 x 3" cellulose nitrate tubes in the Ti50 fixed angle head for a Spinco model L or L-2 ultracentrifuge (manufactured by Spinco Division, Beckman Instruments, inc., Palo Alto, California) at 43,000 r.p.m., 128400g (r_{av} = 5.9cm) at $15^{o}C$, for 36h. The gradient solutions were made up

as follows, or in the same proportions: EB gradients, 4.5g CsCl, 4.6ml DNA solution (30-300µg/ml), 0.2ml EB solution (3mg/ml) adjusted to n_D^{25} = 1.389, sp.gr. 1.5873; PI gradients, 4.5g CsCl, 4ml DNA solution (30-300µg/ml), 1.25ml PI solution (2mg/ml) adjusted to n_D^{25} = 1.383, sp.gr. 1.5221. The gradients were harvested by puncturing the bottom of the tubes with a narrow-bore needle and collecting the two bands batchwise, by visual inspection. The PI or EB was removed by passage through a 2.5 x 40cm column of Dowex-50 equilibrated with BPES; this suffices for an 8 tube harvest. The DNA was assayed for residual dye by a fluorescent assay, the calibration curves for which are shown in Fig. 2.1, which was capable of detecting down to 0.01µg/ml of dye. Emission and absorption wavelengths used were 623nm and 305nm respectively. The two forms, in particular RFI, were assayed for contamination by the other form or any other DNA by band sedimentation as specified in Section 2.2.3.1. This is estimated to assay down to 3% contamination of RFI with RFII.

2.2.2

LIGHT SCATTERING

2.2.2.1

INSTRUMENTATION

The light scattering experiments were performed on a FICA 50 photogonio-diffusometer, manufactured by FICA, F-78 Le Mesnil-St. Denis, Yvelines, France, using unpolarised incident light at 546nm.

2.2.2.2

CALIBRATION

The instrument was originally designed for use by polymer chemists and the sample sits in a benzene vat, so that the refractive index correction for the volume "seen" by the photomultiplier should be $n^2(\text{benzene})/n^2(\text{solution})$, for solutions of refractive index ≥ 1.45 (Hermans & Levinson, 1951; Billmeyer, 1945; FICA, Introductory Manual, 1970); the instrument is equipped with a glass standard, calibrated with respect to the Rayleigh ratio of benzene. However, for solutions with $n < 1.45$ certainly and perhaps for all solutions, using the manufacturer's cylindrical cells, this correction

does not hold, because the receiver now seems to "see" past the edges of the primary beam (Hermans & Levinson, 1951). Various other analyses of this problem have appeared (Brice, Halwer & Speiser, 1950; Carr & Zimm, 1950; Edsall et al., 1950; Bonnelycke & Dandliker, 1959; Stacy & Arnett, 1964; Hardy & Penin, 1932; Wallace et al., 1972). It was not clear initially which, if any, of these should be applied to our instrument. Since then documentation of this problem has appeared and it now seems the correction is intermediate between n^2 and n (Wallace et al., 1972).

At first attempts were made to determine the correction factor experimentally by determining the apparent Rayleigh ratios of a number of pure liquids of known refractive indices and Rayleigh ratios, at 546nm. The literature values were obtained from work of Cohen & Eisenberg (1965), Coumou (1960), Coumou & Mackor (1964), Coumou et al.(1964), Goring & Napier (1954) and Kraut & Dandliker (1955). The organic liquids were dried, distilled and passed over silica gel to remove fluorescent contaminants, and redistilled. Water was distilled over potassium permanganate and redistilled. The liquids were finally clarified by passage through 0.22u pore size GS Millipore filters (from Millipore (U.K.) Ltd., Abbey Road, Park Royal, London N.W.10 7SP) or Sartorius membran filters (from Sartorius, 34 Gottingen, West Germany). The results are shown in Fig. 2.2. There are, however, a number of rather large errors involved in this experiment: (a) the large uncertainty in literature values of the Rayleigh ratios for most of these liquids; (b) the difficulty in measuring accurately the small light intensities scattered by pure liquids; (c) the difficulty in obtaining absolutely pure liquids, free of fluorescent contaminants. Therefore the correction was not considered accurate enough.

Conical cells were then designed according to a verbal description by the FICA instrument designer. These were intended to make the "n^2" correction applicable to a solution with $n < 1.44$ and were manufactured by Messrs. Barr & Stroud Ltd., Anniesland, Glasgow, Scotland; these are shown in Fig. 2.3. They reduced the deviation from the n^2 correction somewhat and

had the merit of reducing the sample volume required from 5ml to under 3ml, so they were retained in the rest of the work.

The instrument and cells were finally calibrated using an aqueous suspension of Ludox colloidal silica, thus avoiding all but very small refractive index corrections. The calibration constant, C, is given by $C.J(90) = R(90) = (3/16)(2.303A/P)$ for unpolarised incident light (McIntyre, 1964; Stacey, 1956) where J(90) is the observed excess instrument reading corresponding to the scattering from a calibrating solution at 90^{o}, R(90) is the Rayleigh ratio, and A is the optical absorbance measured in a cell of length Pcm at the same wavelength used in scattering measurements. Precautions previously recommended were taken (Dezelic & Kratohvil, 1960; Kratohvil et al., 1962). The stock Ludox suspension was centrifuged at 47,000g for 30 min prior to use and all suspensions were in 50mM-NaCl. Absorbances were measured in a Cary 15 spectrophotometer in 10cm pathlength cells enclosed in a temperature controlled Beck box at $25^{o}C \pm 0.1^{o}C$ with slits at either end. These were then compared with the readings in the light scattering instrument with respect to an arbitrary fixed reading for the glass standard. The Ludox suspensions were filtered through 0.45u pore size Millipore filters or Sartorius membran filters. The dissymetry was never greater than 1.05 but always existed as previously reported (Harpst et al., 1968a; Dezelic & Kratohvil, 1960). The Ludox had no depolarisation as measured by the horizontally and vertically polarised components of scattered light at 90^{o}, using polarisation filters supplied with the instrument. The calibration constant was obtained by three methods: (a) direct comparison of A and J(90); (b) the extrapolation method of Goring et al., (1957); (c) the extrapolation method of Maron & Lou (1954); (b) and (c) are shown in Figs. 2.4 and 2.5. These gave calibration constants which agreed to within 2%, which compares well with the uncertainty in the Rayleigh ratio of benzene - the standard for the manufacturer's original calibration. The best values of this are between 15.5×10^{-6} and 16×10^{-6} at 546nm (Kratohvil et al., (1962). When the sensitivity of the instrument was changed from calibration conditions, the calibration constant was changed in proportion to the change

in the glass standard reading. When the glass standard read 47, $C = 0.282 \times 10^{-6}$.

The cylindrical cells originally supplied did not require correction for changes in the scattering volume seen by the receiver at different angles, apart from the usual $\sin\theta/(1 + \cos^2\theta)$ factor, at least from 30° to 150°. For the conical cell, however, this was not so and was corrected for using a fluorescence correction method described by Harpst et al. (1968a). Solutions of fluorescein (9-(0-carboxyphenyl-6-hydroxy-3-150-xanthenone, disodium salt), 5ug/ml or less in 50mM-NaCl, 0.02% (w/v) NaN_3 were illuminated by light at 436nm, and the scattered light intercepted by a Corning sharp cut-off glass filter no. 3-68, glass no. 3484, obtained from Precision Optical Instruments (Fulham) Ltd., 159 Fulham Palace Road, London, W.6. This filter transmits no light at 436nm but does at 546nm, thus only fluorescence reaches the receiver, and this is of uniform intensity in all directions. For fluorescence, therefore, the quantity $i(\theta) \sin\theta$ should be independent of θ, the angle of examination, where $i(\theta)$ is the fluorescent intensity instrument reading. The correction for the volume seen by the receiver at different angles is obtained by calculating the value of the constant required to normalise readings to the 90° value, as this was the angle at which calibration was performed. Thus $S(\theta) = i(90)/i(\theta)\sin\theta$, where $S\theta$ is the normalisation factor at angle θ. The values obtained are shown in Fig. 2.6.

For calculating the absolute value of $R(\theta)$ which is equivalent theoretically to $r^2 I(\theta)/I_0(1 + \cos^2\theta)$, where r is the distance of the receiver from the scattering centre, $I(\theta)$ the scattered intensity at angle θ and I_0 the incident intensity per unit volume, the formula is $R\theta = (C.S(\theta).J(\theta).\sin\theta)/(1 + \cos^2\theta)$ where $J(\theta)$ is the excess instrument reading for scattered intensity at angle θ.

The light scattering experiments were plotted in terms of the quantity $Kc/R\theta$, where $K = 2\pi^2 n^2 (dn/dc)^2/N\lambda^4$, c the concentration; here n is the refractive index of the solvent, dn/dn the refractive index increment at constant chemical potential, λ the wavelength of light used in vacuo, N Avogadro's number. All quantities are in cgs system. When $n = 1.334$

and dn/dc = 0.166 (see Section 2.2.2.7) K = 1.807×10^{-7}.

2.2.2.3

CLARIFICATION

Clarification of DNA solutions has been previously attained in three different ways: (a) centrifugation (Reichmann et al., 1953); (b) dust extraction by an immiscible organic solvent (Bernardi, 1964; Froelich et al., 1963); (c) filtration through absolute membrane filters (Harpst et al., 1968b; Cohen & Eisenberg, 1966). I chose filtration as the most convenient. All solutions and solvents were filtered through 0.45u Millipore filters or Sartorius membranfilters; the solutions were pushed through filters held in Swinnex 25 polypropylene filter holders obtained from Millipore (U.K.) Ltd., by hand operated syringes of various sizes, up to 50ml. All manipulations were carried out on a Model TM36 Horizontal Laminar Flow Clean Bench, obtained from Gelman-Hawksley Ltd., 12 Peter Road, Lancing, Sussex, England, wearing washed disposable triflex gloves. This bench removes all dust particles from the bench atmosphere down to 0.5u. The following procedure was normally followed. Initially a cell and its teflon top were soaked in conc nitric acid for approx. 10 min. The top was then thoroughly rinsed and the cell washed out six times with filtered distilled water. The cell was then considered ready for use. For each solution placed in the cell, the filters were washed through with approx. 100ml solvent or water, as appropriate. The cell was washed once with filtered water, twice with filtered solvent and left full of solvent the second time. The cell was then rapidly emptied, the solution injected through a filter, and the top, washed with filtered solvent, placed on the cell. The cell was then placed in the holder and transferred to the instrument after drying and polishing the external surface of the cell with lens tissue. The concentration measurements were made subsequently. For experiments with RFI DNA the filters were pre-autoclaved in holders to minimise DNA breakdown.

2.2.2.4

TREATMENT OF SOLUTIONS

In all experiments, the initial solution was dialysed to equilibrium and constant chemical potential (Cassasa & Eisenberg, 1964) for at least 16h against the required solvent solution at room temperature. The experiment was then performed using the diffusate as solvent for dilutions.

2.2.2.5

TEMPERATURE EXPERIMENT

Temperature control was achieved with the system fitted to the instrument. Due to difficulties in exact replication of experimental temperatures, these varied by up to $\pm$ 0.3^{o}C for different concentrations at nominally the same temperatures. This was not considered important. Dilutions were made at room temperature and the solutions heated up and cooled down in the scattering cell. This had to be performed carefully to avoid introducing dust into the scattering solutions. This was checked by reading the solution at room temperature after reading at higher temperatures. Concentration measurements were made at room temperature and corrected to the temperature of scattering for water expansion (Fig. 2.7). The refractive indices of BPES at various temperatures at 546nm were measured using an Abbé refractometer, manufactured by Bellingham & Stanley Ltd., London, England, and the temperature was controlled by circulating water with a Haake thermostatic pump (Gebruder-Haake K.G., 1 Berlin 46, Siemenstrasse 27). The required refractive indices were read off the resulting plot (Fig. 2.8). As the cell holder is metal, and in contact with the metal frame of the instrument, the temperature of the benzene bath does not correspond exactly to that of the cell contents, above and below room temperature (22^{o}C approx.), because of heat conduction. All results were corrected for this effect from the temperature correction plot (Fig. 2.8).

2.2.2.6

PROFLAVINE TITRATION EXPERIMENTS

Light scattering experiments were performed at various values of r, the number of moles dye bound/moles nucleotide. The approximate desired value

of r was achieved by adjusting the buffer for dialysis to the corresponding free dye concentration, equilibrating the previously dye-free sample for 8h, exchanging the buffer and dialysing for at least 48h at room temperature in the dark, to achieve complete equilibrium. The dialysis tubing absorbed fairly large amounts of PF but this did not affect the experiment. The filters for clarification also absorbed large amounts of dye, and had to be equilibrated firstly with at least 150ml of diffusate and then, for the sample filter several passages of the DNA solution. Even so there were sometimes small unpredictable absorptions and desorptions of dye, so every scattering solution was analysed spectrophotometrically as described in Section 2.2.4.3 for dye binding and DNA concentration.

That the experiments were not distorted by fluorescence is shown by the fact that the mol. wt. of ϕ X174RF DNA in these experiments was the same as in other experiments, also no fluorescence was visible.

2.2.2.7

REFRACTIVE INDEX INCREMENT

In all experiments except the PF experiment the value of 0.166ml/g for dn/dc of DNA in BPES (Krasna, 1970) was used, which does not change significantly with temperature. For the PF experiments dn/dc was determined at different values of r using CT-DNA, dialysed to equilibrium for more than 48h in BPES, with added PF. The experiments were performed on a Brice-Phoenix differential refractometer (Phoenix Precision Instrument Co., 3808-05 North 5th St., Philadelphia 40, P a., U.S.A.) which has been described by Brice & Halwer (1951), calibrated with NaCl solutions as described in the manual. This gave a value of the calibration constant, K, of 0.9210×10^{-3}, where $\Delta n = K \Delta d$; Δn is the difference in refractive index between a solution and its solvent, and Δd is the total slit image displacement (solvent zero corrected) at $25 \pm 0.1^{0}C$ using unpolarised light at 546nm. The temperature was controlled by a Haake thermostatic pump. Dye binding and DNA concentrations were determined by spectrophotometric analyses as described in Section 2.2.4.3. A range of four DNA concentrations (90-600µg/ml approx.) was used to determine dn/dc at r . 0, 0.098 and 0.102, while at intermediate

values of r, single concentrations of DNA were used. This is shown in Fig. 2.11. In BPES alone (r = 0) a value of 0.1653ml/g was found, in good agreement with the value of Krasna (1970), which was used previously.

2.2.3

ANALYTICAL ULTRACENTRIFUGATION

All experiments were performed using a Beckman Spinco Model E analytical ultracentrifuge equipped with RTIC temperature control unit, photographic u.v. optics, and a single cell An-D rotor with 12mm, single sector cells. Negatives were analysed with a Beckman Analytrol or, in some cases, a Joyce-Loebl microdensitometer. In boundary sedimentation experiments, the boundary was taken as the 50% concentration point.

2.3.3.1

BAND CENTRIFUGATION

This was performed before and after light scattering experiments, and at other times to check for breakdown or contaminating material with a Kel-F band-forming centrepiece at 20 ± 0.05°C using the RTIC temperature control system, at 39460 r.p.m., taking 8 min photographs. The cell was usually loaded with as much material as conveniently possible (up to 35ul of solution) in order to increase sensitivity to contaminants. It was not usually necessary to process these photographs in the Analytrol as visual inspection seemed as sensitive, or more so. Typical analytrol traces of RFI and RFI and II are shown in Fig. 2.9.

2.2.3.2

PROFLAVINE AND ETHIDIUM BROMIDE TITRATIONS

These were performed using boundary sedimentation with Kel-F centrepieces at 25 ± 0.3°C, at 35,600 r.p.m., taking 8 min photographs and following the methodology of Waring (1970). The temperature control system was switched to indicate after reaching speed to avoid convectional disturbances (Studier, 1965) and thereafter during a run the temperature stayed almost constant. The rotor was heated to approx. 25°C in a cool oven and allowed to reach temperature in the vacuum chamber, before starting a run. In the EB experiment a mixture of 3:1 = RFI:RFII in BPES was used, and in the PF experiment

100% RFI. For the RFII sedimentation coefficients around the minimum in the ED titration, 100% RFII was used. The procedure was briefly as follows. Measurement of r (moles dye bound/moles nucleotide) were made as in Section 2.2.4.2. Two cells were loaded with 0.6ml DNA solution adjusted to an absorbance of 0.600 at 260nm and were used alternately. The cells were weighed and one run, while 5µl of an ED solution at 32.7µg/ml or PF solution at 44.9µg/ml in BPES was added to the other with a 10ul Hamilton syringe. The addition was checked by weighing and this cell then run, then reweighed to check for loss of material. The two cells were then used alternately, adding an additional 10ul of dye solution each run and checking for evaporation and drug addition errors by weighing. As found by Waring (1970) up to 6 runs/cell could easily be accomplished with a cumulative error of less than 2%. On each new addition of dye the cell contents were mixed thoroughly and allowed to equilibrate for at least 45 min at room temperature. The sedimentation coefficients obtained were not corrected for buoyancy, to 20^{o}C or extrapolated to zero DNA concentration as they are all internally consistent.

2.2.4

SPECTROPHOTOMETRY

All measurements were made in a Cary 15 spectrophotom eter (Cary Instruments, 2724 South Peck Road., Monrovia, California 91016, U.S.A.) at room temperature unless otherwise specified.

2.2.4.1

DNA CONCENTRATIONS

DNA solutions were scanned in 1cm pathlength micro-cells or 0.2cm pathlength cells from 300 - 230nm. The spectra of a large number of different ø X174-RF DNA solutions were analysed according to the method of Hirschman & Felsenfeld (1966) and Felsenfeld (1968) for native DNA spectra. This gives the concentration and percentage A-T content from a spectrum. Thus an extinction coefficient was obtained using only spectra which correctly predicted the A-T content of ø X174-RF DNA; the range accepted was 58% ± 1.5% (Hayashi et al., 1963). For ø X174-RFI DNA this gave a molar phosphorus

extinction coefficient, $\varepsilon(P)$ at 260nm of 6415 ± 44 (S.D. of 10), which, using a monomer equivalent weight of 331 for NaDNA gives $E^{1\%}_{1cm}$ of 193 ± 1.3. For RFII, this gave $\varepsilon(P)$ of 6425 ± 40 (S.D. of 21), $E^{1\%}_{1cm}$ = 194.1 ± 1.2. Thus, as would be expected, there is no detectable difference in the u.v. spectra of RFI and II. The value of $\varepsilon(P)$ = 6422 ± 42 (S.D. of 31) was used in all concentration measurements.

2.2.4.2

DYE BINDING MEASUREMENTS FOR ULTRACENTRIFUGE EXPERIMENT

Measurements of binding were made using the formulation of Peacocke & Skerret (1956) and following the method of Waring (1965,1970). For EB, measurements were made on three solutions at 470nm in 5cm pathlength cells in a water jacket, thermostated to 25°C ± 0.1°C: (a) BPES, (b) CT DNA at a concentration 500µg/ml in BPES, (c) ϕ X174-RF DNA, I:II = 3:1, E_{260} = 0.600 in BPES. The EB solution at 32.7µg/ml was added in the same proportions as the EB added to the bulk solution in the sedimentation experiment. Thus cell (c) mimics conditions in the sedimentation cell, cell (b) gives the absorbance if all the dye is bound, and cell (a) gives the absorbances if all the dye is free. The absorbances are plotted out as absorbance against dye added and the best line drawn through the points by eye (Fig. 2.10). The dye bound to ϕ X174 DNA is then calculated as follows. Let the total molar nucleotide concentration of DNA = Tn, that of EB = Te, the absorbances when all the EB is free and bound be Df and Db respectively. Then when $[EB] = 0$, $Te = rTn$; so $[EB] + rTn = Te$ and $D = ([EB]/Te)Df + (r.Tn/Te).Db$ where D is the absorbance of the whole solution. Therefore $a = r.Tn/Te$

$$= (Df - D)/(Df - Db)$$

where a is the fraction of EB bound. Thus r can be obtained for each dye concentration. The procedure was virtually the same for PF with the following changes: appropriately 100% RFI was used in cell (c) and the PF solution added was 44.9µg/ml as in the sedimentation experiment; in addition, light at 440nm and 1cm pathlength cells were used.

2.2.4.3

PROFLAVINE BINDING AND DNA CONCENTRATIONS IN DIFFERENTIAL REFRACTOMETRY AND LIGHT SCATTERING

PF binding to DNA was investigated by spectral examination of CT DNA, PF and CT DNA plus PF in the visible using a modification and extension of the method of Peacocke & Skerret (1956) and in the u.v. in BPES at room temperature (20 - 23°C) in 1cm pathlength cells, except where otherwise specified. Previous binding experiments indicated no change in experiments conducted in this manner from those under strict temperature control at 25°C. The usual procedure was to set up cuvettes with 2.4ml of solution and add 20 - 50µl aliquots of stock PF solution, about 45µg/ml, or BPES as required. The cuvettes were then sealed with parafilm, mixed by several inversions and allowed to equilibrate for 5min. In fact, binding seemed to occur very rapidly and the first spectrum it was possible to obtain never altered after up to 2h equilibration. In all these experiments, PF concentrations were found using the well established value of $\epsilon = 4.1 \times 10^4$ for the free dye at the maximum at 443 - 444nm (Haugen & Melhuish, 1964; Gersch & Jordan, 1965; Blake & Peacocke, 1967; Cohen & Eisenberg, 1969). Spectra of free and bound PF (i.e. in a solution of DNA, 1.8×10^{-3} mole nucleotides/l approx.) from 480nm to 400 nm were run first at PF concentrations from 1.34µM to 17.1µM; a DNA blank was used for the bound PF and some measurements at lower concentrations were made in 5cm pathlength cells.

In these experiments and all later ones an isobestic point was observed at 454 ± 0.3nm, as noted first by Peacocke & Skerret (1956). The absorbances at 454nm were plotted against those at 440nm and 460nm of bound and free dye (Fig. 2.12) and the best straight line found by the least squares method. All four sets of points were extremely good straight lines with linear regression coefficients above 0.998, and the ratios $\frac{E(440)}{E(454)}$ and $\frac{E(460)}{E(454)}$ for bound and free dye found from the gradients. E(444) against E(454) was also plotted for the free dye from the gradient of which $\epsilon(454) = 3.399 \times 10^4$ was calculated from $\epsilon(444)$ 4.1×10^4. Results of these analyses are included in Table 2.1. From one visible spectrum of DNA + PF it was then

possible to obtain the total PF concn. and the absorbances of totally bound and free dye of the same concentration at 440 and 460nm, from the absorbance at 454nm. This, together with the actual absorbances at 440 and 460nm allows the use of the method described in Section 2.2.2.4 to determine the amount of dye bound from readings at 440 and 460nm. Peacocke & Skerret (1956) found that the specific absorbance of bound PF at 460nm varied with r, the moles of dye bound/nucleotide pair. As witnessed by the linearity of the absorbance value plots (Fig. 2.12), this has not been observed; neither do binding results calculated from absorbances at 460nm in later experiments differ in a significant manner from results from 440nm, although the error of the former is somewhat larger. However, Peacocke & Skerret were working to a large extent at values of r above those in this investigation, and this may account for the discrepancy.

Further spectra from 480 to 400nm and 300 to 220nm were run for PF alone, in the presence of moderate DNA concentrations (1×10^{-4} and 1.3×10^{-4} mole nucleotides/l approx.) and the same DNA solutions without dye. A further isobestic point at 225.5nm was found, as reported by Cohen & Eisenberg (1969). Plotting E(225.5) against E(444) for free dye (Fig. 2.13) gave a straight line and ϵ(225.5) of 1.312×10^{4} for PF. Thus for any DNA + PF solution within certain limits, the absorbances at 480, 454, 440 and 225.5nm lead to accurate values of bound dye, DNA concentration and hence r. The value of ϵ(225.5) for the CT DNA used in all these experiments and in differential refractometry was 3101 (ϵ(260) = 6541). DNA concentrations and r values in the refractive index increment experiments were determined this way.

However, in the light scattering experiments a u.v. absorbing contaminant in the membrane filters, which has been previously noted (Dawson & Harpst, 1971) makes readings in the far u.v. at 225.5nm unreliable despite thorough prerinsing of the filters. However, at least as far as 240nm, readings are always completely unaffected, if prerinsing is thorough, and for light scattering samples concentrations were determined by E(260). It was, therefore, necessary to determine ϵ(260) of bound and free PF, from the

previous results. For the free dye, absorbances at 444 and 260nm were plotted as usual, giving $\varepsilon(260) = 5.593 \times 10^4$. For bound dye, the concentration of this, Cb, was found from the visible spectra; then from

$$(Df - D) = Cb(\varepsilon f - \varepsilon b)$$

where Df is the absorbance if all the dye is free, D is the absorbance of bound and free dye (DNA absorbance subtracted) and εf and εb are the free and bound dye extinction coefficients respectively, a plot of (Df - D) against Cb should give a straight line, gradient $(\varepsilon f - \varepsilon b)$. This is the case (Fig. 2.13) and $\varepsilon b = 3.143 \times 10^4$ at 260nm. Thus knowing the concentration of bound and free dye from the visible spectrum and the extinction coefficient at 260nm an absorbance at 260nm is obtained for the DNA, which is readily convertible to concentration.

It was desirable to check the accuracy of these two methods of DNA concentration measurement and this was done by examining five solution of CT DNA (1.01×10^{-4} mole nucleotides/l) at different total PF concentrations (3 - 12μM). By both methods, the known DNA concentration was refound to within 0.5%.

A table of extinction coefficients etc. is given in Table 2.1.

2.2.5

COMPUTATION OF RESULTS

Light scattering Zimm and Berry plot results, sedimentation coefficients, Felsenfeld-Hirschman and PF binding spectral analyses, and theoretical P(θ) calculations were all computed on a PDP-8/L computer using specially written programmes.

Table 2.1

EXTINCTION COEFFICIENTS FOR FREE AND BOUND PF AT VARIOUS WAVELENGTHS

These are the results of the spectral ratios plotted in Figs. 2.12 and 2.13; the y axis and x axis are those in these diagrams, the numbers in these columns indicate the wavelength of light in nm, the absorbances at which are plotted on that particular axis and b and f indicate bound and free PF respectively. The final column gives the calculated molar extinction coefficients at the wavelength and conditions defined in the y axis column.

The bottom line refers to the plot in Fig.2.13 to determine the extinction coefficient of bound PF at 260nm (given in the final column); Df, D and Cb are explained in the legend to Fig.2.13, and in section 2.2.4.3.

Table 2.1

y axis	x axis	Figure	gradient	regression coefficient	$\epsilon \times 10^{-4}$	
454	444f	2.12	0.8287	0.9984	3.398	
440f	454	2.12	1.1947	0.9984	4.060	
460f	454	2.12	0.7668	0.9988	2.606	
440b	454	2.12	0.7129	0.9980	2.422	
460b	454	2.12	1.0401	0.9983	3.534	
225.5	444f	2.13	0.3201	0.9999	1.312	
260f	444f	2.13	1.3641	1.0000	5.593	
(Df-D) x 100	Cb(μM)	2.13	2.4450	0.9991	3.143	(bound, at 260nm)

Fig.2.1

CALIBRATION CURVES FOR ASSAYING THE PRESCENCE OF PI IN DNA SOLUTIONS BY FLUORESCENCE

The solvent is BPES and the curves were constructed from experiments done at room temperature. The DNA used in this was: A, calf thymus; B, 3:2 approx. mixture of RFI:RFII. In B the fluorescence is apparent, and due to light scattering probably. The assay was performed in 1cm cells using an Aminco-Bowman single beam spectrofluorimeter (American Instrument Co. Inc., Silver Springs, Maryland, U.S.A.).

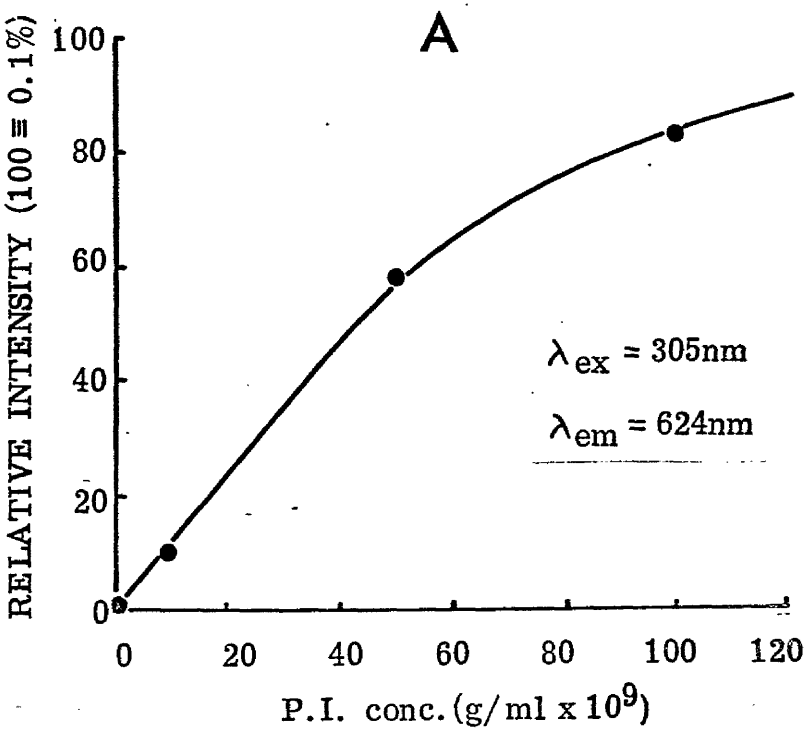

Fluorescence of Propidium Iodide in presence of excess DNA (40 μg/ml), using DNA blank.

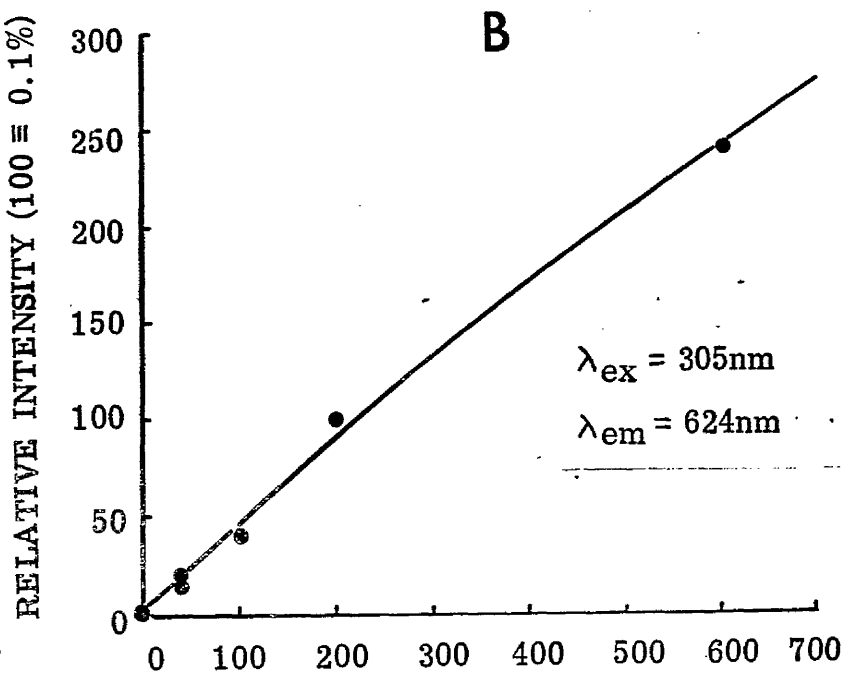

Fluorescence of native DNA

Fig.2.2

REFRACTIVE INDEX CORRECTION CURVE FROM PURE LIQUID SCATTERING

R_{lit} is the literature value of the Rayleigh ratio, R_{exp} the value calculated from the instrument readings using the makers' calibration with benzene and ignoring refractive index corrections. The ratio of the two values should then represent the correction to be applied at a certain value of the refractive index, n. The plot is not a straight line indicating deviation from the suggested "n^2" correction.

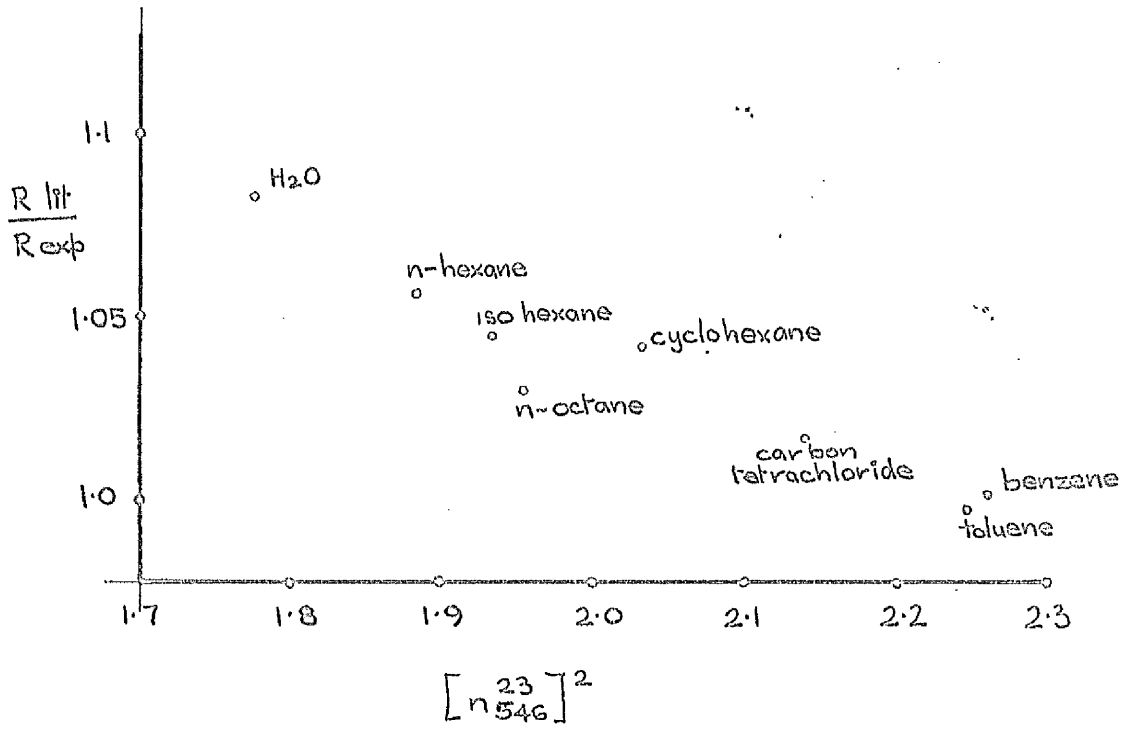
1·1
1·05
1·0
R lit / R exp
H2O
n-hexane
iso hexane
cyclohexane
n-octane
carbon tetrachloride
benzene
toluene
1·7
1·8
1·9
2·0
2·1
2·2
2·3
$[n_{546}^{23}]^2$

Fig.2.3

CONICAL LIGHT SCATTERING CELL

This cell is the type used in all the exprimental work described herein; all calibration detail apply to this cell. The cell material was glass, refractive index at the sodium D line, 1.5084 (material E.SC.3791, Barr & Stroud Ltd., Glasgow).

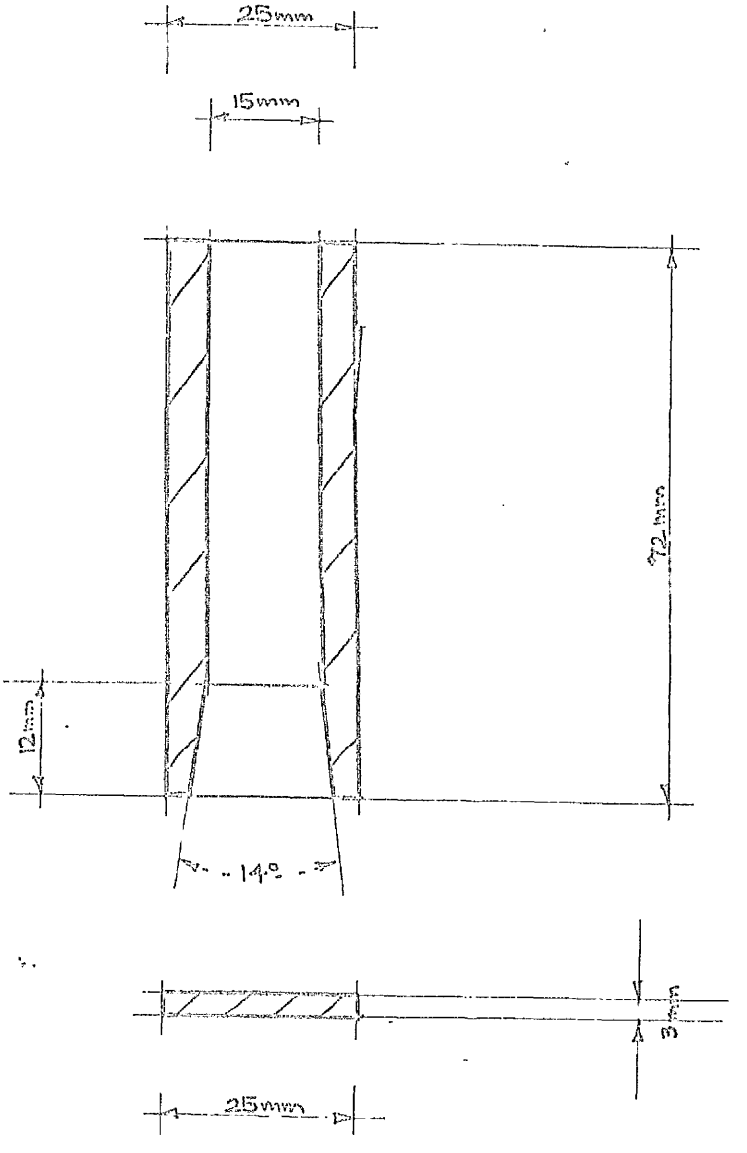
25mm
15mm
72 mm
12mm
14°
3mm
25mm

Fig.2.4

PLOTS TO DETERMINE THE LIGHT SCATTERING CALIBRATION CONSTANT ACCORDING TO THE METHOD OF GORING ET AL. (1957)

These experiments were carried out using Ludox colloidal silica. Here R90 is the Rayleigh ratio calculated from spectrophotometric data, S90 is the instrument reading for Ludox scattering and c is the concentration determined by evaporation to dryness and weighing. The calibration constant, $C = (c/S90)_{c=o}/(c/R90)_{c=o}$ is the ratio of the intercepts of these two plots; this was found by drawing the best straight lines by the least squares method. This method is used to allow for interference from attenuation of incident and scattered light, secondary scattering and intermolecular interaction.

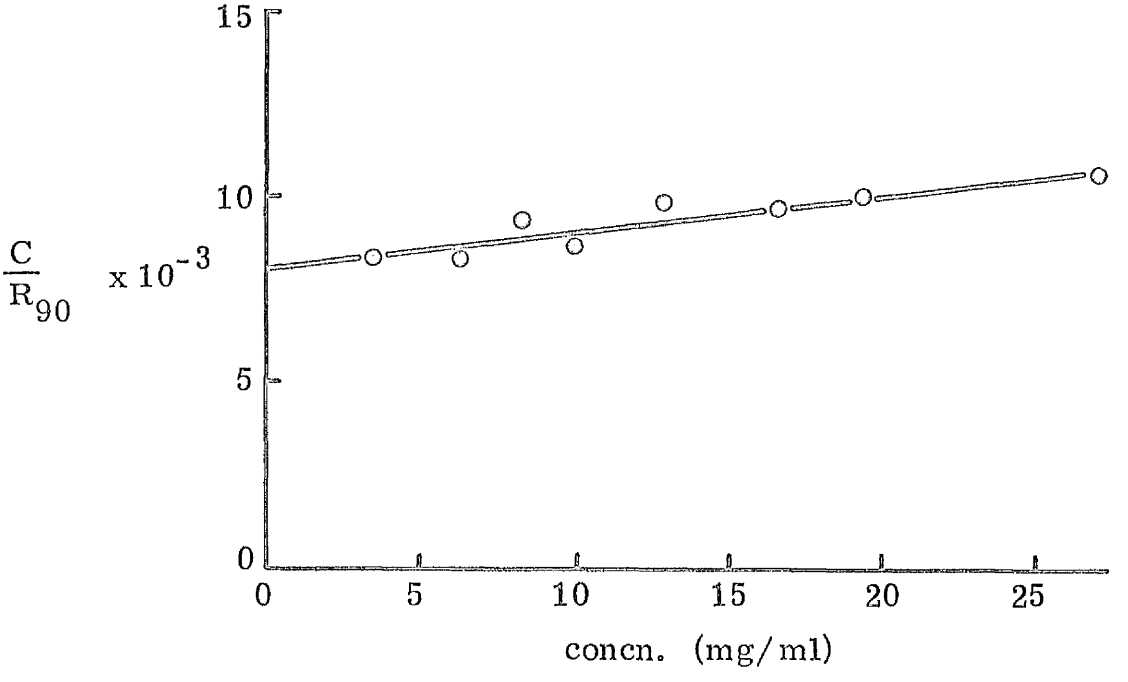
15
10
5
0
C/R90 x 10-3
0
5
10
15
20
25
concn. (mg/ml)

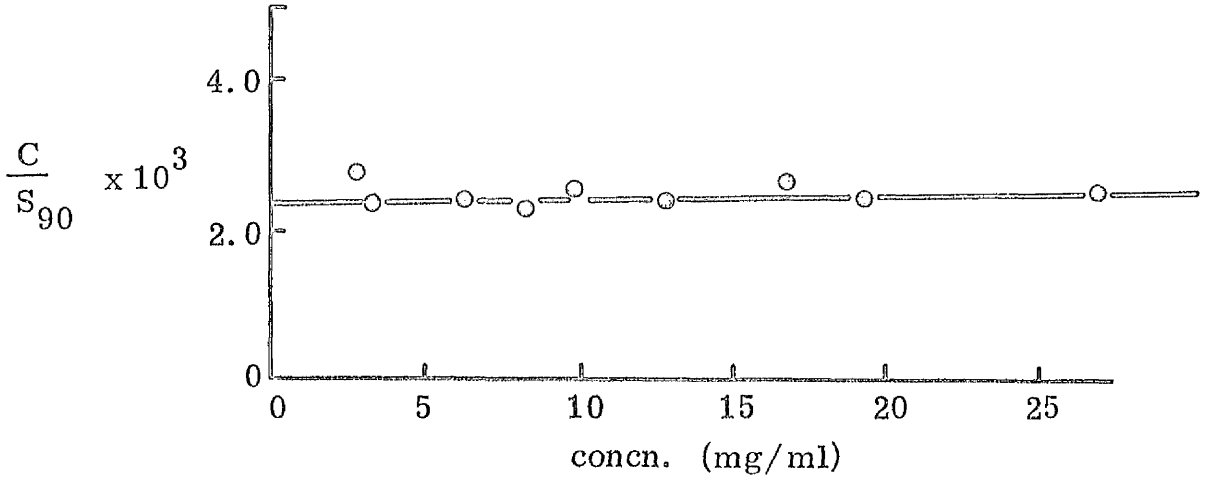
4.0
2.0
0
C/S90 x 10^3
0
5
10
15
20
25
concn. (mg/ml)

Fig.2.5

PLOT TO DETERMINE THE LIGHT SCATTERING CALIBRATION CONSTANT ACCORDING TO THE METHOD OF MARON & LOU (1954)

These experiments were carried out using Ludox colloidal silica. Here R90 is the Rayleigh ratio calculated from spectrphotometric data, I90 is the instrument reading for the Ludox scattering. The best straight line was drawn through the points by the least squares method giving the plot the form $\log(R90/I90) = k_1 + k_2 R90$; then if k_1 is small as is the case here, $k_2 = C$, the calibration constant. This method is used to allow for secondary scattering and attenuation of the incident and scattered light.

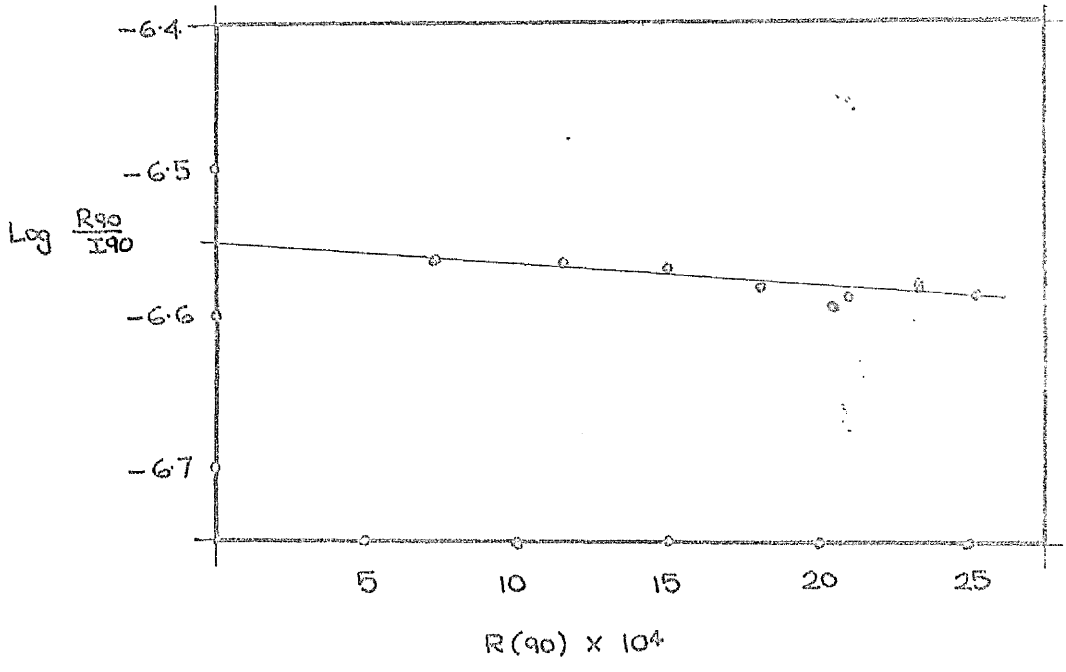

Maron + Lou calibration
glass standard = 47.

Fig.2.6

CORRECTION CURVE FOR THE SCATTERING VOLUME SEEN AT DIFFERENT ANGLES, CONSTRUCTED BY A FLUORESCENCE METHOD

$S\theta$ is the normalisation factor for light scattering at angle θ described in section 2.2.2.2 and $= i(90)/i(\theta)\sin\theta$ where $i(\theta)$ is the instrument reading for the fluorescent intensity at angle θ.

FLUORESCENT CORRECTION CURVE

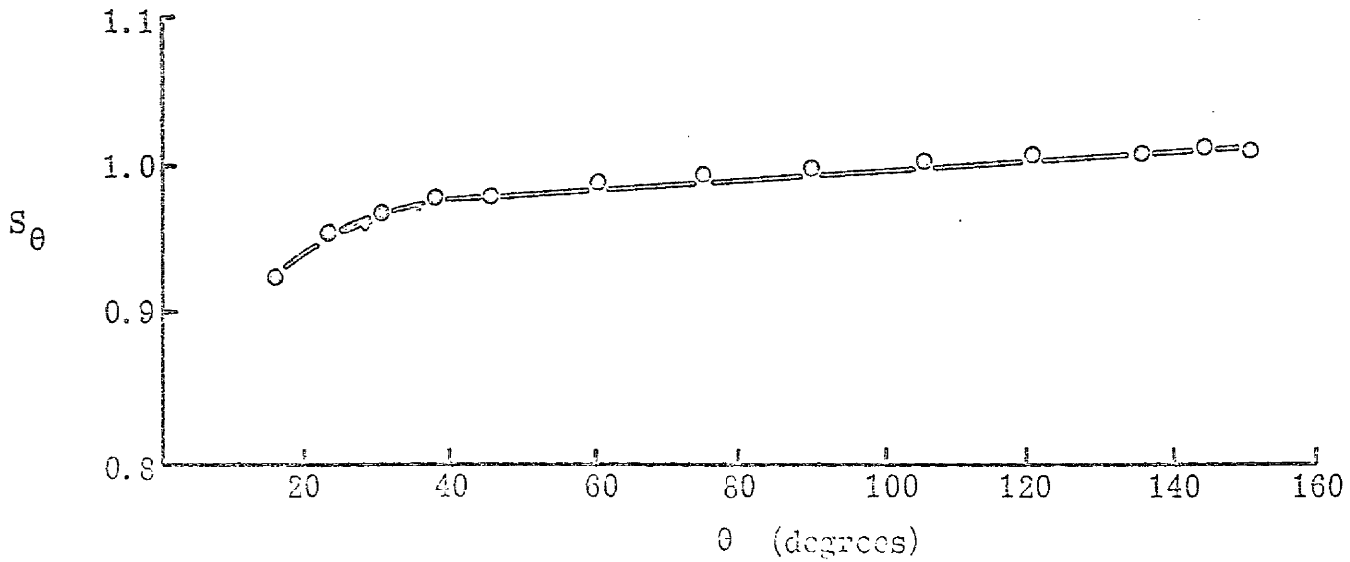

Fig.2.7

VOLUME OF 1g OF WATER AS A FUNCTION OF TEMPERATURE

The data is from the International Critical Tables (1926b). This plot was used to allow for the expansion of solutions in concentration measurements in the temperature experiment (section 2.2.2.5).

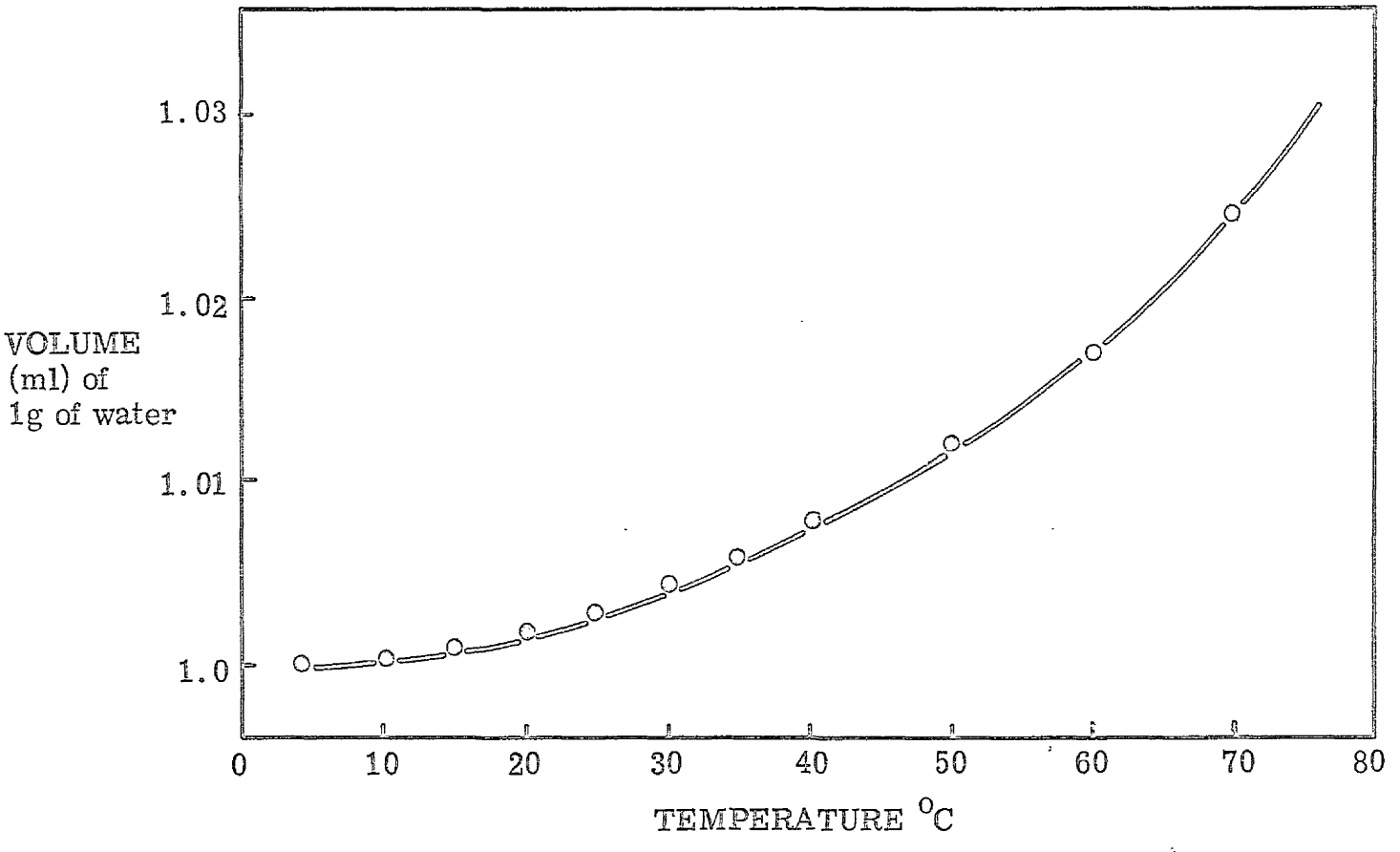
1.03
1.02
1.01
1.0
VOLUME
(ml) of
1g of water
0
10
20
30
40
50
60
70
80
TEMPERATURE °C

Fig.2.8

CORRECTION PLOTS FOR TEMPERATURE EXPERIMENT (SECTION 2.2.2.5)

Top: refractive index of DPES at 546nm at temperature, t (n_{546}^{t}) as a function of temperature.

Bottom: deviation of the temperature of the scattering cell contents from that of the benzene bath (Δt) in the light scattering instrument when room temperature was $23^{o}C$.

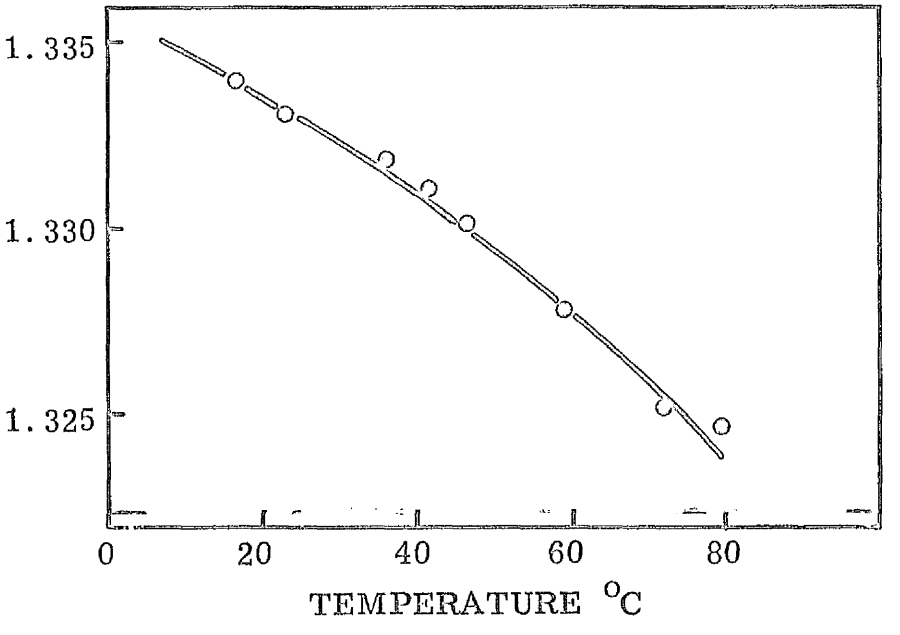
1.335
1.330
1.325
n_{546}^{t}
0
20
40
60
80
TEMPERATURE °C

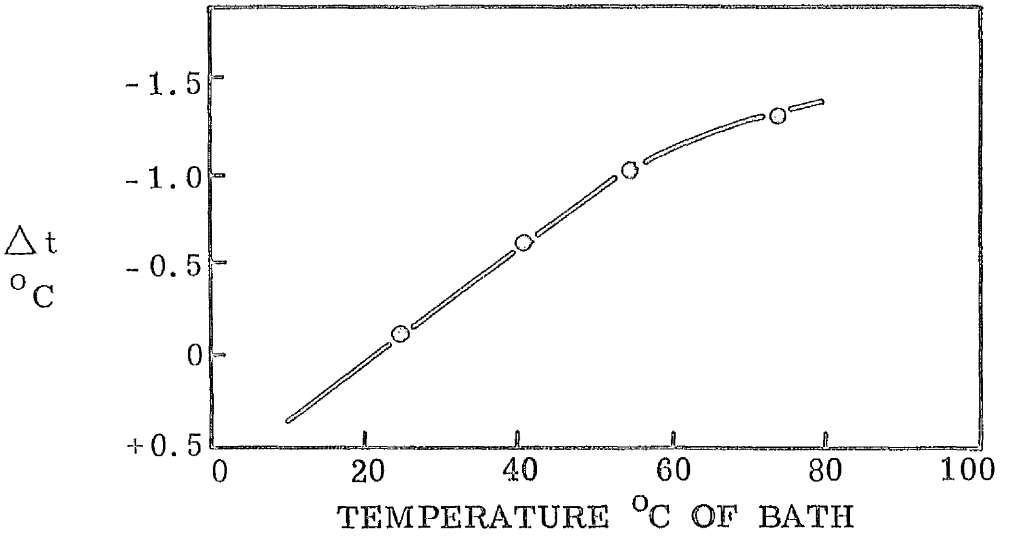
-1.5
-1.0
-0.5
0
+0.5
Δt °C
0
20
40
60
80
100
TEMPERATURE °C OF BATH

Fig.2.9

ANALYTROL TRACES OF ϕX174-RF DNA FROM U.V. PHOTOGRAPHS OF BAND SEDIMENTATION RUNS

Runs were under the conditions given in section 2.3.3.1. The top of the centrifuge cell is at the bottom of the diagram page.

A: a mixture of approx 7:3 RFI:RFII; pictures taken after 24 min approx.

B: RFI alone; picture taken after about 16 min.

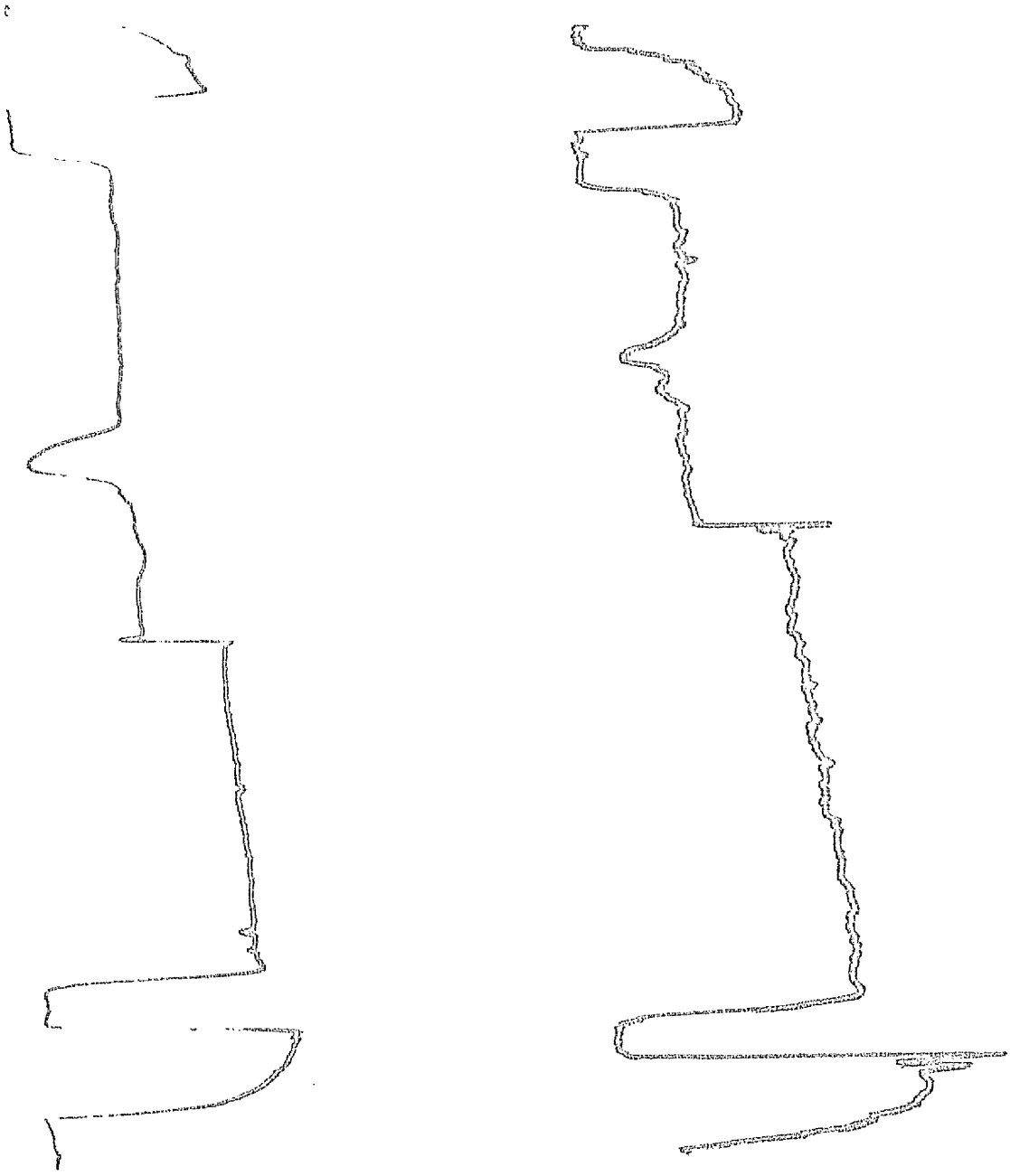

A

B

Fig.2.10

SPECTROPHOTOMETRIC RESULTS FOR EB BINDING TO ϕX174-RF DNA.

These are results of experiments described in section 3.2.4.2. The ordinate represents the increases in absorbance as small aliquots of EB solution were added to each cell: (a) EPES; (b) CT DNA at 500μg/ml in EPES; (c) ϕX174-RF DNA, I:II = 3:1, E_{260} = 0.6, in EPES. The lines are slightly curved rather than straight and the smoothest curve through them was drawn by eye.

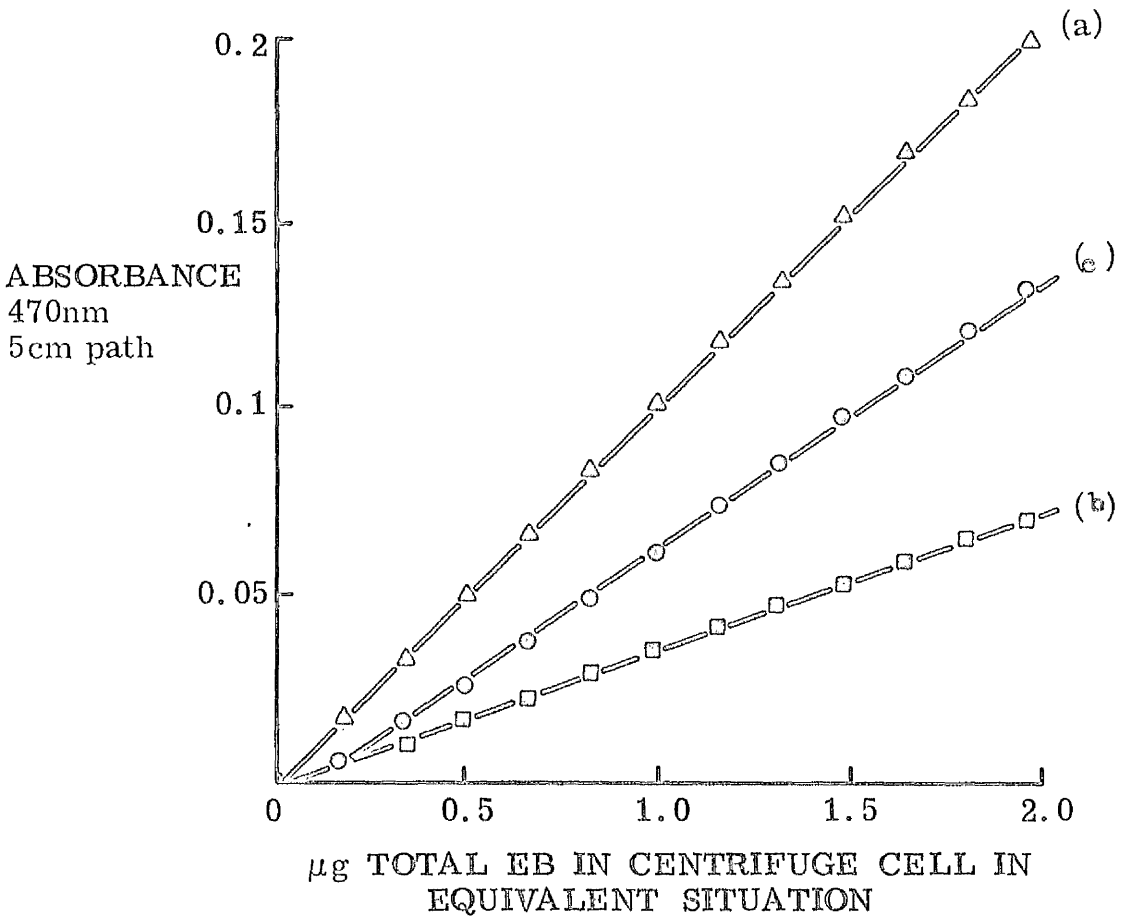
0.2
0.15
0.1
0.05
ABSORBANCE
470nm
5cm path
(a)
(c)
(b)
0
0.5
1.0
1.5
2.0
μg TOTAL EB IN CENTRIFUGE CELL IN EQUIVALENT SITUATION

Fig.2.11

REFRACTIVE INDEX INCREMENT OF DNA AT VARIOUS VALUES OF BOUND DRUG, PF

$(\frac{dn}{dc})_{\mu}$ is the refractive index increment at constant chemical potential, μ; the DNA used was CT. o, dn/dc from one concentration of DNA; o, dn/dc from a range of 4-5 concentrations of DNA. The line is a weighted fit of the points (o:o = 4:1) to a straight line by the least squares method. The dn/dc at various values of bound dye were read off this plot for use in light scattering experiments.

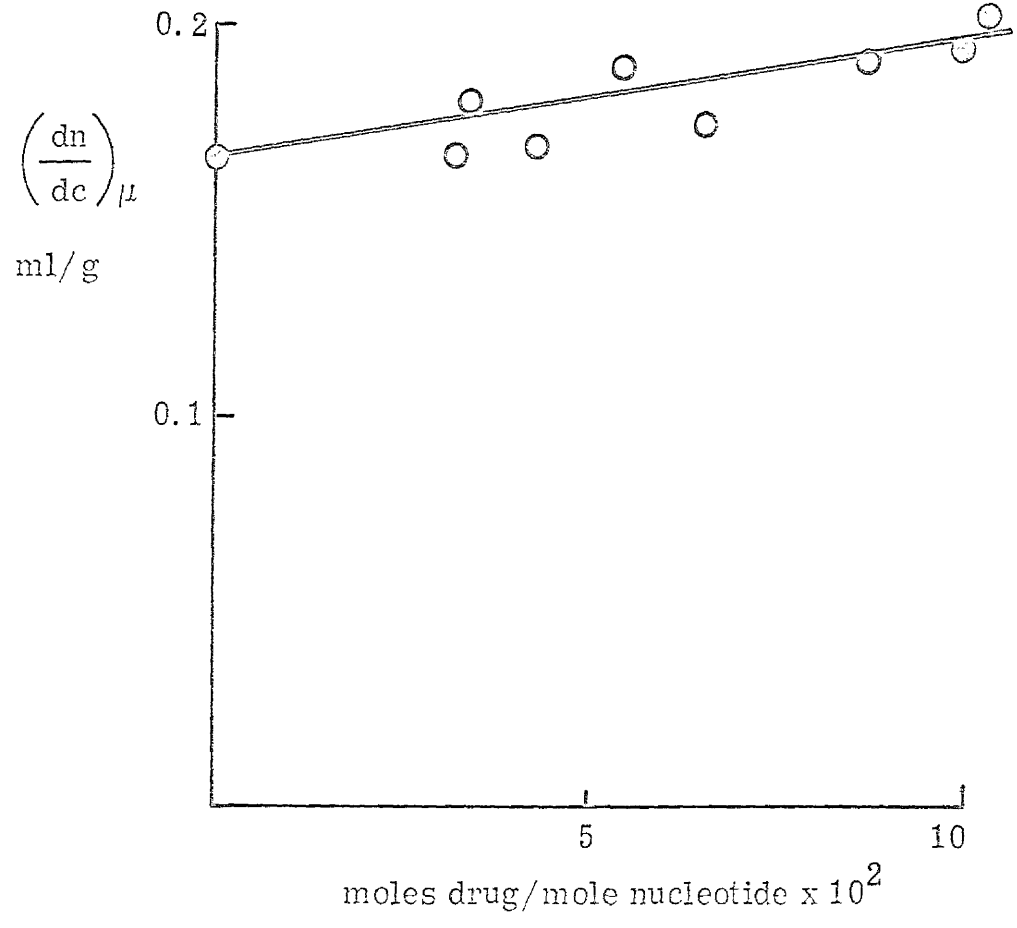
0.2
0.1
$\left(\frac{dn}{dc}\right)_{\mu}$
ml/g
5
10
moles drug/mole nucleotide x 10^2

Fig.2.12

PROFLAVINE VISIBLE SPECTRAL RATIOS

Absorbances of bound (b) and free (f) PF at the different wavelengths of light in nm indicated, for different PF concentrations; thus E444f is the absorbance of the free dye at 444nm. 454nm is the isobestic point where the absorbances of the free and bound dye is the same. Lines are the best straight lines by the least squares method. The relative extinction coefficients etc. calculated from these plots are given in Table 2.1. The circled points are from 5cm pathlength cells.

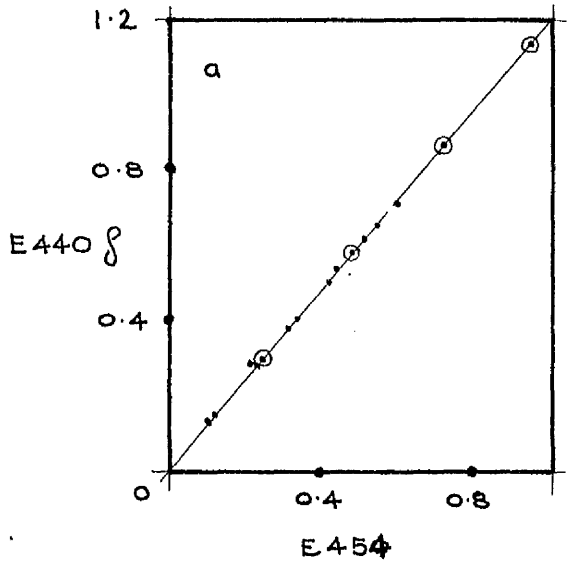
a
1·2
0·8
E440 δ
0·4
0
0·4
0·8
E454

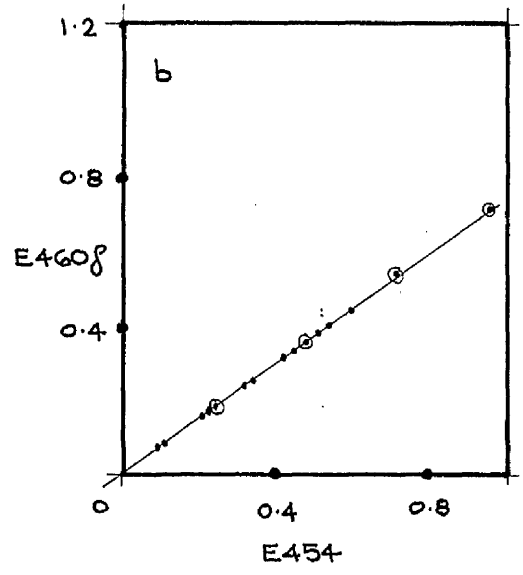
b
1·2
0·8
E460δ
0·4
0
0·4
0·8
E454

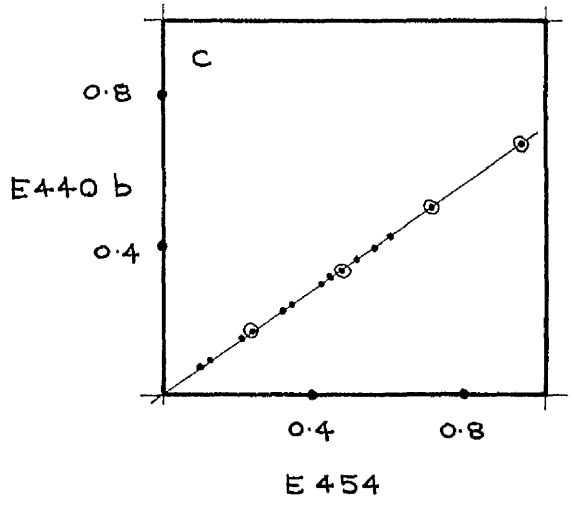
c
0·8
E440 b
0·4
0·4
0·8
E454

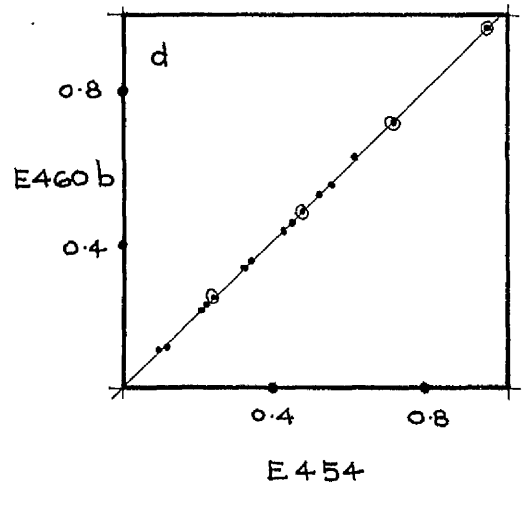
d
0·8
E460b
0·4
0·4
0·8
E454

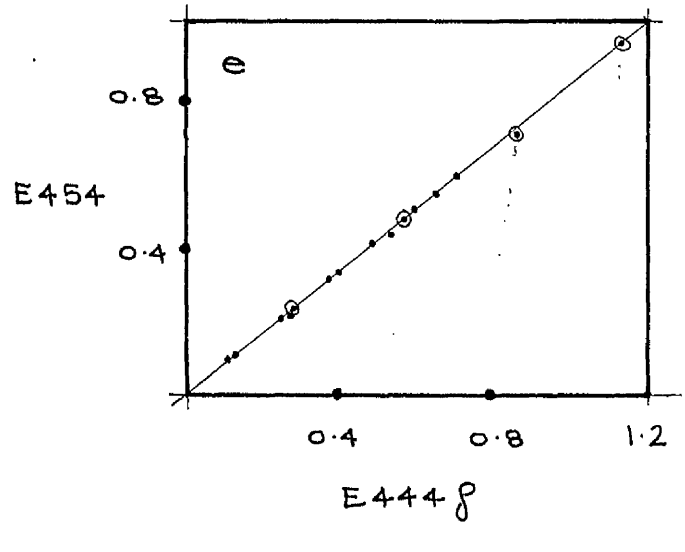
e
0·8
E454
0·4
0·4
0·8
1·2
E444 δ

Fig.2.13

PROFLAVINE U.V. & VISIBLE SPECTRAL RATIOS ·

Absorbances of bound (b) and free (f) PF at different concentrations at the different wavelengths of light in nm indicated; 225.5 is an isobestic point where the absorbance (after subtraction of DNA absorbance) is the same for free and bound dye.. In the third diagram Df is the absorbance when all the dye is free, D is the absorbance of a mixture bound and free dye (DNA absorbance subtracted)„ bothat 260nm„ and Cb is the concentration of bound dye. This leads to an extinction coefficient for bound PF at 260nm as explained in section 2.2.4.3. The extinction coefficients etc. calculated from these plots are shown in Table 2.1.

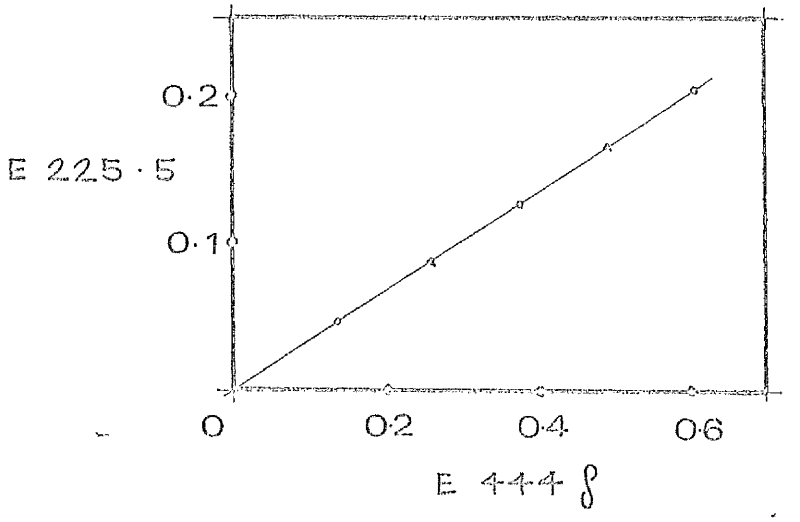
0·2
E 225·5
0·1
0
0·2
0·4
0·6
E 444 f

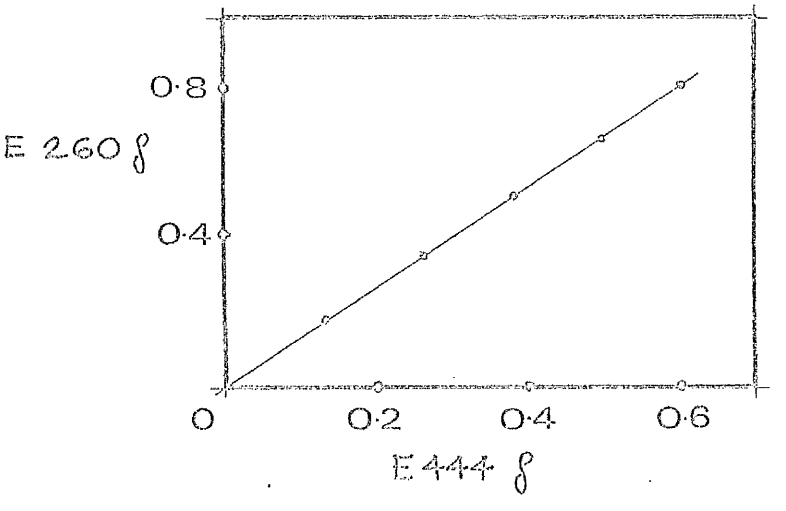
0·8
E 260 f
0·4
0
0·2
0·4
0·6
E444 f

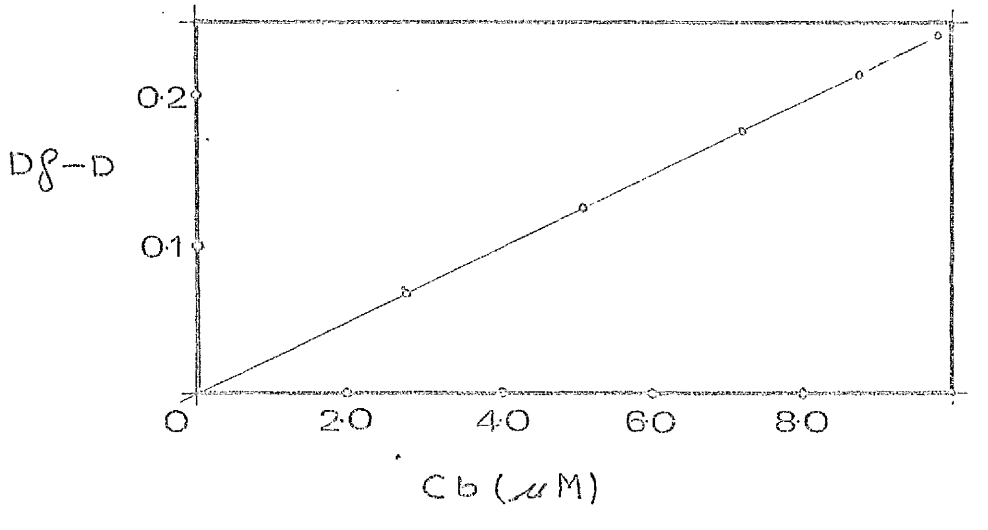
0·2
Df−D
0·1
0
2·0
4·0
6·0
8·0
Cb (μM)

3. [illegible]

3

RESULTS

3.1

SUPERCOILED ϕ X174-RF DNA

3.1.1

NUMBER OF SUPERHELICAL TURNS, EB TITRATION

The changes in sedimentation coefficient with bound EB of RFI and II are shown in Fig. 3.1. The critical value r (= r_c) (moles dye bound/moles nucleotide), where I and II have apparently equivalent conformations and the number of superhelical turns (τ) is zero, was 0.037 ± 0.005. The sedimentation coefficients are not corrected to standard conditions for viscosity, temperature or buoyancy, nor extrapolated to zero concentration as the results are internally consistent. From eqn. (6) in Section 1 this gives τ = -11.8 ± 1.6 corresponding to a superhelix density (σ) of -0.025 ± 0.003, using values for the equation parameters as follows: $\theta_1 = \theta_0$; the unwinding angle for EB, ϕ, 12° (Fuller & Waring, 1964); β_0 = 484; this last value (one tenth the number of base pairs) was calculated from a mol. wt. of 3.2×10^6 (see Sections 3.1, 3.2) and monomer equivalent weight per nucleotide of 331 for Na^+ DNA. The error is the estimation of the exact minimum of the curve and the value of τ agrees with that found by Waring (1970) of 13.3 ± 2.7 for ϕ X174-RFI DNA under somewhat different conditions.

On comparison of the curve for RFI with the schematic curve summarising the results of Upholt et al. (1971) (Fig. 1.3) it is apparent that there is good correspondence. Fig. 3.1 starts at σ = -0.025 (r = 0), equivalent to region II in Fig. 1.3, and the sedimentation coefficient increases to a local maximum at σ = -0.017 (r = 0.012 moles dye/moles nucleotide) before decreasing rapidly to σ = 0, (r = 0.037) in what corresponds to region III in Fig. 1.3.

3.1.2

CONFORMATION OF ϕ X174-RFI DNA AT 25°C

3.1.2.1

EXPERIMENTAL

Three separate light scattering experiments were performed on different DNA

samples in BPES, pH 6.8, ionic strength 0.2 at $25^{o} \pm 0.2^{o}C$. The results were plotted by the method of Zimm (1948) to extrapolate to zero concentration and scattering angle, as shown in Fig. 3.2; information was extracted as described in the legend. No optical anisotropy was detectable by measuring the polarisation of the scattered beam at 90^{o}, even without extrapolation to zero concentration

The mean mol. wt. was $3.17 \pm 0.19 \times 10^{6}$, the mean root-mean-square (r.m.s.) radius (Rg) was 103.5 ± 12nm (error from the least good initial slopes) and the mean second virial coefficient (B) was $-2.6 \pm 2 \times 10^{-4}$ mole cm^{3}/g^{2}. The molecular weight is discussed later, with results from later experiments. The r.m.s. radius was perhaps somewhat larger than expected in view of the value of 109.4nm found for relaxed circular DNA (see Section 3.2) implying that the molecule is not all that compact despite the superturns; in fact the rigidity presumably imparted to the molecule by the superturns may account for Rg not being smaller. There have been no previous light scattering investigations of supercoiled DNA with which to compare these experiments, nor any theoretical predictions of the r.m.s. radius or P(θ) function; as discussed in Section 1.3.3.2, theoretical calculations of the sedimentation coefficient have been attempted (Fukatsu & Kurata, 1966; Bloomfield, 1966; Gray, 1967). Wang (1969a) found the calculations of Fukatsu & Kurata and Bloomfield inappropriate. A treatment predicting the P(θ) values for ϕ X174-RFI based on the method of Gray (1967) is presented below.

The small negative value of B is a measure of deviation from ideality and theta conditions (Flory, 1953), when B = 0. In fact, the error in B could make B almost zero; however, in view of the repeatability of the negative value in these and later experiments, this is thought tentatively to be real.

3.1.2.2

THEORETICAL MODELS

In Fig. 1.3 are shown some suggested structures of supercoiled DNA in solution: (a) the straight interwound model; (b) the toroidal model; (c) branched

interwound model (Y-shape). Other branched structures such as H-shapes may be possible at high superhelix density. To try and determine which, if any, of these exist in solution, theoretical curves of $P\theta^{-1}$ against $\sin^2(\theta/2)$ have been calculated.

The particle scattering factor, $P\theta$ was calculated in all cases from the equation

$$P\theta = \frac{1}{N^2} \sum_{n}^{N} \sum_{m}^{N} \frac{\sin hr_{nm}}{hr_{nm}} \qquad (7)$$

where N is total number of scattering points in the molecule, h is $4 \sin(\theta/2)/\lambda'$, r_{nm} is the absolute value of the vector between scattering points n and m (Goiduschek & Holtzer, 1953) and λ' is the wavelength of light in solution. Our approach was to calculate the dimensions of these models from the molecular weight and root-mean-square radius. $P\theta^{-1}$ was then calculated for each model and compared with the experimental values.

The problem is to formulate r_{nm} by some general expression for all n,m. Each r_{nm} is then evaluated numerically, substituted into the above expression and a running total kept. This can be easily done on a modern digital computer, and the calculation repeated at various designated angles.

The number of superhelical turns had to be an integer, and was taken as -12. The contour length of the molecule was taken as 1625.6nm. This was calculated from the molecular weight assuming a linear mass density of 1950 daltons/nm; i.e. the DNA duplex is assumed to be in the B form in the supercoil (Maestre & Wang, 1971; Campbell & Lochhead, 1971).

Straight Interwound Model

The $P\theta^{-1}$ curve was calculated for the model in Fig. 1.3a. The model molecule contained 12 crossovers (i.e. physical superhelical turns), and was treated as a rod of length $L = (12Rg^2)^{\frac{1}{2}}$. The equation

$$d/2 = (P/2K)^2 - 12(Rg/K)^{2\,\frac{1}{2}}/\pi \qquad (8)$$

when d is the diameter of the cylinder, K is the number of superhelical turns, Rg is the root-mean-square radius and P is the contour length, was used to calculate d.

The molecule was then imagined to be sliced into 4 x K segments with centres of mass in a straight line up the middle; each segment was of small enough dimension to be considered a point scatterer.

There are then 2(4K-1) inter-point distances which are L/4K, 2(4K-2) which are 2L/4K, 2(4K-3) which are 3L/4K, etc. The factor 2 in the expression 2(4K-1) is to allow for the fact that both the distances r_{ab} and r_{ba} must be counted. Thus the molecule was assumed to be essentially rigid, a reasonable assumption for such a small DNA molecule (Cohen & Eisenberg, 1966) and end effects were neglected. Using the above formulae d/2 = 19.35nm and L = 358.5nm. The reciprocal particle scattering function $P\theta^{-1}$ calculated from this is shown in Fig. 3.4.

The Toroidal Model

The toroidal model is shown in Fig. 1.3.b. The dimensions were related to the r.m.s. radius as follows (Tanford, 1961):

$$Rg^2 = \sum_i m_i b_i^2 / \sum_i m_i$$
$$= \sum_i b_i^2 / N \quad \text{, if all } m_i \text{ are equal,} \qquad (9)$$

where b_i is the distance of the i th mass element of mass m_i from the centre of mass, N is the number of mass elements, and Rg the r.m.s. radius. The centre of mass of the toroid is obviously the centre of the large ring of the toroid. Fig. 3.3.a shows a cross-section of the toroid, so that:

$$b_i^2 = R^2 + r^2 + 2Rr\cos(n_i) \qquad (10)$$
$$= c + m\cos(n_i) \qquad \text{where } c = R^2 + r^2$$
$$\text{and } m = 2Rr$$

$$\therefore Rg^2 = \frac{1}{N}\sum_{i=0}^{N}\left(c + m\cos\left(\frac{2\pi Ki}{N}\right)\right) \qquad (11)$$

where K is the number of superhelical turns

This summation can, conventionally, be changed to an integration, where N is large.

$$\therefore Rg^2 = \frac{1}{N}\int_0^N \left[c + m\cos\left(\frac{2\pi Ki}{N}\right)\right] di \qquad (12)$$
$$= c + \frac{m}{2K}\sin(2\pi K)$$

K is an integer

$$\therefore Rg^2 = c = R^2 + r^2 \qquad (13)$$

R and r can also be related by imagining the toroidal structure to be cut at one point and straightened out into a single superhelix of axial length $2\pi R$. Then

$$2\pi R = \left[P^2 - (2\pi Kr)^2\right]^{\frac{1}{2}} \qquad (14)$$

Hence both R and r can be obtained from Rg if P, the contour length is known.

The derivation of the interpoint distances which follows, is largely based on the treatment of Gray (1967). A more exhaustive treatment is available (Fuller, 1971), but in our case was thought to be not worthwhile, because, firstly, of the complexity of the mathematical manipulations involved and, secondly, the resolution of our method did not seem to merit it.

The problem with this model is that for each successive identical distance along the contour of the molecule the angle m in Fig. 3.3.b swept out by the large radius varies smoothly about a mean value. This can be represented graphically (Fig. 3.3.c).

Here

$$(m_s)\ \text{average} = 2\ \arcsin\ (\pi/N) \qquad (15a)$$

and generally

$$m_s = 2\ \arcsin\ \left[2\pi R/2N(R + r\cos n)\right] \qquad (15b)$$

Hence

$$(m_s)\ \max = 2\ \arcsin\ \left[2\pi R/2N(R - r)\right] \qquad (15c)$$

$$(m_s)\ \min = 2\ \arcsin\ \left[2\pi R/2N(R + r)\right] \qquad (15d)$$

The variation has a sinusoidal appearance and this formulation was used to describe the variation. Thus

$$(m_i - i\ (m_s)av) = t\cos\left(\frac{r_i 2\pi}{P}\right) \qquad (16)$$

where m_i is the angle m at the i th element, r_i is the distance along the contour length to the i th element and t is a constant.

When $r_i = P/K$, $i = N/K$ and then

$$(m_i - i\ (m_s)av) - (m_s)\max - (m_s)av$$

$$= 2\ \arcsin\ (2\pi R/2N(R - r)) - 2\ \arcsin\ (\pi/N)$$

$$= t\cos(2\pi)$$

$$= t$$

Therefore generally

$$m_i = 2 \arcsin\left(\pi R/N(R - r)\right) - \arcsin\left(\pi/N\right) \cos\left(\frac{r_i 2\pi}{p}\right) + i\, 2 \arcsin\left(\pi/N\right) \qquad (17)$$

$$= 2 \arcsin\left(\pi R/N(R - r)\right) - \arcsin\left(\pi/N\right) \cos\left(\frac{r_i 2\pi}{p}\right) + i\, 2\pi/N \quad \text{if N is large}$$

The second term is the expression expected for m_i if each step $(r_{i+1} - r_i)$ corresponded to an equal increment in m_i. The first term represents the variation in the change of r_i. The angle $n_i = 2\pi K_{i/N}$ for all i.

By using the axes in Fig. 3.3a, b, the parametric equations describing the toroid are:

$$x = \left[R + r \cos(n)\right] \sin m$$
$$y = \left[R + r \cos(n)\right] \cos m \qquad (18)$$
$$z = r \sin n$$

Then any interpoint distance

$$r_{ij} = \left[(x_i - x_j)^2 + (y_i - y_i)^2 + (z_i - z_j)^2\right]^{\frac{1}{2}}$$

which leads to the expression

$$r_{ij}^2 = (1 - \cos(m_i - m_j))(2R^2 + 2Rr\left[\cos(n_i) + \cos(n_j)\right]) \qquad (19)$$
$$+ 2r^2\left[1 - \cos(m_i - m_j)\cos(n_i)\cos(n_j) - \sin(n_i)\sin(n_j)\right]$$

The model was divided into 15 x K scattering elements of equal mass. These were treated as having their centres of mass at the mid-point of the contour length they occupied.

Using the above formulae, the large radius was 101.6 nm and the small radius 19.8nm, on fitting the model to our experimental root-mean-square radius and molecular weight. The reciprocal particle scattering function $P\theta^{-1}$ calculated from this is shown in Fig. 3.4.

Y-shaped Model

This model is shown in Fig.1.3cand is the supposed three dimensional solution structure of the Y-shapes frequently noted in electron micrographs of superhelical DNA. The angle between the arms and their respective lengths could be varied in the computer model and a number of different sets of values for these parameters were used to compare with the experimental

results. The model was then treated as three linked cylinders of similar form to the rod model. For the sake of generality of applicability of the computer programme to all Y-shapes the defining parameter used was d, the diameter of the cylinders; d was chosen and empirically varied until Rg was obtained at the same as the experimental value. Rg was computer calculated from the formula (Tanford, 1961; Flory, 1969)

$$Rg^2 = \frac{1}{2N^2} \sum_{i=1}^{N} \sum_{j=1}^{N} r_{ij}^2 \qquad (20)$$

For Y-shapes where Rg was easily arithmetically calculable, the computer calculated Rg values were the same. With d defined the length of each arm was calculated from the formula

$$L_c = N_c \left[(L/2N)^2 - (\pi d/2)^2 \right]^{\frac{1}{2}}$$

where L_c and N_c are the length and number of supercoils respectively in the arm.

If the arms are numbered 1, 2, 3 with N_1, N_2 and N_3 the numbers of supercoils respectively in each arm and m_{12}, m_{23}, m_{31} are the angles between arms 1 and 2, 2 and 3, 3 and 1 respectively, then the set of dimensions shown in Table 3.1 are dictated for the various variations on the Y-shape chosen. For the PB calculation (and the Rg), the model was, as in the rod, imagined sliced into four segments per superturn. The intersegment distances r_{ij} were calculated as for the rod for the segments i, j on the same arm. If they were on different arms r_{ij} was calculated from

$$r_{ij} = (r_{io}^2 + r_{jo}^2 - 2r_{io} \cdot r_{jo} \cos m)^{\frac{1}{2}}$$

where m is the angle between the arms on which i and j are, r_{io} and r_{jo} are the distances from the i th and j th segment respectively to the intersection of the three arms.

Empirically one would imagine the minimum thermodynamic energy state for the Y model would be that with all three arms planar, and most of the models chosen assume this. However, conceivably some torsional strain in the structure might cause the lowest energy conformation to be non-planar and we have, therefore, included an example of this in our calculated curves.

The molecule has again been assumed essentially rigid and end effects neglected and the curves are shown in Fig. 3.5.

Computer programmes for calculating PB for all these models are given in Appendix II.

3.1.2.3

FIT OF EXPERIMENTAL RESULTS TO THEORETICAL MODELS

The errors involved in the experimental results used to calculate the theoretical curves in Figs. 3.4, 3.5 are fairly large, in particular in the r.m.s. radius and number of superturns. To assess the effect of these on the resolution of the method, theoretical curves were computed using maximum error data and are also shown in Figs. 3.4, 3.5. Examination of these plots shows that the straight interwound superhelix was totally incompatible with the experimental results and that the toroid model was at best unlikely. Some kind of Y-shape was, therefore, indicated and curves for these straddle the experimental points. However, no really good fit was found, despite varying arm lengths and interarm angles, as shown in Fig. 3.5. A large number of other combinations besides those shown were tried, without markedly improving the fit. In later experiments (see Section 3.1.3) slightly lower values of the last three points (at the highest angles) were found, which would improve the fit; also a slightly lower value of the r.m.s. radius was found, but this is easily encompassed by the maximum error limits. The deviations from predicted curves could, however, be due to a number of factors, such as further branching, some breakdown of normal secondary structure (Dean & Lebowitz, 1971) or some limited flexibility remaining in the molecule. Nevertheless, these experiments indicate strongly that at $\sigma = -0.025$, ϕ X174-RFI DNA has a Y-shaped structure, with possibly the characteristics of curve (1) in Fig. 3.5 as this gives the best fit.

3.1.3

EFFECT OF TEMPERATURE ON RFI CONFORMATION

3.1.3.1

EXPERIMENTAL

The experiments were performed at 10 temperatures from 14.9^{o} to 74.5^{o}C as

described in Section 2.2.2.5. The results were interpreted as usual by means of Zimm plots; in all cases the concentration ranges were approx. 30 to 80µg/ml except at 74.5°C, where it was 40 to 180µg/ml. In all experiments the molecular weight was in the range $3.2 \pm 0.12 \times 10^6$. The results for the r.m.s. radii, second virial coefficients and temperatures at which experiments were performed are given in Table 3.2, five typical Zimm plots are shown in Fig. 3.6, the resulting $P\theta^{-1}$ curves in Fig. 3.7 and a plot of r.m.s. radius against temperature in Fig. 3.8. The dependence of the superhelix density on temperature has been investigated by Wang (1969a) and Upholt et al. (1971). Because of the insensitivity of the sedimentation coefficient to superhelix density in region II in Fig. 1.1, however, estimates of the temperature coefficients have been made only in regions I and III. In these regions for SV40 DNA (mol. wt. 3×10^6) Upholt et al. (1971) found $\Delta\sigma$/degree was 1.5×10^{-4} and 1.6×10^{-4} respectively, while Wang found 1.4×10^{-4} for λb2b5c DNA (mol. wt. 25×10^6) in region I. Hence, a value of 1.5×10^{-4} was used for ϕ X174-RFI DNA (mol. wt. 3.2×10^6) in region II for conversion of temperature to σ dependence. These coefficients, however, were determined from 0° to 40°C and have been used here from 14.9°C to 74.5°C. This seems reasonable and any doubt would centre on the highest temperature, where it would be conceivable that some early melting might have occurred. However, Vinograd et al. (1968) estimated the Tm of polyoma-I DNA, which has G-C% = 48% (ϕ X174-RF DNA, 42%), as 108°C in buffer equivalent to PPES; in addition they estimated a Tm of 77°C and an onset of melting at 72°C for the early melting which seems to occur in the A-T richest sections of the duplex, due to the destabilising effect of the superhelical turns, in the alkaline titration of polyoma-I monitored by buoyant density, if a linear relationship between pH and temperature melting is assumed. This, however, does not seem to have affected the results of this experiment as indicated by the compatibility of the proflavine experiment (Section 3.1.3.2).

The plot of the r.m.s. radius against σ making the above assumptions is shown in Fig. 3.8; also included, for reference, are sedimentation

coefficients from the EB titration (Fig. 3.1) converted to dependence on σ, ignoring differential binding of dye by RFI and II. It can be seen that although there are some apparent small variations in the r.m.s. radius from $\sigma = -0.0205$ to -0.0207, a major transition in solution structure occurs between $\sigma = -0.0207$ and -0.0170. This is borne out by the change in the $P\theta^{-1}$ plots (Fig. 3.7). Notably, the sedimentation coefficient only increases slightly in this region, indicating that the molecule has become considerably less free-draining (Tanford, 1961). The actual conformation of this structure is interesting and three possibilities are shown in Fig. 3.9; A and B are variations of the straight interwound and toroidal models, and C, related to B, has been considered by Glaubiger & Hearst (1967).

3.1.3.2

THEORETICAL MODELS

Theoretical $P\theta^{-1}$ curves for A and B in Fig. 3.9 were computed as in Section 3.1.2 from equation (7), using -8 as the integral number of superhelical turns, and assuming a linear mass density of 1950 daltons/nm. For the straight interwound model, A, the superhelix radius has become much too large to treat it as a simple rod and, therefore, the formulation of Gray (1967) was used to describe it.

Straight Interwound Model with Large Radius

The geometrical representation of the model is shown in Fig. 3.10. The molecule is considered, neglecting end effects as two interwound helices, each with half the contour length of the molecule, with the z axis equivalent to the superhelix axis and the two helices beginning 180° apart in a plane parallel to the x-y plane. The parametric equations for a helix are then:

$$\begin{aligned} x &= (\cos t)\, d/2 \\ y &= (\sin t)\, d/2 \\ z &= pt/2 \end{aligned} \qquad (21)$$

where d is the superhelix diameter, t is the polar angle in the x-y plane and p is the superhelix pitch.

The intersegment distances, r_{nm}, fall into two categories: interhelix distances when n, m are on different helices and intrahelix distances when

they are on the same helix. Then, for interhelix distances

$$r_{nm}^2 = 2r^2\left[1 - \cos((n-m)t_b - \pi)\right] + (p^2/4\pi^2)\left[(n-m)t_b\right]^2 \qquad (22a)$$

and for intrahelix distances

$$r_{nm}^2 = 2r^2\left[1 - \cos((n-m)t_b\right] + (p^2/4\pi^2)\left[(n-m)t_b\right]^2 \qquad (22b)$$

where t_b is the projection in the x-y plane of the angle between adjacent segments and is 2 arcsin $(\pi K/N)$. Therefore,

$$P\theta^{-1} = 2/N^2\left[\sum_{n}^{N/2}\sum_{m}^{N/2}\frac{\sin h\, r_{nm}}{h\, r_{nm}}\ (\text{interhelix}) + \sum_{n}^{N/2}\sum_{m}^{N/2}\frac{\sin h\, r_{nm}}{h\, r_{nm}}\ (\text{intrahelix})\right] \qquad (23)$$

where h, r_{nm} and N are as in eqn. (7). The equation

$$p^2 = (P/K)^2 - (\pi d)^2 \qquad (24)$$

where P is the contour length and K is the number of superhelical turns, relates these quantities and is analogous to eqn. (8). The procedure was to use eqn. (20) to calculate the r.m.s. radius, Rg, from a specified superhelix diameter and vary this by trial and error until the calculated Rg matched the experimental. The dimensions thus specified were used to calculate $P\theta$ values from eqn. (23) by computer summation; the computer programme for this is given in Appendix II. Using the above formulae for this model d = 63.8nm and p = 45.4nm. The $P\theta^{-1}$ curve is shown in Fig. 3.11.

Toroid model

The $P\theta^{-1}$ curve for this model (Fig. 3.9b) was calculated for the dimensions dictated by Rg, exactly as in Section 3.1.2. This gave a large radius of 53.1nm and small radius of 32.0nm. The $P\theta^{-1}$ curve is shown in Fig. 311.

3.1.3.3

FIT OF EXPERIMENTAL RESULTS

The experimental points, theoretical curves for the two models and theoretical curves using maximum error data are shown in Fig. 3.11. The experimental points fall just outside the max. error curve for the toroid and well outside

that for the interwound model. Thus no hard conclusion can be drawn from these experiments alone, although some toroid-like structure is suggested, e.g. Fig. 3.9c, and these results are discussed later in conjunction with the proflavine experiment

3.1.4

PROFLAVINE TITRATION OF ϕ X174-RF DNA

It is fairly well established that PF binds as an intercalating ligand to DNA at moderate ionic strength and high polymer-to-dye ratios (Blake & Peacocke, 1968). Titrations of supercoiled DNA using PF instead of EB have been performed (Waring, 1970; Saucier et al., 1971). As it does not absorb light at 546nm, it was possible to perform light scattering experiments at various points along the dye titration curve.

3.1.4.1

SEDIMENTATION COEFFICIENT DEPENDENCE ON DYE BINDING

The values found are plotted in Fig. 3.12 The minimum is assumed to be where the open circular conformation is achieved. The critical binding ratio at this point, r_c, is 0.061 ± 0.003 moles dye/mole nucleotide. Assuming that both the value of $\tau = -11.8 \pm 1.6$ from the EB experiment and an unwinding angle of 12^o per EB molecule are correct, this gives an apparent unwinding angle of $7.3^o \pm 1.3^o$ per bound PF molecule, in excellent agreement with the values of 8^o and $8.4^o \pm 2.4^o$ found by Saucier et al. (1971) and Waring (1970) respectively. The curve is the same shape, biphasic, as the EB titration curve (Fig. 3.1) with the maximum occurring at $r = 0.0208$, $\sigma = -0.017$, which coincides with the maximum in the EB titration. There is a possibility that not all the PF bound intercalates (Ramstein et al., 1972) and the real unwinding angle per intercalating molecule is larger, but this has no effect on the results from this or later experiments.

3.1.4.2

BINDING OF PF TO RFI

The binding curve found using the solutions from light scattering experiments is shown in Fig. 3.13. As mentioned in Section 2.2.4.3, each complete light scattering experiment encompasses a small range of r, and the values

in Fig. 3.13 are these values meaned and plotted one point per light scattering experiment; in fact the ranges encompassed are either smaller than or just larger than the points. There are no previous curves published for PF binding to supercoiled DNA, but the curve seems qualitatively compatible with binding curves for linear DNA (Peacocke & Skerret, 1956; Cohen & Eisenberg, 1969) taking into account of the higher initial affinity of supercoiled DNA for intercalating ligands (Bauer & Vinograd, 1968, 1970a)

3.1.4.3

LIGHT SCATTERING ON DNA-PF COMPLEX

Zimm plots of results obtained at four values of r from 0.017 to 0.052 moles dye/moles nucleotide are shown in Fig. 3.14. Zimm and Berry (1966) plots of results at r = 0.06 are shown in Fig. 3.15. The Berry plot is useful for extending somewhat the range of molecular dimensions examinable by light scattering down to 30^{o} by eliminating some of the curvature at low angles; it has been used also with RFII in Section 3.2, where it is discussed more fully. No anisotropy was detectable from the zero value of the horizontally polarised light component at a scattering angle of 90^{o} extrapolated to zero concentration. Molecular weights for the four lower r values were all, after subtraction of bound PF, in the range $3.2 \pm 0.05 \times 10^{6}$. For r = 0.06 the Zimm plot gave a mol. wt. of 3.32×10^{6}, while the Berry plot gave 3.15×10^{6}, thus justifying its use. The results for the r.m.s. radius, Rg, and second virial coefficient, B, as functions of r and σ are tabulated in Table 3.3. The Rg values are plotted as a function of r on the same diagram as the sedimentation coefficient plot against r in Fig. 3.12. The sharp drop in Rg at around $r = 0.02$ where $\sigma = -0.017$ is again evident, in agreement with the temperature experiment, before increasing again to a value corresponding to an open circle at r = 0.00. The curves of $D_{20,w}^{-1}$ in Fig. 3.16 also indicate these trends in conformation transitions; the curve for r = 0.06 was constructed using the intercept from the Berry plot at zero angle, and the extrapolation to zero concentration at finite angles from the Zimm plot .

3.1.4.4

FIT OF EXPERIMENTAL RESULTS TO THEORETICAL MODELS

The $P\theta^{-1}$ curves at $r = 0.017$ and 0.024 were compared to the same two types of models (Fig. 3.9A,B) as considered for the compact structure in the temperature experiment; it was assumed that each bound dye molecule extended the DNA length by 0.335nm. The results of this are shown in Fig. 3.17. At $r = 0.017$, the experimental points fall well within the error range for the toroid and well outside that for the interwound. At $r = 0.024$ the experimental points fall outside the error ranges of both models but nearer the toroid limit, reminiscent of the situation in the temperature experiment (Fig. 3.11).

For $r = 0.017$, the dimensions of the models from experimental results were: toroid, large radius 74.2nm, small radius 28.9nm; straight interwound model, superhelix diameter 57.4nm, pitch 56.1nm. For $r = 0.024$ the dimensions were: toroid, large radius 56.8nm, small radius 38.3nm; straight interwound model, diameter 76.4nm, pitch 54.3nm. It seems, therefore, that at $\sigma = -0.018$ the rigid toroid is a reasonable model for the molecule, but at $\sigma = -0.0154$ this model breaks down somewhat, in some way.

At $r = 0.06$ the molecule is almost exactly equivalent to RFII DNA, i.e. it is in an open circular form. Since there was a theoretical $P\theta$ function available for open circular DNA (see Section 3.2 and Appendix I) it was possible to use it to obtain $P\theta^{-1}$ curves for different persistence lengths. This was done, again assuming an extension of 0.335nm per bound dye molecule for the DNA thread, and using the following parameters for the calculation in Appendix I: $N = 612$; segment size, 3.0nm; excluded volume factor, $\epsilon = 0.141$; persistence lengths from 350 - 450nm. The experimental points and theoretical curves are shown in Fig. 3.18. The persistence length of the DNA in this situation is estimated as 36.0 ± 3.0nm from this plot.

3.2

RELAXED CIRCULAR DNA

3.2.1.

EXPERIMENTAL

No anistropy was detectable in solutions of ϕ X174-RFII DNA, after solvent subtraction. At 90^{o}, no horizontally polarised light was detectable even before extrapolation to zero concentration, and on extrapolation to 0^{o}, the ratio of the vertical to horizontally polarised components became one, as expected. Two different experiments with different samples were performed and the results of these were totally compatible.

The results were initially plotted as Zimm plots (Zimm, 1948), Fig. 3.19. This gave a mol. wt. of $3.38 \pm 0.17 \times 10^{6}$ which is somewhat higher than the values of 3.2×10^{6} approx. previously found for RFI DNA. The explanation for this seems to be the curvature observed at the lower angles, and in fact, extrapolation to 0^{o} relies heavily on the two lowest angles. The semi-empirical method of Berry (1966) was, therefore, used where $(Kc/R\theta)^{\frac{1}{2}}$, not $Kc/R\theta$, is plotted on the ordinate, to attempt to eliminate the curvature at low angles (Fig. 3.20). This gives a mol. wt. of $3.18 \pm 0.18 \times 10^{6}$, which is in very good agreement with previous results, so a correct extrapolation to 0^{o} seems to have been achieved, although there is still some curvature at low angles. The r.m.s. radius, Rg, and second virial coefficient B were extracted from the Berry plot as explained in the legent to Fig. 3.15.

This gave a value of 109.4 ± 15nm for Rg, which is nearer perhaps than expected to the final average value from all experiments on RFI at 25^{o}C of 97.4 ± 8.0nm (S.D. of 5), and value of approx. zero for B.

3.2.2

FIT OF EXPERIMENTAL RESULTS TO THEORETICAL

The experimental $P\theta^{-1}$ points in Figs. 3.21, 3.22 were obtained using the extrapolation to zero concentration of the values at zero scattering angle from the Berry plot and the extrapolations to zero concentration at finite angles from the Zimm plot. These points were compared with a theoretical $P\theta^{-1}$ curve for circular worm-like coil (Kratky & Porod, 1949) which was

calculated using a Daniels (1952) distribution function modified for excluded volume effects (Gray et al., 1967; Sharp & Bloomfield, 1968b) and made applicable to circular molecules (Zimm, 1948) in conjunction with the exact worm-like coil distribution without excluded volume effect (Kratky & Porod, 1949). The calculations for this are given in Appendix I. For the theoretical curves, the parameters used were: number of segments, N, 547; segment length, 3.0nm; persistence length, values from 30 - 70nm. The excluded volume factor, ϵ, was used at two values; these were 0.11, the value accepted for linear DNA and 0.141, the corresponding value for a circular DNA of mol. wt. 3.2×10^6 (Gray et al., 1967).

The comparisons of experimental and theoretical results are shown in Figs. 3.21, 3.22 for $\epsilon = 0.141$ and 0.11 respectively. As can be seen this makes only a small difference to the theoretical curves, although the former is more appropriate. By visual examination, at $\epsilon = 0.141$ the experimental points fit the theoretical curves well for a value of the persistence length around or just over 40nm. A value of 41.0 ± 3.5nm was estimated for this. For $\epsilon = 0.11$, there is no great difference and the persistence length appears only marginally higher. Thus, even if the value of ϵ is not certain, the error in the persistence length is not increased much.

It is also worth noting that the general form of the experimental and theoretical curves agrees with that predicted for circular flexible chains by Casassa (1965).

Table 3.1

GEOMETRY OF Y SHAPES AS DICTATED BY THE EXPERIMENTAL R.M.S. RADIUS

Dimensions of three possible Y shapes are given, which would have the experimental r.m.s. radius of 103.5nm and the theoretical $P\theta^{-1}$ curves for which have been computed and are given in Fig.3.5. The symbols are explained in section 3.1.2.2 on the Y shaped model.

Table 3.1

Features chosen						Resulting dimensions (nm)				Curve no. in Fig.3.5
N_1	N_2	N_3	m_{12}	m_{23}	m_{31}	d	L_1	L_2	L_3	
4	4	4	120°	120°	120°	31.1	185.6	185.6	185.6	1
2	4	6	120°	120°	120°	32	84.2	168.4	252.6	4
4	4	4	90°	90°	90°	30	198.4	198.4	198.4	5

Table 3.2

THE DEPENDENCE OF MOLECULAR PARAMETERS OF ϕX174-RFI DNA ON TEMPERATURE

These results are for section 3.1.3.1, and the correlation of σ with temperature was made as described there.

Table 3.2

Temperature ^{o}C	Rg nm	$10^5 xB$ mole cm^3/g^2	$-\sigma \times 10^2$	$-\tau$
14.9	85.4 ± 11	7.15 ± 4	2.65	12.5
20.3	85.3 ± 11	6.76 ± 4	2.57	12.1
25.4	92.0 ± 12	-8.57 ± 5	2.50	11.8
30.3	92.8 ± 12	1.47 ± 1.5	2.42	11.4
35.4	93.2 ± 12	2.06 ± 2	2.34	11.0
39.8	92.5 ± 12	3.05 ± 3	2.28	10.8
45.0	95.2 ± 12	4.14 ± 3	2.20	10.4
49.5	88.0 ± 11	8.24 ± 5	2.15	10.1
53.4	83.2 ± 11	1.47 ± 1.5	2.07	9.8
74.5	62.0 ± 9	2.0 + 2.0	1.76	8.3

Table 3.3

THE DEPENDENCE OF MOLECULAR PARAMETERS OF ϕX174-RFI DNA ON THE BOUND PF/NUCLEOTIDE RATIO

These are the results for section 3.1.4.3

Table 3.3

$-\tau$	r mole dye/ mole nucleotide	$-\sigma^2 \times 10^2$	Rg nm	B_2 (mole cm^3/g^2) $\times 10^5$
11.8	0	2.5	92.0 ± 12	-8.57 ± 5
8.5	0.017	1.80	79.6 ± 10	-2.94 ± 3.0
7.2	0.024	1.53	68.5 ± 9	-4.17 ± 3.9
4.6	0.037	0.97	82.9 + 11	-2.94 ± 3.0
1.7	0.052	0.36	109.0 ± 13	0 ± 3.0
0.2	0.060	0.04	119.9 ± 15	0 ± 2.0

Fig.3.1

EB TITRATION OF SUPERCOILED ϕX174-RFI AND II DNA

The solvent was BPES and all runs were performed at 25° + 0.05°C. Sedimentation coefficients were not corrected to standard conditions for viscosity, buoyancy, temperature or concentration effects. All experiments were with a 3:1 mixture of RFI:RFII except the three points for RFII near the minimum of the RFI curve which were performed using 100% RFII. At this point the binding of EB by I and II is very similar (Bauer & Vinograd, 1968) and for the purpose of these experiments, the binding was assumed tobe the same as in the 3:1 mixture.

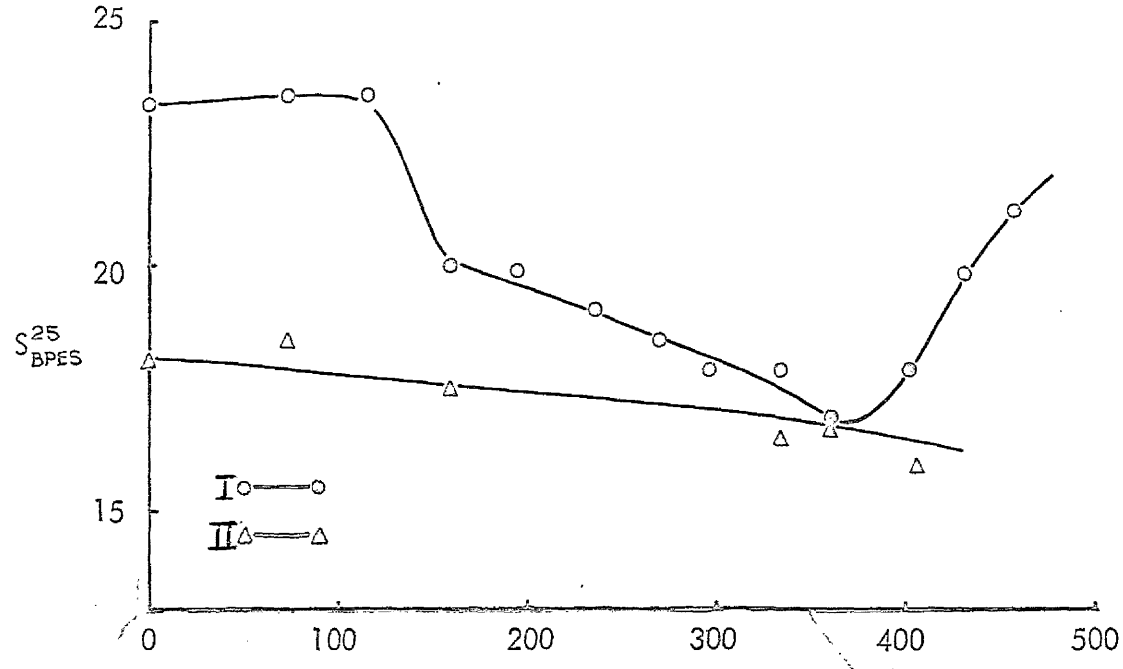

Ethidium bromide titration of Φ x 174 RF I, II

Fig.3.2

TYPICAL ZIMM PLOT OF ϕX174-RFI DNA IN EPES AT 25°C

The scattering angle, θ, varied from 30 to 150°; the concentration range was 33 to 80μg/ml. All units are in the cgs system. The formula $\left[Kc/R\theta\right]_{\substack{c=0\\ \theta=0}} = 1/M$ allows estimation of the mol. wt., M, from the intersection on the ordinate of the extrapolation to zero angle and concentration. The meaning of K and Rθ are defined in section 2.2.2.2. The formula $(Kc/R\theta)_{c=0} = (1/M)(1/P\theta)$ $=(1/M)(1 + 16\pi^2 Rg^2 \sin^2(\theta/2)/3(\lambda')^2 + \ldots\ldots)$ allows estimation of the r.m.s. radius, 'Rg, where λ' is the wavelength of light in solution and Pθ is the particle scattering factor which is 1 at 0°, from the initial slope of Kc/Rθ at zero concentration. The formula $(Kc/R\theta)_{\theta=0} = 1/M + 2Bc + \ldots\ldots$ allows estimation of the second virial coefficient, B. $P\theta^{-1}$ = (scattered intensity at θ)/(scattered intensity at 0°) $= (Kc/R\theta)_{c=0} / \left[Kc/R\theta\right]_{\substack{c=0\\ \theta=0}}$ and is calculated from this latter formula.

These are standard equations for dealing with light scattering results (see, for example, Geiduschek & Holtzer, 1958).

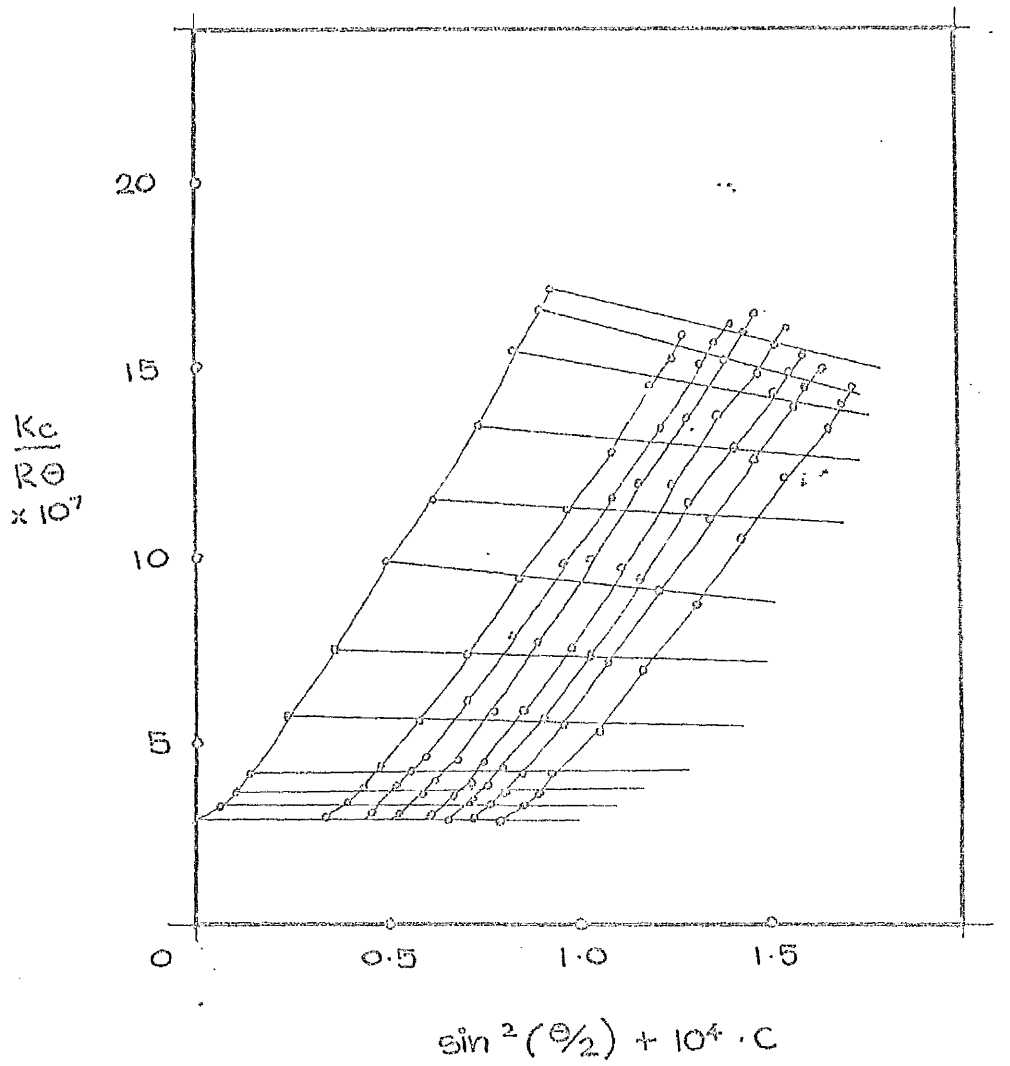
20
15
10
5
0
0·5
1·0
1·5
Kc / Rθ × 10⁻⁷
sin²(θ/2) + 10⁴ · C

Fig.3.3

GEOMETRY OF THE TOROID MODEL (FIG.1.3.b) USED TO CALCULATE THE GENERAL R.M.S RADIUS AND PΘ FUNCTION

The meanings of the symbols are defined in the calculation in section 3.1.2 on the geometry of the toroid; (a) cross-section of toroid on the z and y axes; (b) cross-section of the toroid on the x and y axes; (c) variation of the angle m between adjacent elements (m_s), with distance along the contour length.

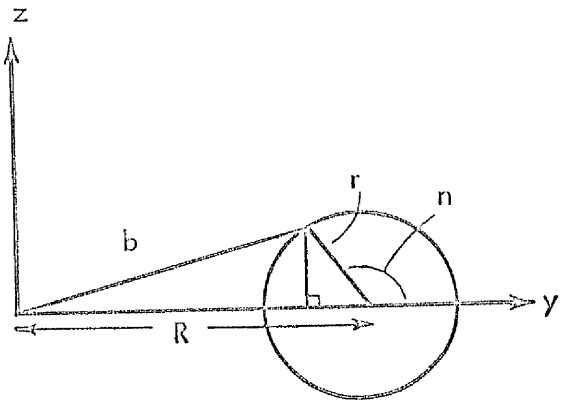

(a)

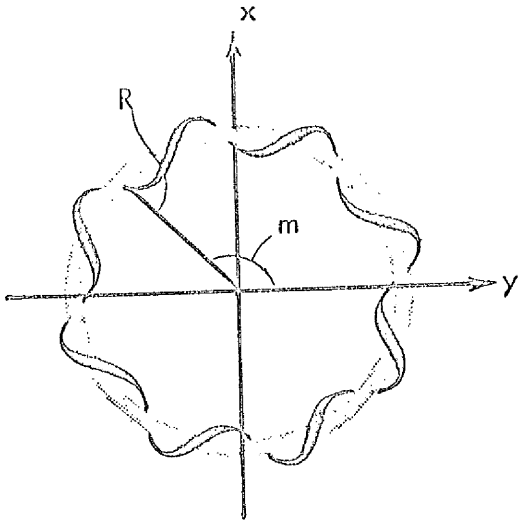

(b)

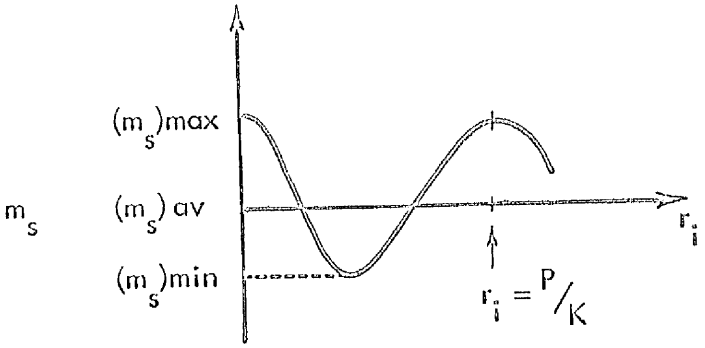

(c)

Fig.3.4

COMPARISON OF COMPUTER DRAWN CURVES FOR THE TOROID AND INTERWOUND MODELS WITH EXPERIMENTAL DATA

The reciprocal particle scattering factor of the various models are compared with experimental points. Vertical bars represent the spread of experimental values obtained ata particular angle. Curve (1): toroidal model from experimental data, r.m.s. radius, Rg 103.5nm, number of superhelical turns, K 12. Curve (2): rod model from experimental data, Rg = 103.5nm, K=12. Curves (3) and (4): toroidal model, max. error limits, Rg = 116.0 and 91.5mm, K = 10 and 13 respectively. Curves (5) and (6): rod model, max. error limits, Rg = 116.0 and 91.5mm, K = 10 and 13 respectively.

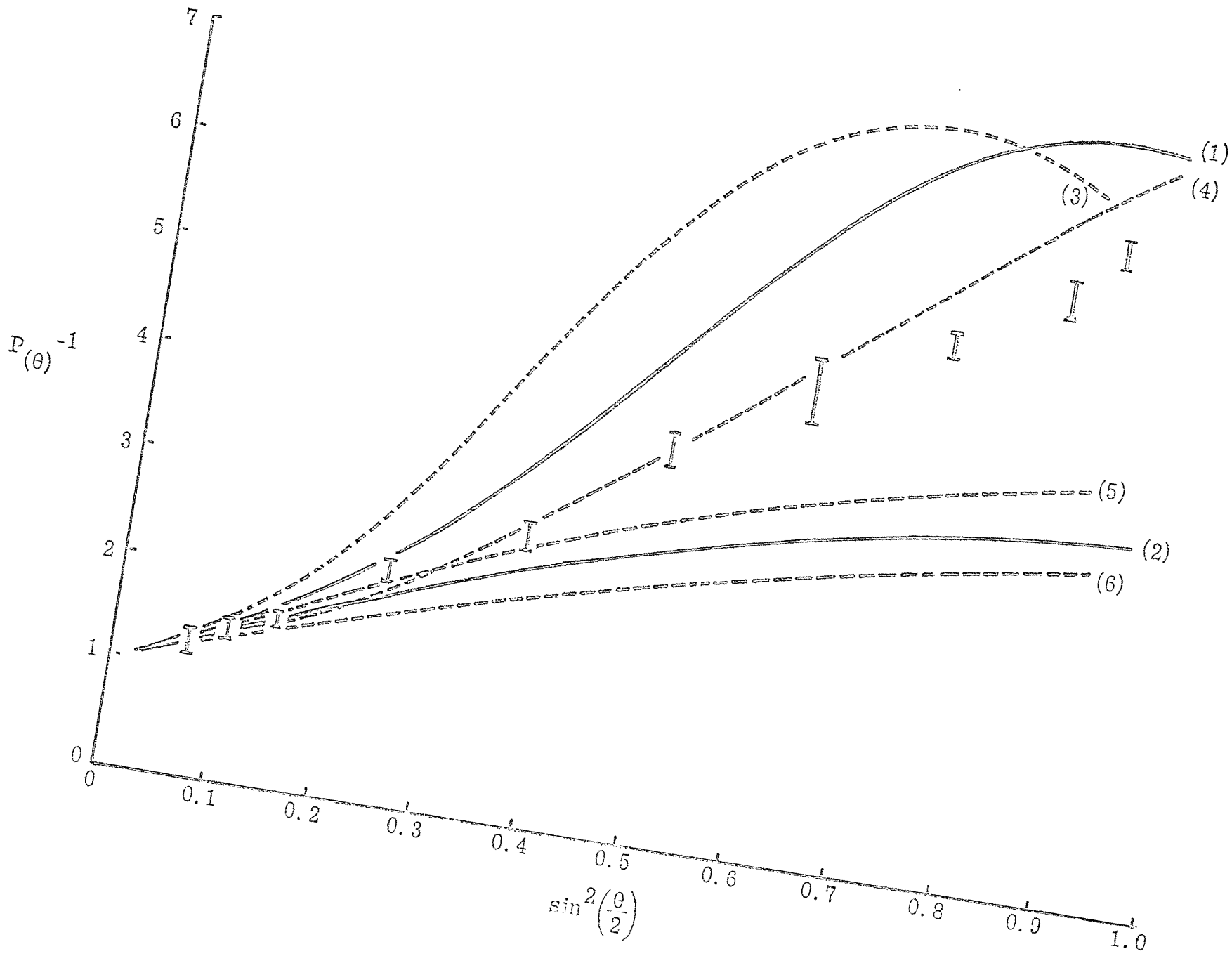
$P_{(\theta)}$-1
7
6
5
4
3
2
1
0
0
0.1
0.2
0.3
0.4
0.5
0.6
0.7
0.8
0.9
1.0
$\sin^2\left(\frac{\theta}{2}\right)$
(1)
(2)
(3)
(4)
(5)
(6)

Fig.3.5

COMPARISON OF COMPUTER DRAWN CURVES FOR Y SHAPED MODELS WITH EXPERIMENTAL DATA

The reciprocal particle scattering factors for Y-shaped models are compared with the experimental points. Vertical bars represent the spread of experimental values obtained at each angle Θ. Curves (1),(4),(5): r.m.s. radius, Rg, 103.5nm, number of superhelical turns, K, 12 for various arm lengths and inter-arm angles shown in Table 3.1. Curves (2),(3): max. error data curves for (1): Rg = 116.0 and 91.5nm with 4, 3, and 3, and 4, 4, and 5 superhelical turns per arm respectively, 120° inter-arm angles.

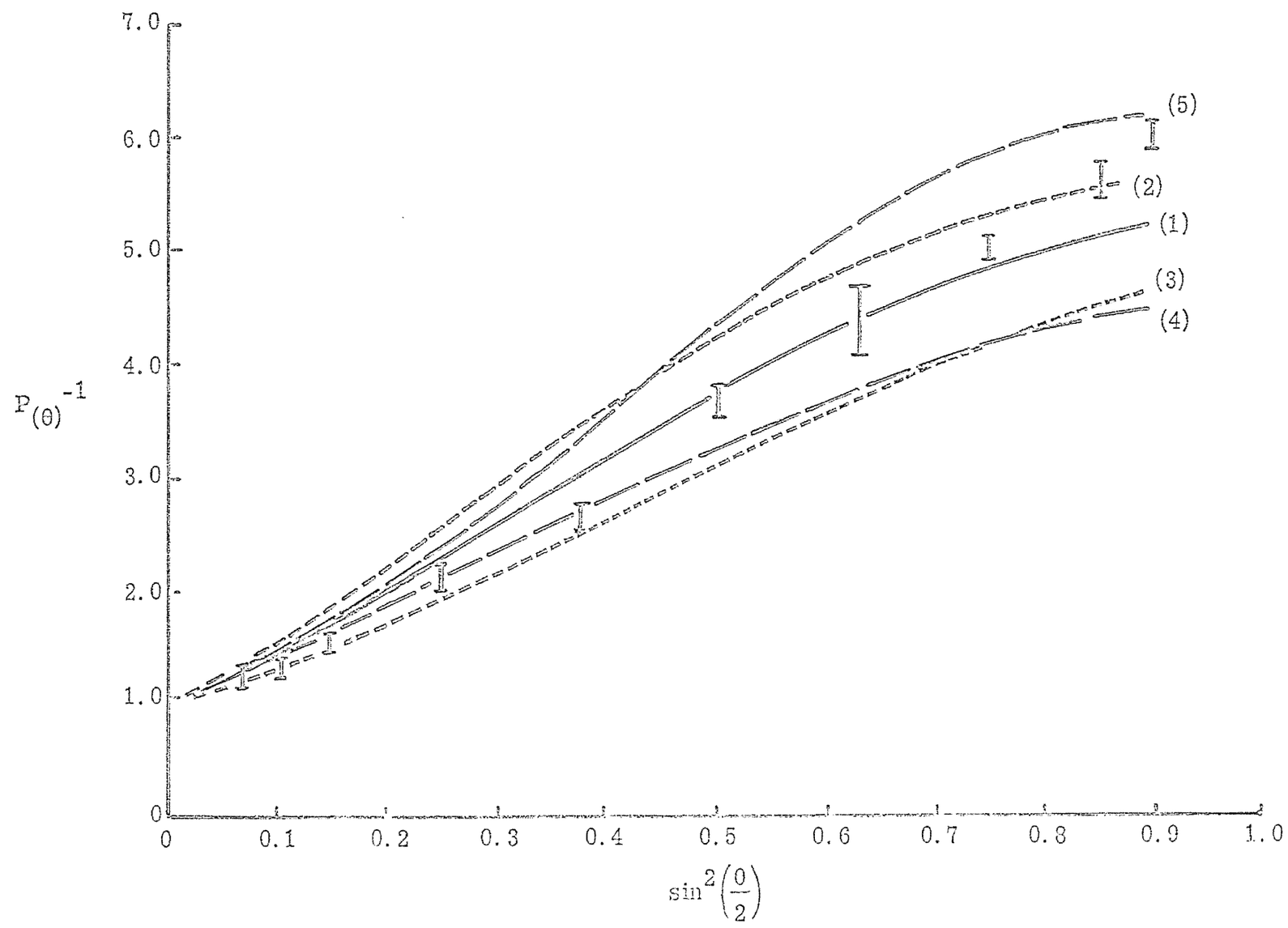
7.0
6.0
5.0
4.0
3.0
2.0
1.0
0
$P_{(\theta)}^{-1}$
(5)
(2)
(1)
(3)
(4)
0
0.1
0.2
0.3
0.4
0.5
0.6
0.7
0.8
0.9
1.0
$\sin^2\left(\frac{\theta}{2}\right)$

Fig.3.6

ZIMM PLOTS OF ϕX174-RFI DNA AT TEMPERATURES FROM 14.9°C TO 74.5°C

The scattering angle varied from 30 to 150°, the concentration range was 33 to 80μg/ml approx. in all experiments except at 74.5°C where it was 40 to 180μg/ml. All units are in the cgs system. The mol. wts., r.m.s.radii, second virial coefficients and PΘ functions were extracted from the plot as described in the legend to Fig.3.2.

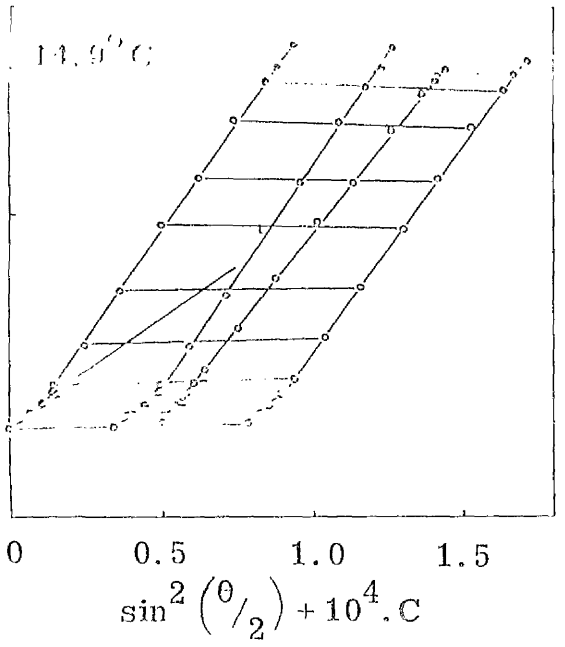
14.9°C
0
0.5
1.0
1.5
$\sin^2\left(\theta/_2\right) + 10^4.C$

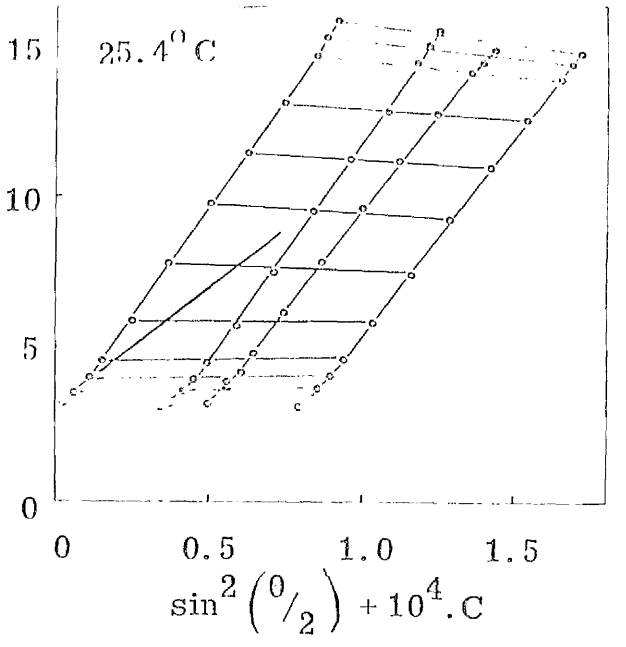
25.4°C
15
10
5
0
0
0.5
1.0
1.5
$\sin^2\left(\theta/_2\right) + 10^4.C$

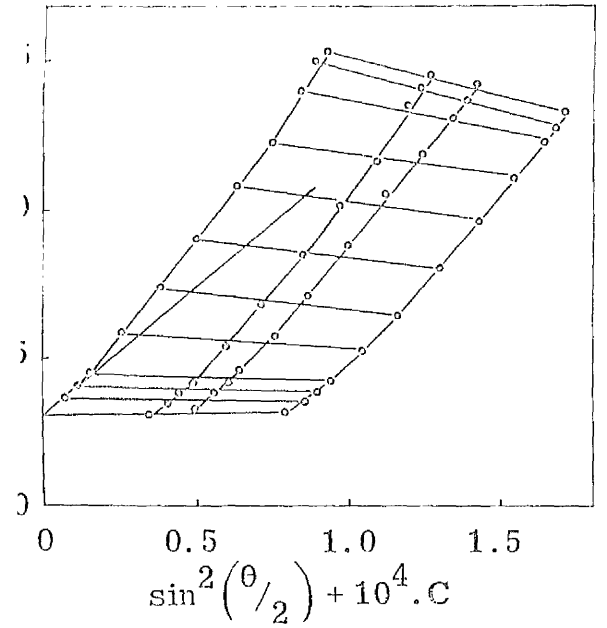
0
0.5
1.0
1.5
$\sin^2\left(\theta/_2\right) + 10^4.C$

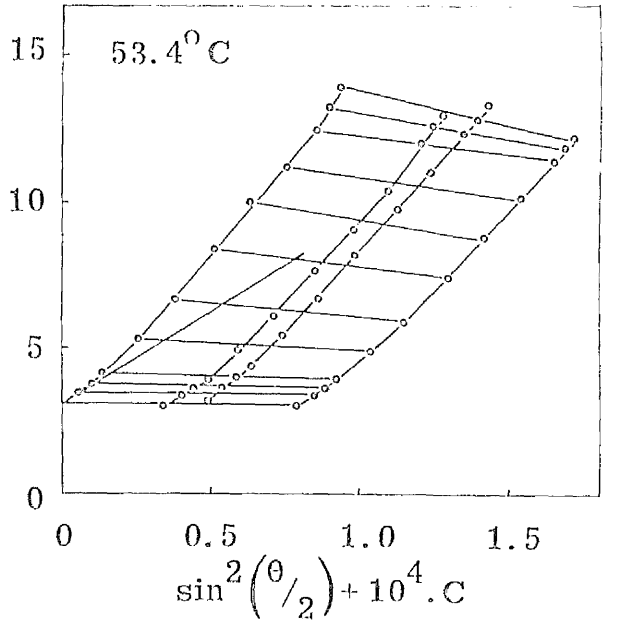
53.4°C
15
10
5
0
0
0.5
1.0
1.5
$\sin^2\left(\theta/_2\right) + 10^4.C$

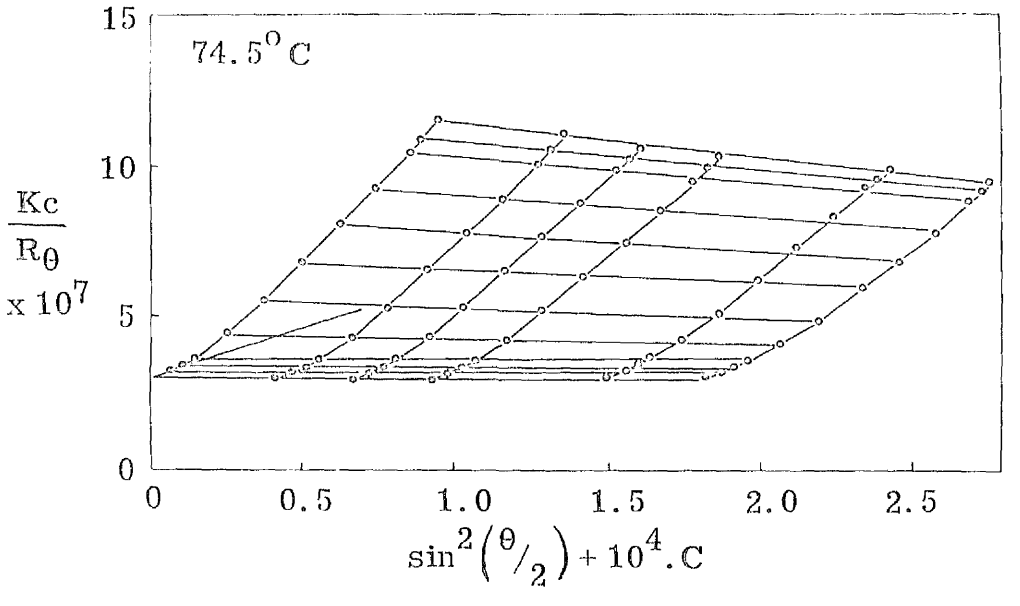
74.5°C
15
10
5
0
$\frac{Kc}{R_\theta} \times 10^7$
0
0.5
1.0
1.5
2.0
2.5
$\sin^2\left(\theta/_2\right) + 10^4.C$

Fig.3.7

VARIATION OF THE CURVES OF $P\theta^{-1}$ AGAINST $SIN^2(\theta/2)$ WITH TEMPERATURE FOR ϕX174-RFI

θ is the scattering angle. The curves at temperatures intermediate to those for which curves are shown, were intermediate in position. Details of results at these and other temperatures are given in Table 3.2.

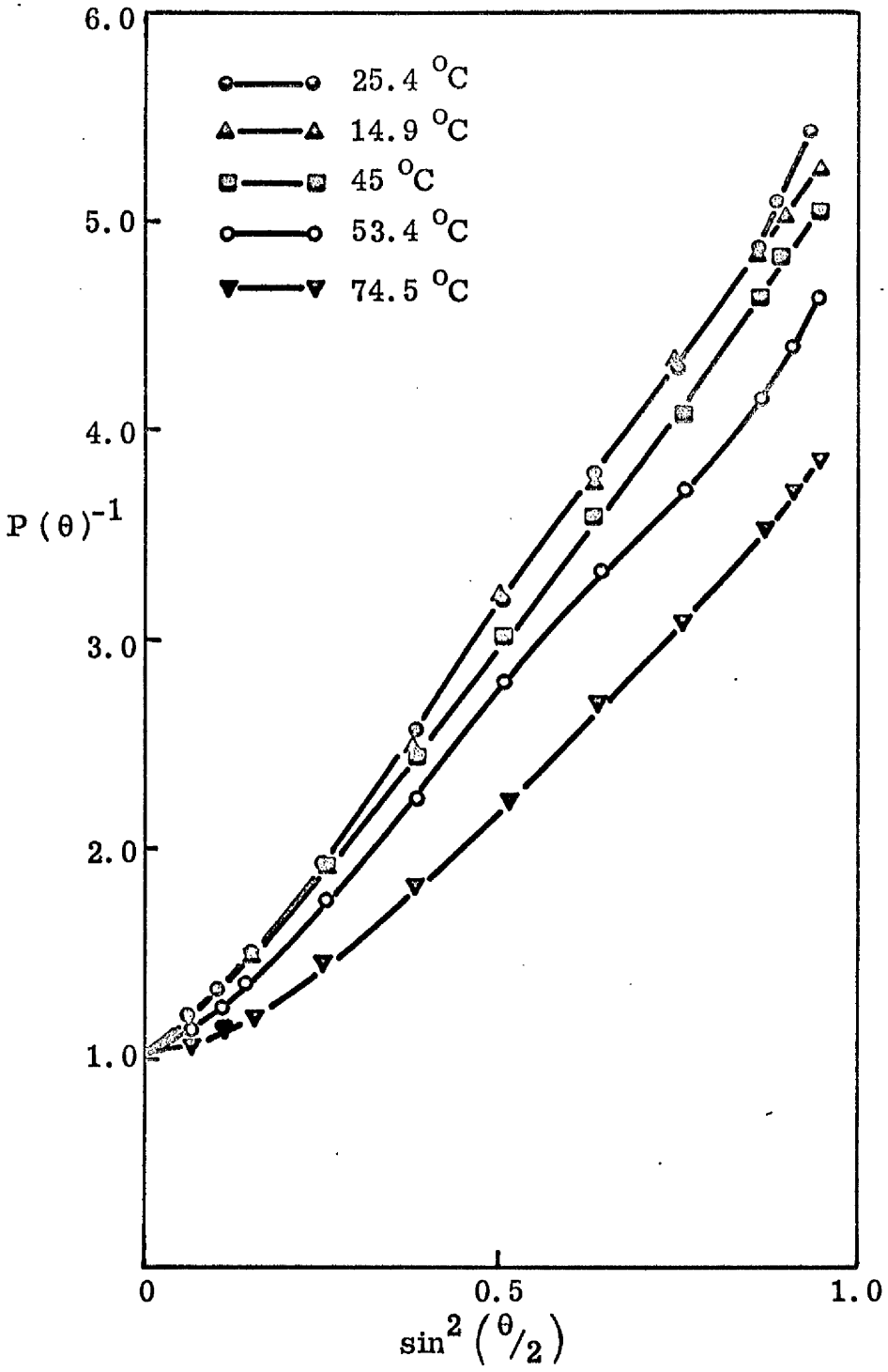
6.0
5.0
4.0
3.0
2.0
1.0
P (θ)-1
25.4 °C
14.9 °C
45 °C
53.4 °C
74.5 °C
0
0.5
1.0
sin2 (θ/2)

Fig.3.8

VARIATION OF THE R.M.S. RADIUS OF ϕX174-RFI DNA WITH TEMPERATURE AND SUPERHELIX DENSITY

Top: variation of the r.m.s. radius with temperature; errors were estimated from worst initial slopes on the Zimm plots. Bottom: the same results translated into a dependence on superhelix density by means of a temperature coefficient as described in the text (section 3.1.2.1); the errors in the r.m.s. radii are the same as in the top figure, but are not shown, for clarity. Also shown, for reference, are points from the EB titration (Fig.3.1) converted to dependence on superhelix density.

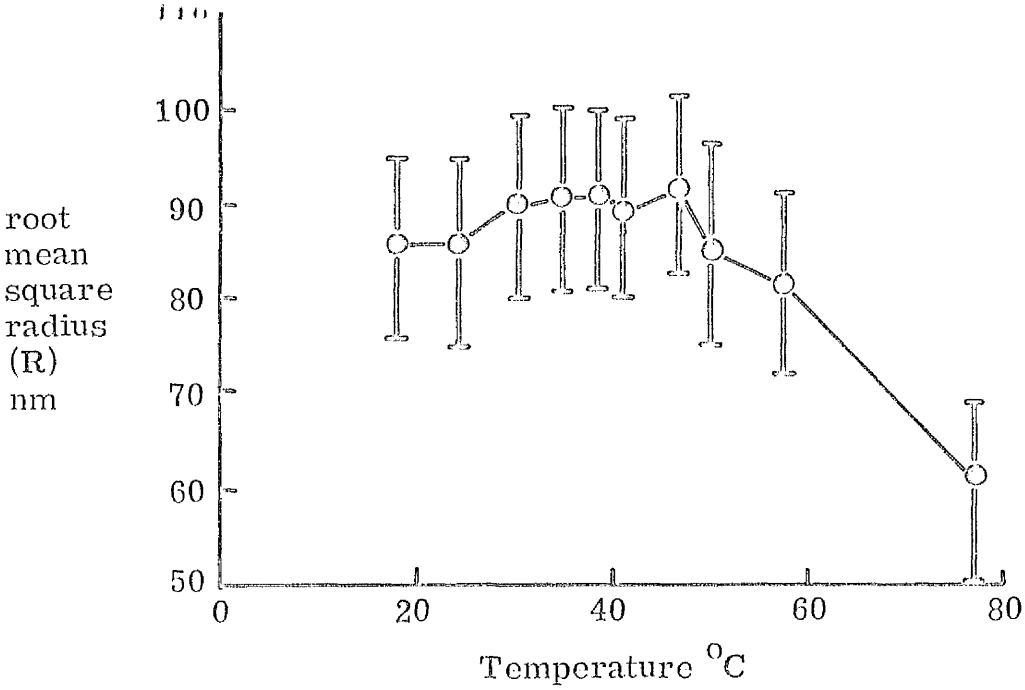
root mean square radius (R) nm
100
90
80
70
60
50
0
20
40
60
80
Temperature °C

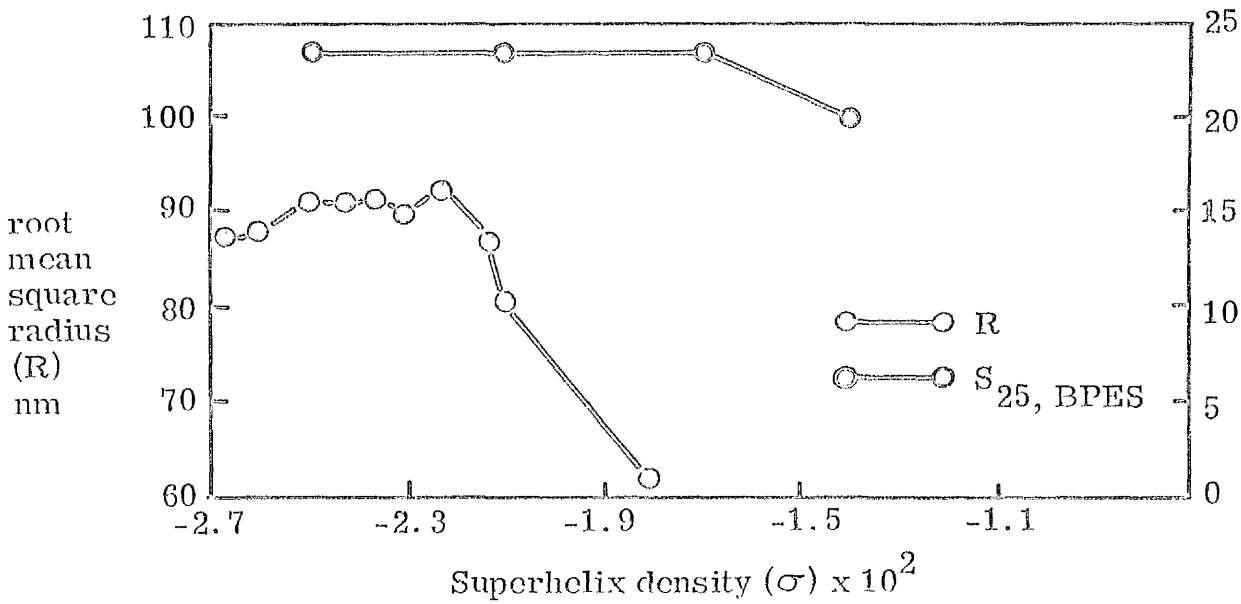
root mean square radius (R) nm
110
100
90
80
70
60
25
20
15
10
5
0
-2.7
-2.3
-1.9
-1.5
-1.1
R
S25, BPES
Superhelix density (σ) x 10²

Fig.3.9

HYPOTHETICAL STRUCTURES FOR VARIOUS FORMS OF SUPERCOILED DNA, WITH 8 SUPERHELICAL TURNS

A: straight interwound model with larger superhelix radius, of the same order of dimensions as the length; this is closely related to the structure in Fig.1.2.a.

B: toroidal model with the small and large radii (r and R in Fig.3.3) almost the same size; this closely related to the structure in Fig.1.2.b.

C: flattened toroid model; this is related to B and has been considered by Glaubiger & Hearst (1967).

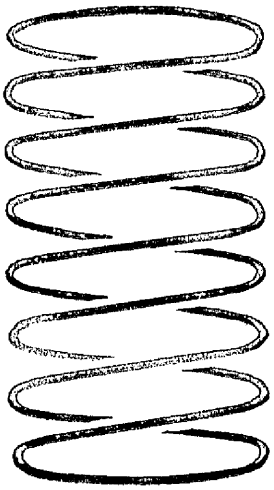

A

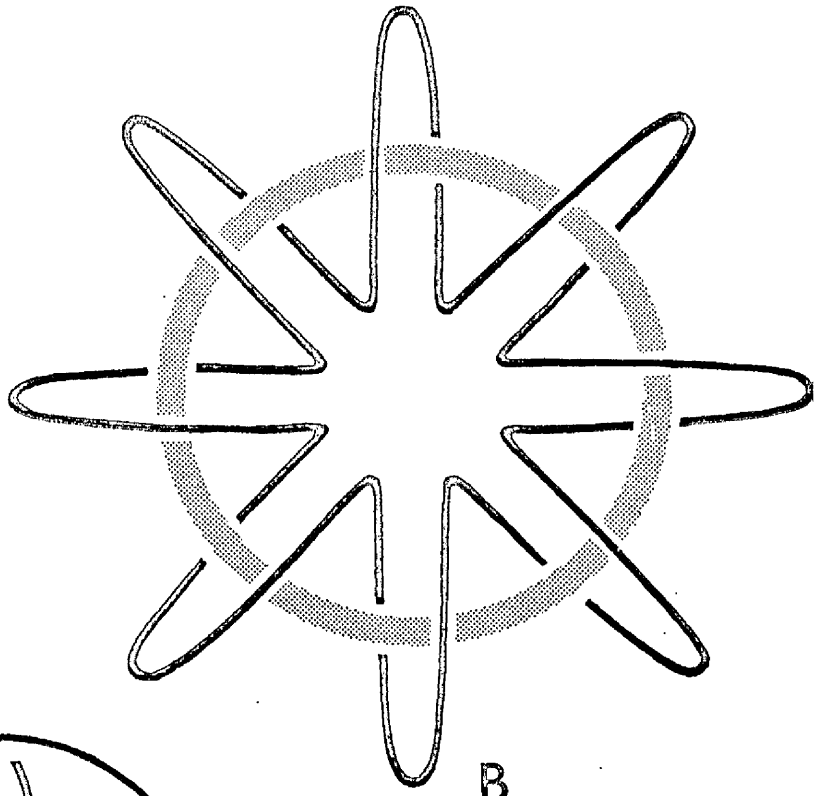

B

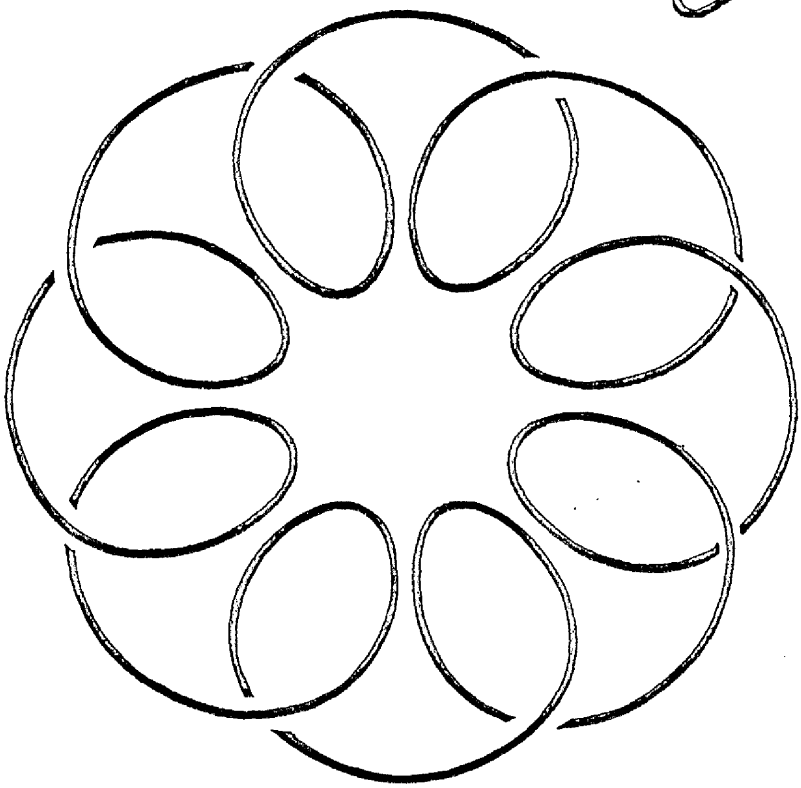

C

Fig.3.10

GEOMETRY OF A RIGID INTERWOUND SUPERHELICAL MODEL

Two superhelices are shown interwound; d is the superhelix diameter and p the pitch. No ends are shown joining the two helices, indicating that end effects have been ignored.

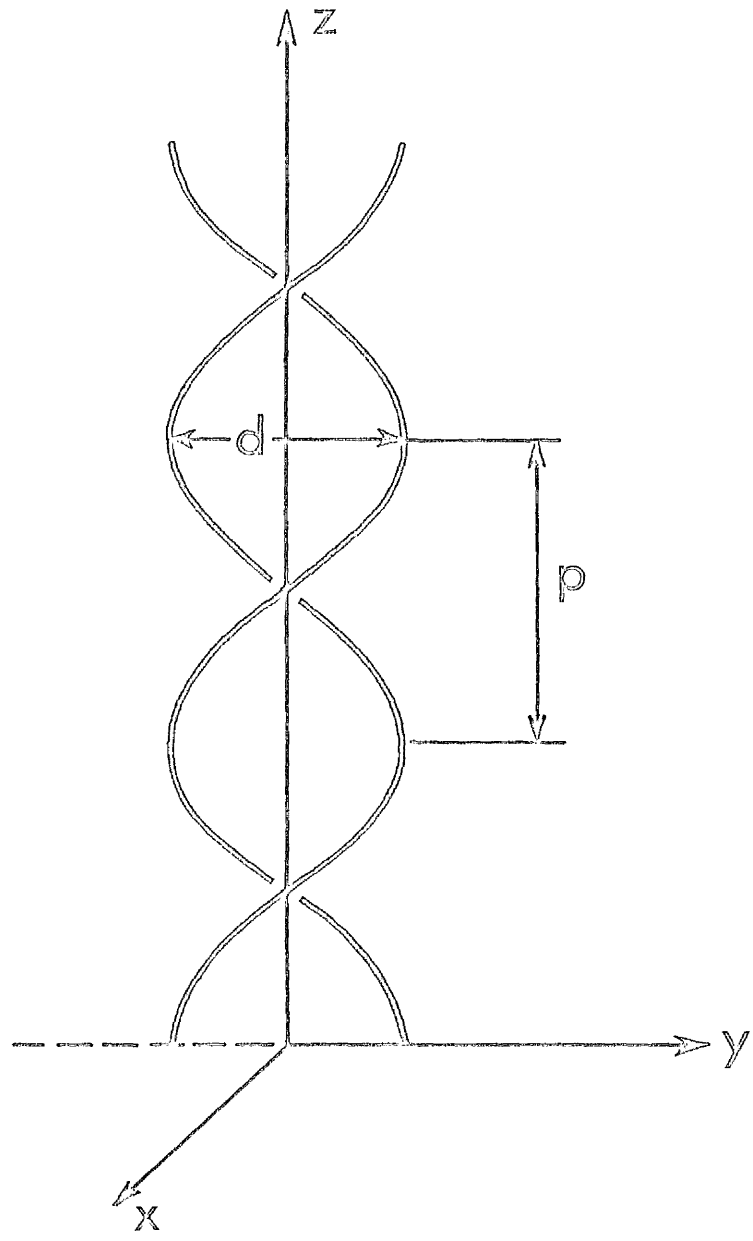
z
d
p
y
x

Fig.3.11

COMPARISON OF EXPERIMENTAL AND THEORETICAL $P\Theta^{-1\frac{1}{4}}$ CURVES FOR THE COMPACT STRUCTURE FORMED BY ϕX174-RFI DNA AT 74.5°C

The points indicate the experimental results, the lines computer calculated curves for theoretical models. Curve (1): toroidal model, Rg = 620nm, K = 8; curve (2): interwound model, Rg = 620nm, K = 8; curve (3): toroidal model upper max. error data, Rg = 710nm, K = 10; curve (4): interwound model, upper max. error data, Rg = 710nm, K = 10.

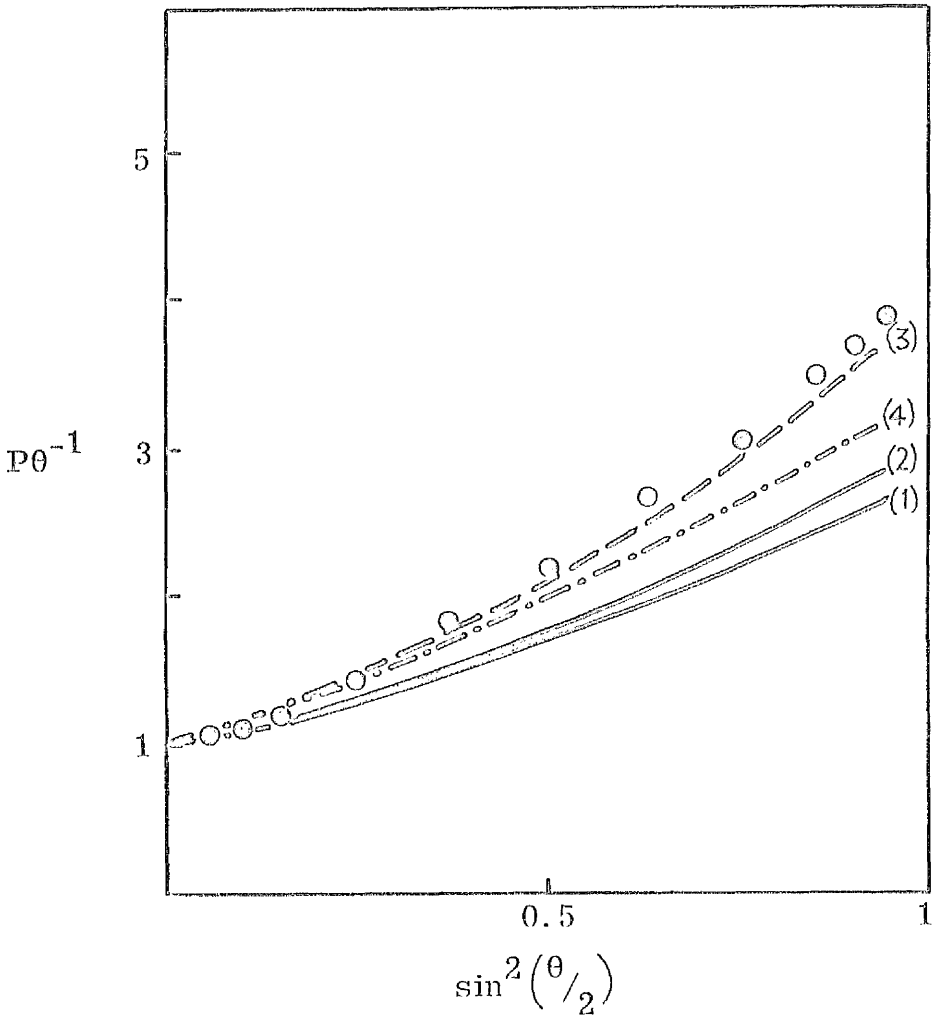
5
3
1
$P\theta^{-1}$
(3)
(4)
(2)
(1)
0.5
1
$\sin^2\left(\theta/2\right)$

Fig.3.12

THE SEDIMENTATION COEFFICIENT AND R.M.S. RADIUS OF ϕX174-RFI DNA AS FUNCTIONS OF THE BINDING OF PROFLAVINE

All experiments were at 25° ± 0.2°C and the solvent was BPES. Sedimentation coefficients were not corrected to standard conditions. The errors for Rg (large vertical bars) were estimated by worst initial slopes in the Zimm and Berry plots; the errors for r (small horizontal bars) represent the variation in r for samples used in the same Zimm or Berry plot to estimate the r.m.s. radius. Any other errors are negligible compared to this. The data are given in Table 3.3.

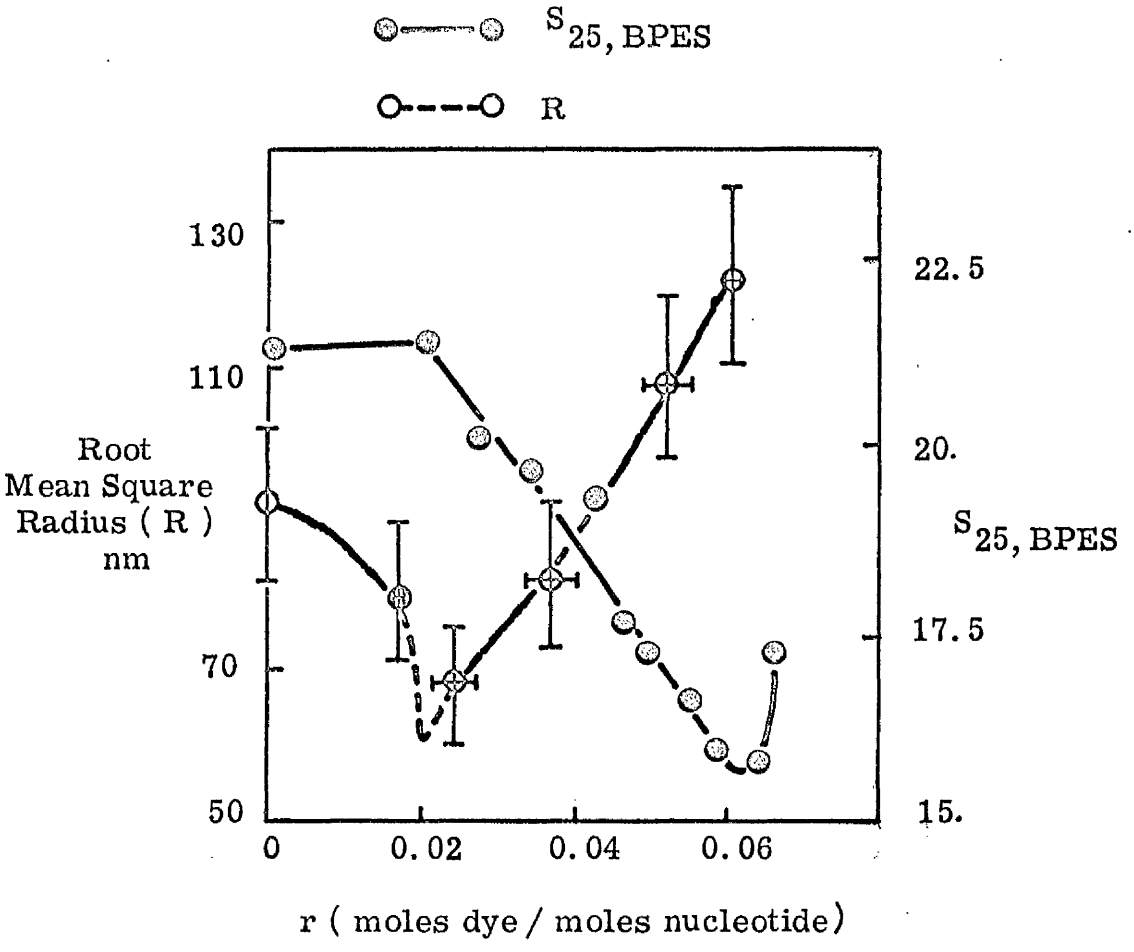
$S_{25, BPES}$
R
130
110
70
50
Root
Mean Square
Radius (R)
nm
22.5
20.
17.5
15.
$S_{25, BPES}$
0
0.02
0.04
0.06
r (moles dye / moles nucleotide)

Fig.3.13

BINDING OF PROFLAVINE TO ϕX174-RFI DNA

C_f is the concentration of free dye and r is the moles dye bound/mole nucleotide. The results are from the solutions used for light scattering and each point represents meaned results from the solutions of one complete light scattering experiment. Hence the DNA concentration was from 20 to 50μg/ml. The solvent was BPES and the temperature 20-23°C.

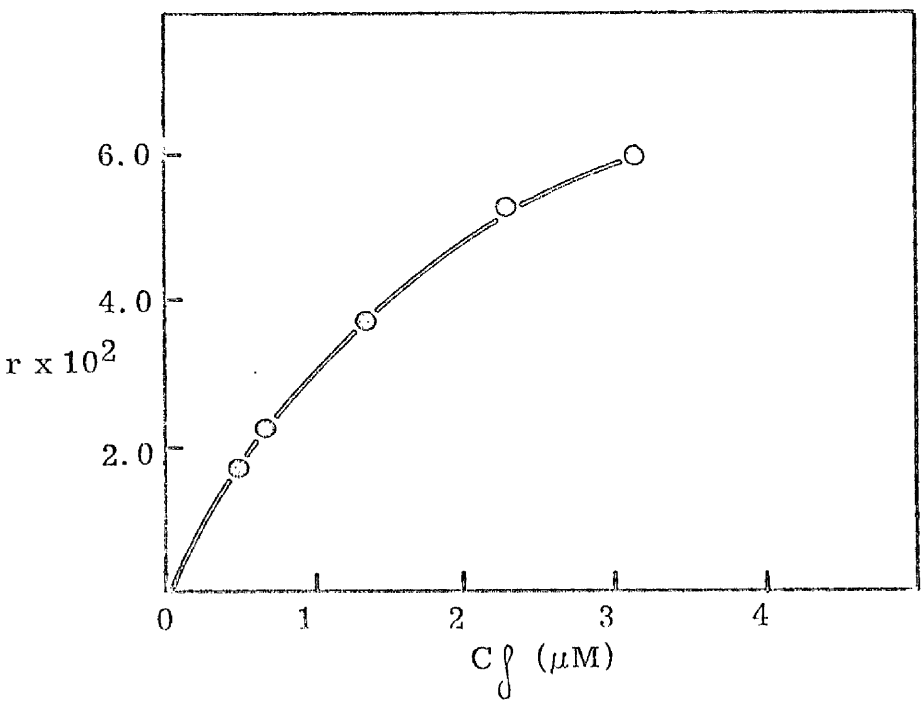
6.0
4.0
r x 10²
2.0
0
1
2
3
4
C f (μM)

Fig.3.14

ZIMM PLOTS OF ϕX174-RFI DNA AT DIFFERENT VALUES OF BOUND PROFLAVINE

All units are in the cgs system. The scattering angles were 30 - 150°, and DNA concentrations 20 - 45μg/ml approx. All experiments were at 25° ± 0.2°C and in BPES. The mol. wts., r.m.s. radii, second virial coefficients and PQ values were obtained as described in the legend to Fig.3.2.

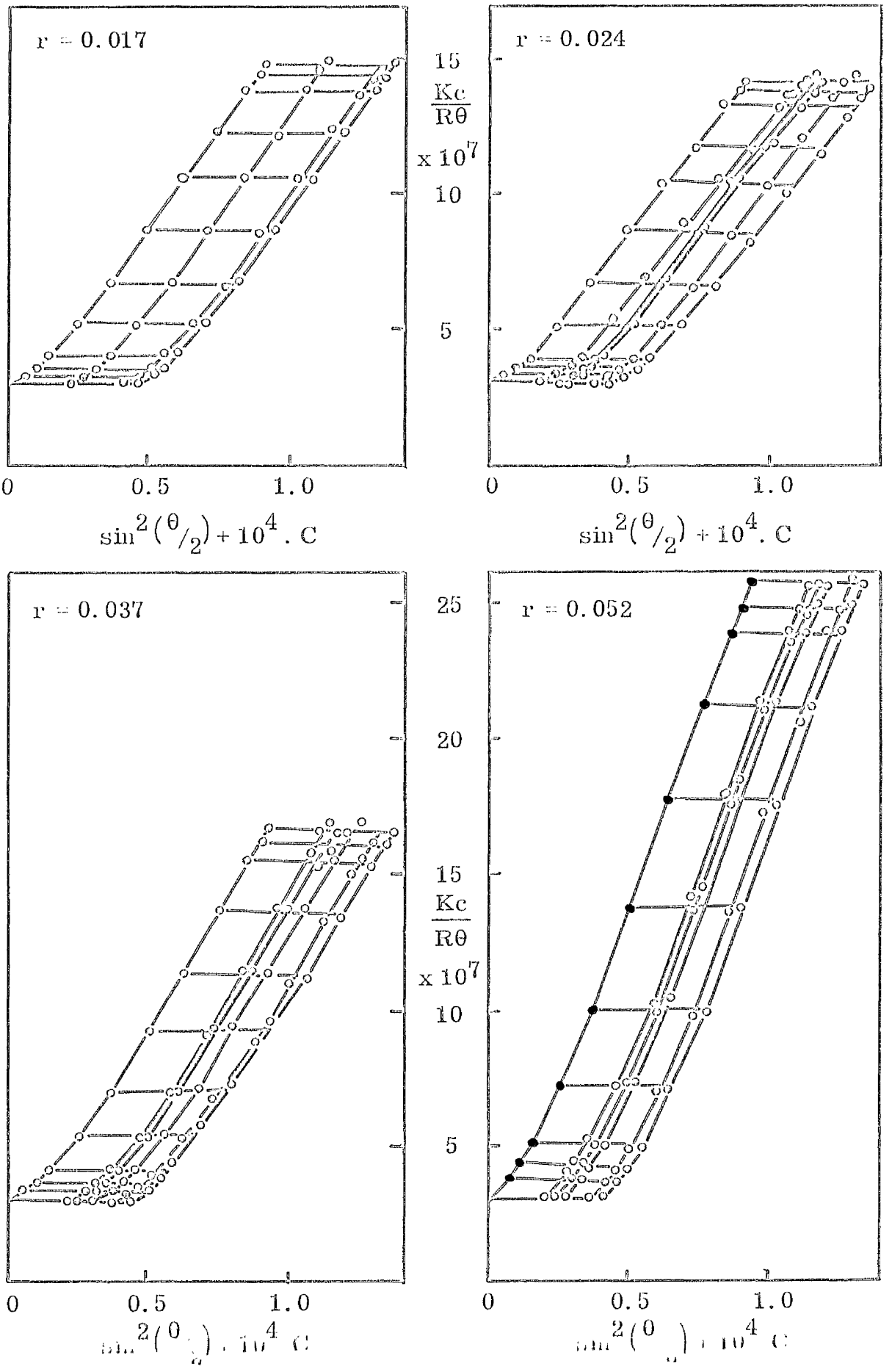
r = 0.017
r = 0.024
r = 0.037
r = 0.052
$\frac{Kc}{R\theta} \times 10^7$
15
10
5
25
20
0
0.5
1.0
$\sin^2(\theta/2) + 10^4 . C$

Fig.3.15

ZIMM AND BERRY PLOTS FOR ϕX174-RFI DNA WITH 0.06 MOLES PF/MOLES NUCLEOTIDE BOUND

The scattering angle range was 30 - 150° and the concentration range 20 - 50μg/ml. The temperature was 25° ± 0.2°C and the solvent BPES. All units are in cgs system.

Top: Zimm plot; information was obtained from this plot as before (Fig.3.2), with respect to the mol. wt.

Bottom: Berry plot of the same data as inthe Zimm.plot. The formula $\left[(Kc/R\theta)^{\frac{1}{2}}\right]_{\substack{c=0\\ \theta=0}} = 1/M^{\frac{1}{2}}$ gives the mol. wt. $(Kc/R\theta)^{\frac{1}{2}}_{c=0} = (1/M)^{\frac{1}{2}}(1/P\theta)^{\frac{1}{2}} = (1/M)^{\frac{1}{2}}(1 + 8\pi^2 Rg^2 \sin^2(\theta/2)/3(\lambda')^2 + \ldots\ldots)$ gives the r.m.s. radius, Rg, from the initial slope of $(Kc/R\theta)^{\frac{1}{2}}_{c=0}$, where λ' is the wavelength of light in solution. $(Kc/R\theta)^{\frac{1}{2}}_{\theta=0} = (1/M + 2Bc + \ldots\ldots)^{\frac{1}{2}} = (1/M)^{\frac{1}{2}} + BM^{\frac{1}{2}}c + \ldots\ldots$ allows estimation of B the second virial coefficient, when B is small, from the slope of $(Kc/R\theta)^{\frac{1}{2}}_{\theta=0}$. $P\theta^{-1} = (Kc/R\theta)_{c=0} / \left[(Kc/R\theta)^{\frac{1}{2}}\right]^2_{\substack{c=0\\ \theta=0}}$ is calculated using the denominator from the Berry plot and the numerator from the Zimm plot at finite angles.

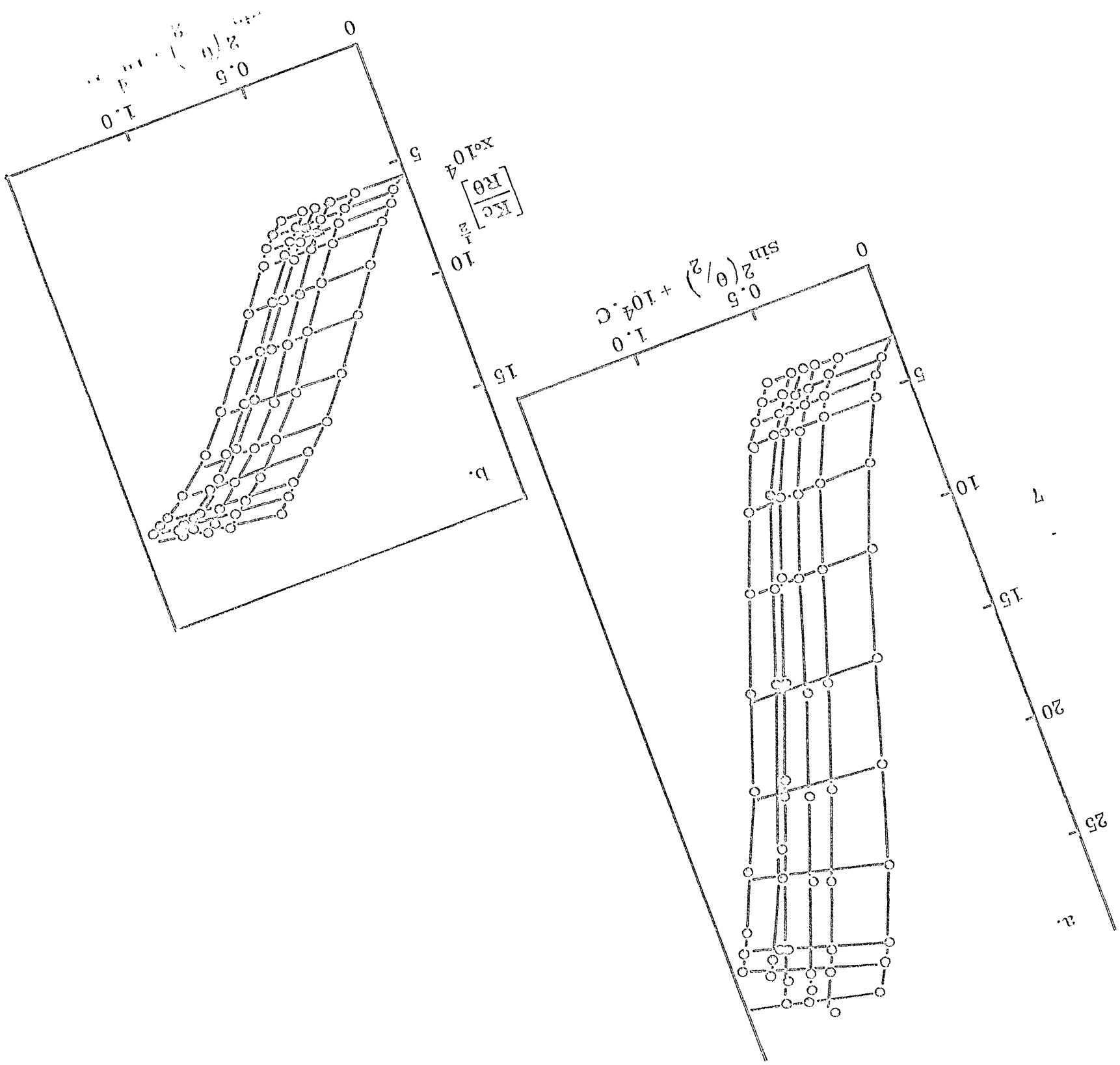
a.
b.
$\left[\frac{Kc}{R\theta}\right]^{\frac{1}{2}}$
$\sin^2(\theta/2) + 10^4 \cdot C$
$\times 10^4$
0
5
10
15
20
25
0.5
1.0

Fig.3.16

RECIPROCAL PARTICLE SCATTERING FACTORS FOR ϕX174-RFI DNA AT DIFFERENT BOUND PF TO DNA RATIOS

The curves were constructed from the respective Zimm and Berry plots as detailed in the legends to Figs.3.2 and 3.15 and section 3.1.4.3. The values of r (moles dye bound/mol.equiv. nucleotide) at which the curves were obtained were: 1. 0.017, 2. 0.024, 3. 0.037, 4. 0.052, 5. 0.060. As before, θ is the angle at which scattering measurements were made.

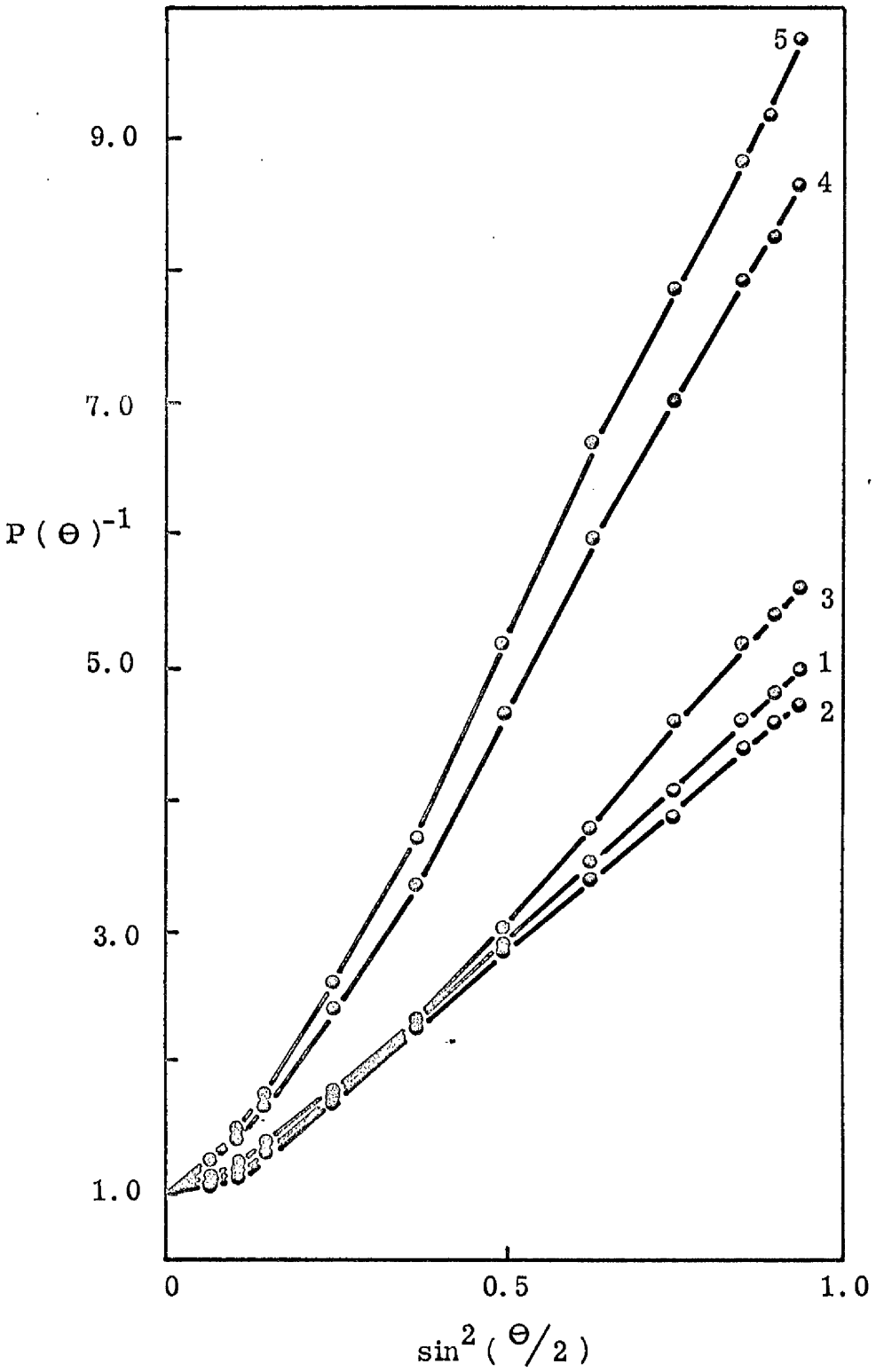
9.0
7.0
5.0
3.0
1.0
P (Θ)-1
0
0.5
1.0
sin2 (Θ/2)
5
4
3
1
2

Fig.3.17

COMPARISON OF EXPERIMENTAL AND THEORETICAL $P\Theta^{-1}$ FUNCTIONS FOR THE COMPACT SUPERCOIL CONFORMATION FROM PF TITRATION

The points indicate the experimental results, the lines computer calculated curves for theoretical models (Fig.3.9.A & B).
(a): r (mol dye/mol equiv. nucleotide) = 0.024, σ = -0.0153; curve (1), interwound model, Rg = 68.5nm, number of superturns, K = 7; curve (2) toroid, Rg = 68.5nm, K = 7; curves (5),(6) interwound model, max. error data, Rg = 78 and 59nm, K = 8 and 6 respectively; curves (3),(4) toroid, max. error data, Rg = 78 and 59nm, K = 8 and 6 respectively.

(b): r = 0.017, σ = -0.0180; curve (1), toroid, Rg = 79.6nm, K = 9; curve (2), interwound model, Rg = 79.6nm, K = 9; curves (3),(4) toroid, max. error data, Rg = 89.5 and 70nm, K = 10 and 8; curves (5),(6) interwound model, max. error data, Rg = 89.5 and 67nm, K = 10 and 8.

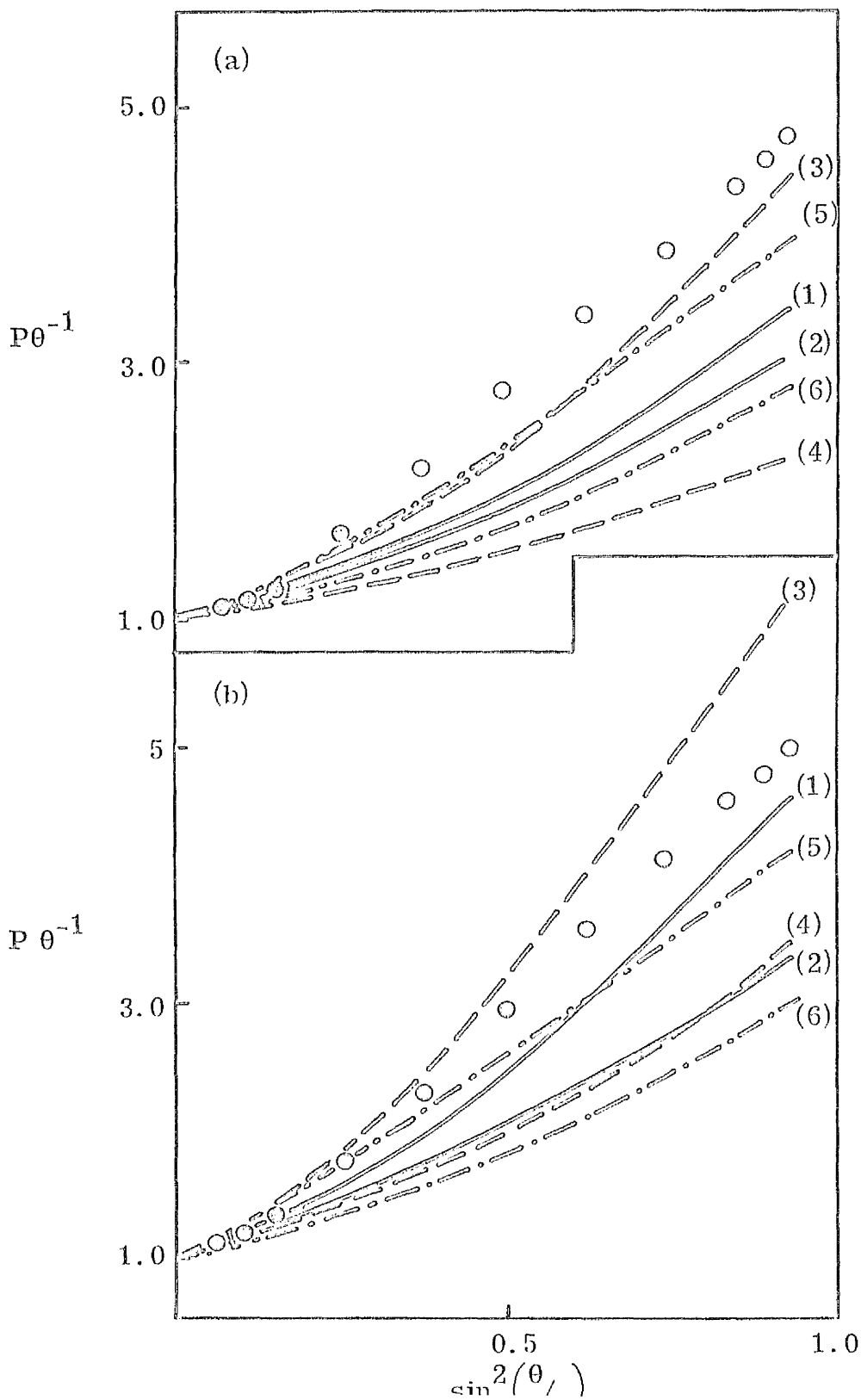
(a)
5.0
3.0
1.0
$P\theta^{-1}$
(3)
(5)
(1)
(2)
(6)
(4)
(b)
5
3.0
1.0
$P\theta^{-1}$
(3)
(1)
(5)
(4)
(2)
(6)
0.5
1.0
$\sin^2(\theta/\ )$

Fig.3.18

COMPARISON OF EXPERIMENTAL AND THEORETICAL $P\theta^{-1}$ CURVES FOR ϕX174-RFI TITRATED TO AN OPEN CIRCLE WITH PROFLAVINE

● RFI with 0.060 mol dye bound/mol equiv. nucleotide, that is, σ virtually zero; ▲ RFII, no dye present (cf. Figs.3.21 and 3.22). The lines are the computed curves using the theoretical $P\theta^{-1}$ function from the calculations in Appendix I and parameter values given in section 3.1.4.4; the numbers on the lines indicates the value of the persistence length used in nm. the points for RFI are above those for RFII, due to extension of the duplex by intercalation.

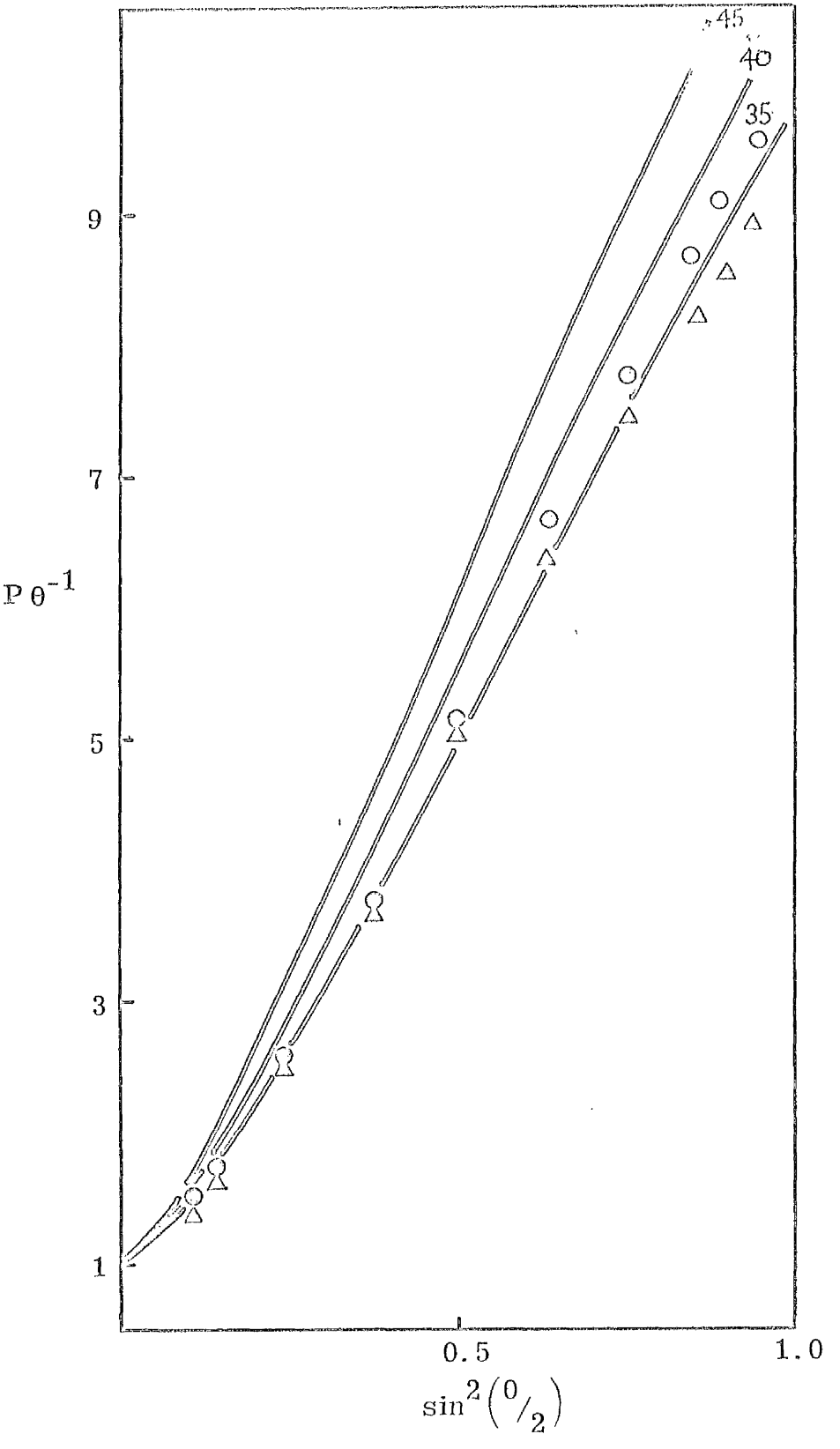
45
40
35
9
7
5
3
1
P θ⁻¹
0.5
1.0
sin²(θ/2)

Fig.3.19

A ZIMM PLOT OF ϕX174-RFII DNA IN EPES AT 25°C

The scattering angle, θ, varied from 30 - 150°C. On the abcissa, c, the concentration is in mg/ml; otherwise all units are in the cgs system. The temperature was 25° $\pm$ 0.2°C and the concentration range, 19 - 45μg/ml approx. The mol. wt. was extracted as described in the legend to Fig.3.2

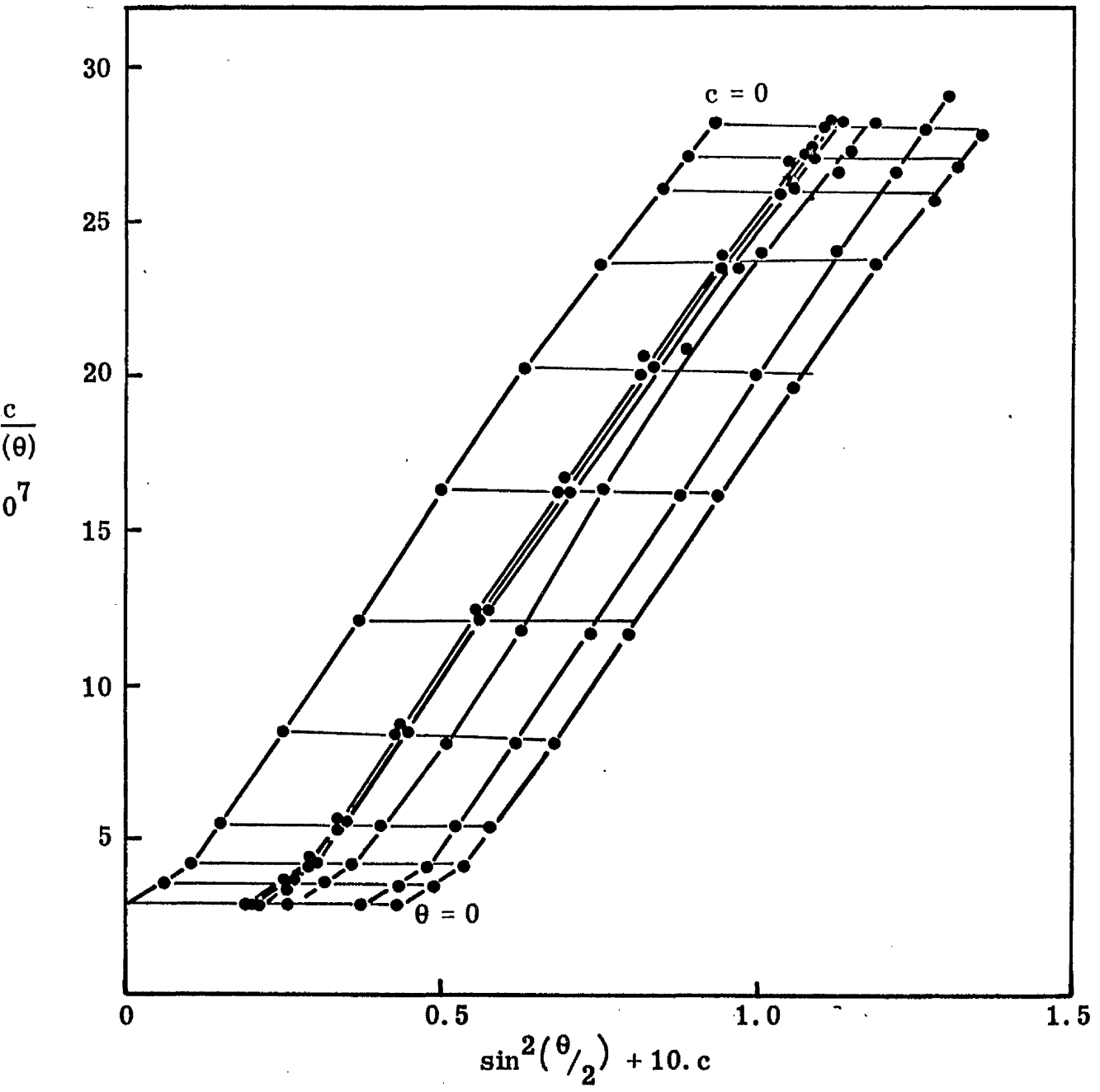
30
25
20
15
10
5
c = 0
θ = 0
0
0.5
1.0
1.5
sin²(θ/2) + 10. c

Fig.3.20

A BERRY PLOT OF ϕX174-RFII DNA IN PPES AT 25°C

The experimental data used here was the same as in Fig.3.19. All units arein the cgs system except c, the concentration, on the abcissa, which is in mg/ml. The mol. wt., r.m.s radius, the second virial coefficient and PΘ function were estimated from the plot as described in the legend to Fig.3.15.

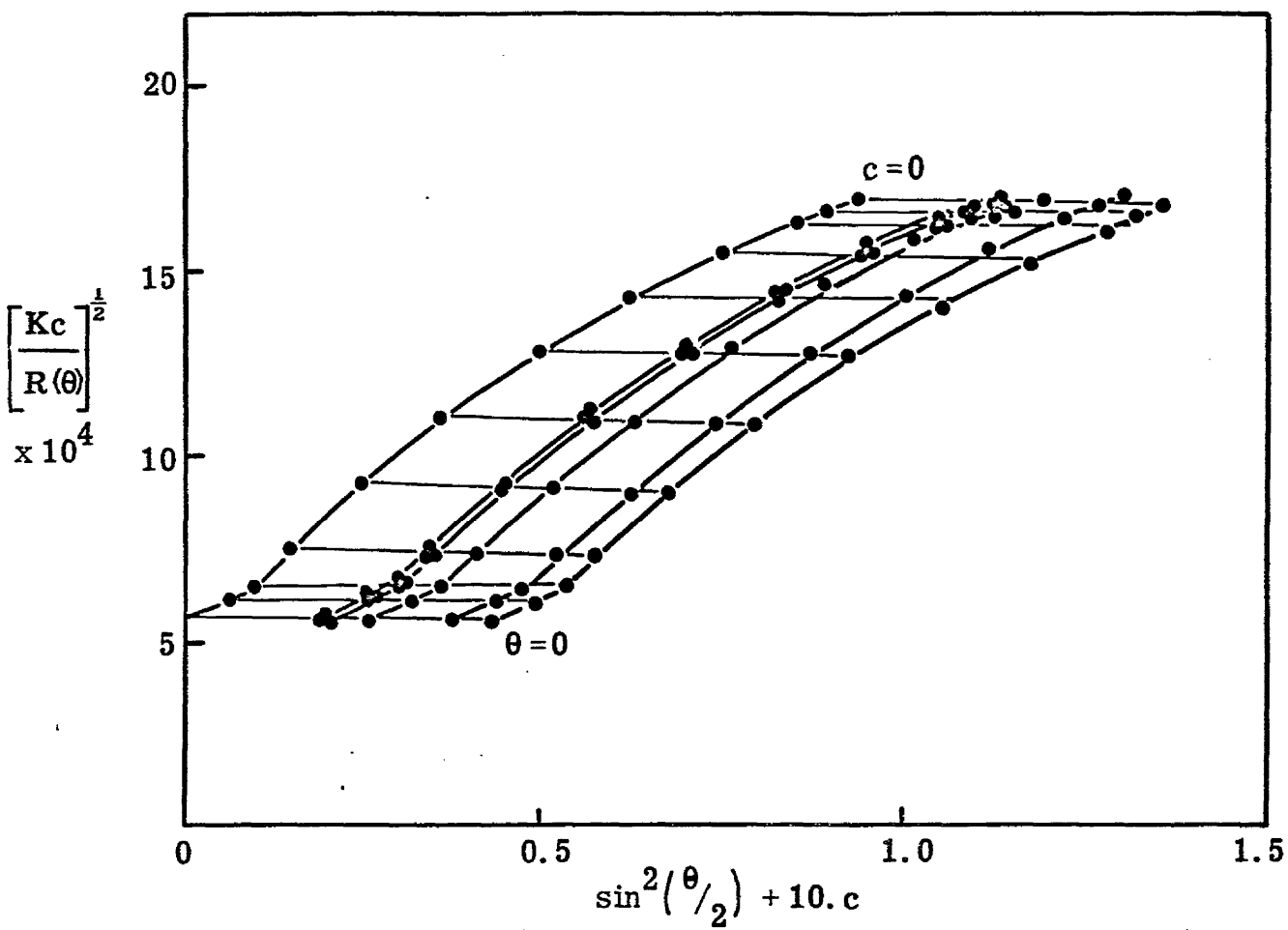
20
15
10
5
0
0.5
1.0
1.5
c = 0
θ = 0
$\left[\frac{Kc}{R(\theta)}\right]^{\frac{1}{2}}$
x 10^4
$\sin^2(\theta/2) + 10.c$

Fig.3.21

COMPARISON OF EXPERIMENTAL AND THEORETICAL $P\theta^{-1}$ CURVES FOR RFII WITH $\epsilon = 0.141$

The solid lines are the theoretical curves for the indicated persistence lengths in nm, $\epsilon = 0.141$ and other parameter values as given in section 3.2.2. The points are experimental values obtained by pooling results from two separate experiments for the extrapolations to zero angle and concentration. The two sets of points were totally compatible

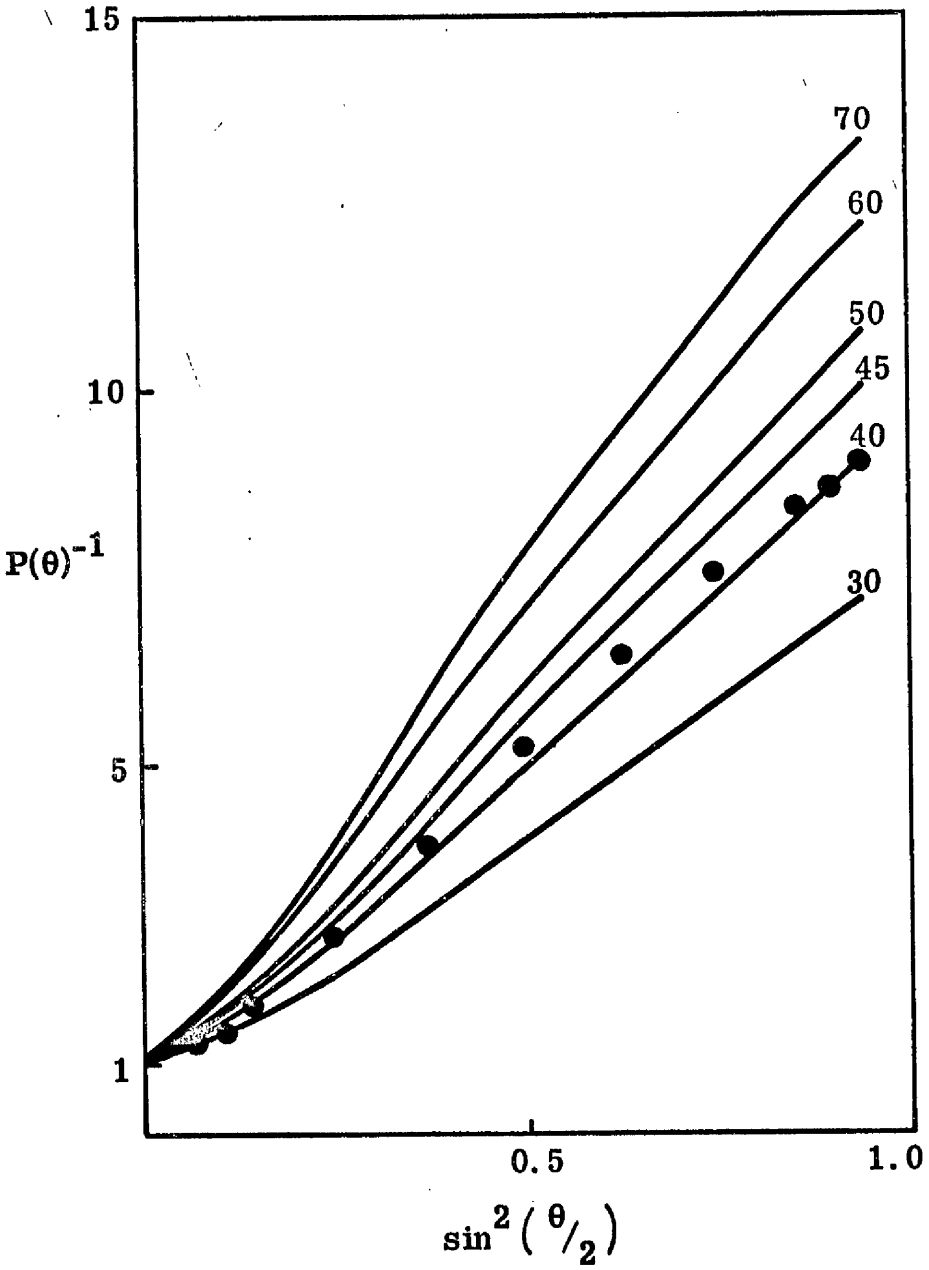
15
10
5
1
70
60
50
45
40
30
0.5
1.0
P(θ)^-1
sin^2 (θ/2)

Fig.3.22

COMPARISON OF EXPERIMENTAL AND THEORETICAL Pe^{-1} CURVES FOR RFII WITH $\epsilon = 0.11$

The meanings of the points lines and numbers is the same as in Fig.3.21. Using this value of ϵ does not seem to give as good a fit to the experimental curve shape as in Fig.3.21.

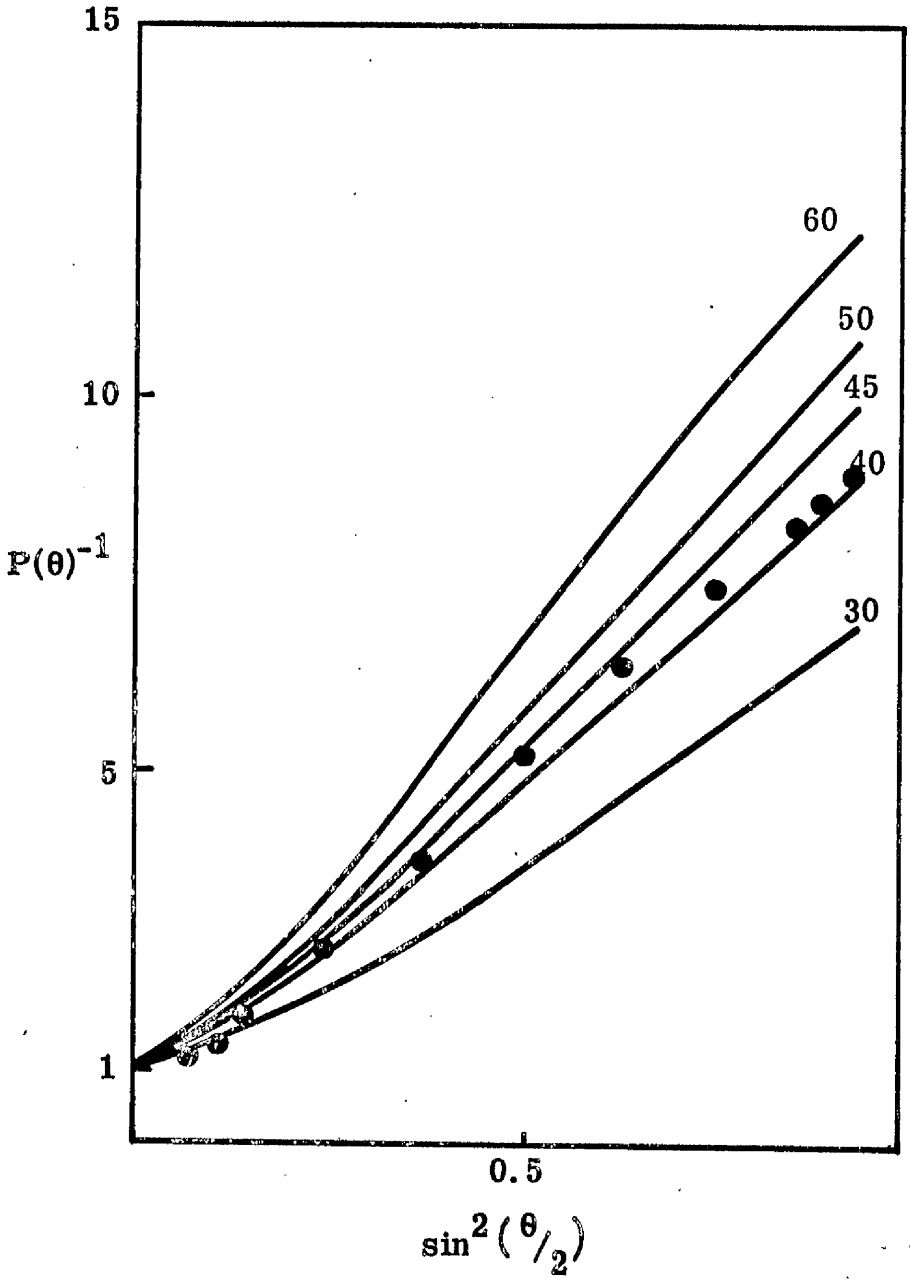
15
10
5
1
$P(\theta)^{-1}$
60
50
45
40
30
0.5
$\sin^2(\theta/2)$

4. DISCUSSION

4

DISCUSSION

4.1

MOLECULAR WEIGHTS AND EXTRAPOLATION TO ZERO ANGLE

The results for the molecular weight of ϕ X174-RF DNA are obviously very dependent on correct extrapolation to zero angle as are the other experimental results, the r.m.s. radius, the second virial coefficient B, and the $P\theta$ function. As mentioned in Section 1.3.4, previous light scattering results have been considered unreliable because of difficulties in this extrapolation (Sharp & Bloomfield, 1968b; Freifelder, 1970; Schmid et al., 1971). From the theoretical $P\theta^{-1}$ curves of Benoit & Doty (1953), Schmid et al. (1971) have estimated that linear extrapolations from values of $P\theta^{-1} > 1.3$ for Zimm plots and $P\theta^{-\frac{1}{2}} > 1.3$ for Berry plots will be in error. Zimm (1948) also estimated that extrapolations to 0^{o} were only valid for $P\theta^{-1}$ less than 1.3. Examination of the various $P\theta^{-1}$ curves (Figs. 3.5, 3.7, 3.16, 3.21) reveals that extrapolation has been made from at least two points below $P\theta^{-\frac{1}{2}} = 1.3$ where Berry plots have been used. Thus correct extrapolations are believed to have been made. The Berry plots used in Sections 3.1.4.3 and 3.2.1 seem to provide a valid method of allowing correct extrapolation to 0^{o} for molecules with dimensions just over those correctly examinable by the Zimm method. Thus the molecular weights are reduced marginally from Zimm plot values to values compatible with other experiments and curvature at low angles is reduced.

The other main factor rendering light scattering results suspect has been anisotropy (Schmid et al., 1971); this has been found to be negligible.

The molecular weight of ϕ X174-RF DNA found by pooling information from all experiments is $3.22 \pm 0.05 \times 10^{6}$ (S.D. of 20). Sinsheimer (1959) obtained a value of $1.7 \pm 0.1 \times 10^{6}$ for single-stranded ϕ X174 DNA by light scattering and hence the value for the double-stranded form should be 3.4×10^{6}. Sinsheimer, however, used a value of the refractive index increment (dn/dc) of 0.201ml/g at 436nm. More recent work has suggested that the value is much lower (Cohen & Eisenberg, 1968; Krasna, 1970) so

that Sinsheimer's results should have given a mol. wt. of 4.5×10^6 approx. for the double-stranded form, using the corrected value of 0.175ml/g for dn/dc at 436nm. The value of 3.22×10^6 is considerably lower than this, a fact that can probably be attributed to stringent modern dust-clearing procedures; other factors such as variations in the proportions of linear and circular molecules in Sinsheimer's preparations may contribute.

It has become apparent recently (Freifelder, 1970; Schmid & Hearst, 1969) that previously accepted values of molecular weights (Thomas & MacHattie, 1967) were somewhat high in particular λ and T4 DNA. These and other workers (see Freifelder, 1970 for a review) have started to establish soundly based values for DNA molecular weights by absolute methods, e.g. sedimentation equilibrium in a density gradient, to allow their use as standards in relative methods, e.g. electron microscopy, sedimentation velocity. These redeterminations have indicated a reduction of the "best" molecular weights for a number of commonly used phage DNA molecules - T4, T5, T7 and λ by approx. 10% to about 110, 68, 25 and 30 millions respectively. The re-evaluation of the molecular weight of ϕ X174 RF, with respect to the previously used value of 3.4×10^6 which seemed compatible with other DNA molecular weight evaluations, to 3.22×10^6 is in agreement with this trend, though somewhat less quantitatively, the reduction being 5 - 6%. It seems that this mol. wt. for ϕ X174-RF DNA is quite accurate and, therefore, usable as a standard, with, if necessary, allowance for circularity.

4.2

ROOT MEAN SQUARE RADII

The final value of the r.m.s. radius of RFI at room temperature was found from pooling all available experiments to be 97.4 ± 8.0nm (S.D. of 5), which is well within the error allowed in calculating $P\theta^{-1}$ curves in Section 3.1.2. The variations in the r.m.s. radius with σ slot together well (Figs. 3.8, 3.12) forming a clean composite picture. From σ = -0.027 to -0.021 approx. there are small variations which presumably represent small variations within one structure; from σ = -0.021 to -0.017 approx. the r.m.s. radius drops from over 90nm to between 60 and 70nm, obviously indicating some major structural transition. At the same time the sedimentation coefficient only increases slightly; the most plausible explanation for this is a change in the free-draining properties of the molecule (Tanford, 1961; Flory, 1953). For example, if the structure changes from a Y shape (Fig. 1.2c) to a condensed toroid (Fig. 3.9.b), then the molecule will intuitively be expected to become more flexible and less free-draining. This could account for such a small increase in the sedimentation coefficient as the dimensions of the molecule shrink rapidly.

From σ = -0.017, the r.m.s. radius increases monotonically to a value of 120nm approx. at σ = 0 at the open circular conformation; the increase in this value over the one of 109.4nm for RFII without dye, is presumably due to the extension of the molecule by dye intercalation.

The persistence length of DNA falls with increasing temperature (Gray & Hearst, 1968) and increasing dye bound (Sections 3.1.4.4, 3.2.2), and dye intercalation causes a lengthening of the molecule. Thus the transitions observed here cannot be quantitatively identical to those in supercoiled DNA molecules at different values of σ at room temperature. However, it seems very unlikely that the same qualitative transitions do not occur.

4.3

SECOND VIRIAL COEFFICIENT

The second virial coefficient, B, is a measure of the deviation of the solution from ideality and theta conditions (Flory, 1953), when B = 0. Harpst et al. (1968) and Dawson & Harpst (1971) have found slightly positive values of B in BPES buffer, for large intact T7 and λ DNA molecules and Dawson and Harpst (1971) found λ circular DNA to have a marginally higher value than λ linear DNA. Other workers, however, have found a zero value of B in similar solvents, for linear DNA (Froelich et al., 1963; Reichmann et al., 1954; Cohen & Eisenberg, 1966) and there is probably a molecular weight dependence for B as predicted theoretically (Flory, 1953; Tanford, 1961) and found experimentally, for example with polystyrene in organic solvents (Berry, 1966). Thus the zero value of B for RFII is not surprising.

For RFI, although the non-zero values of B found are only just significantly different from zero, some qualitative discussion is possible. The small negative value obtained at 25°C was found repeatable and does seem to exist. From comparing the kinetics of reaction with formaldehyde of Forms I and II of PM2 and ϕ X174-RF DNA moleucles at $\sigma = -0.04$, Dean & Lebowitz(1971) concluded that there was alteration of the secondary structure of the DNA duplex, which meant increased exposure of normally buried base-base hydrogen bonding groups, if not an actual rupture of the duplex hydrogen bonds. This could be imagined to disturb solution structure, with a negative value of ΔS (Sinanoglue & Abdalnur, 1964) with respect to the unstrained duplex, and hence to decrease B. The negative value of B has, therefore been tentatively attributed to the increased exposure of hydrophobic bases due to torsional strain by the superhelix; although the DNA has $\sigma = -0.025$, not -0.04, the effect noted by Dean & Lebowitz(1971) could still be significant. One consequence of this is that the partial specific volume, density increment and other such properties of superhelical DNA may be slightly different from normal linear DNA and hence adoption of well-established values with respect to normal DNA for such parameters may affect the accuracy of hydrodynamic experiments with supercoiled DNA. The

refractive index increment, however, would remain the same as conformational changes, such as denaturation, appear to have a negligible effect on this parameter (Krasna, 1970).

Bauer & Vinograd (1970a) have calculated, from the binding of EB to supercoiled SV40 DNA an expression for the free energy of supercoiling, Gsc, which is the energy which would be released as the molecule relaxed to an open circular form, if one of the duplex strands were nicked. Thus the supercoil is thermodynamically unstable and does not relax to an open circle, merely because the activation energy necessary (to break a covalent bond) is very high. The greater initial affinity of supercoils over nicked circular DNA for intercalating ligands is a reflection of the negative value of Gsc. The Bauer & Vinograd (1970a) equation is:

$$Gsc/RF = 0.88\tau^2 - 0.038\tau^3 \qquad (25)$$

where R is the gas constant and T is the absolute temperature. The corresponding equation, using intensive quantities, assuming Gsc proportional to molecular length, is (Davidson, 1972),

$$g(\sigma)/RT = 422\sigma^2 - 880\sigma^3 \qquad (26)$$

where $g(\sigma)$ is the free energy of supercoiling per ten base pairs. ϕ X174-RF and SV40 DNA have similar molecular weights (3.22×10^6 and 3.1×10^6 respectively) and G-C contents (42 and 41% respectively) so that even if Gsc is not proportional to molecular length, or if dye binding depends on G-C content eqn. (26) should be a good description of ϕ X174-RFI DNA. From this, at $\sigma = -0.025$, Gsc = 78kcal/mole DNA, so that the free energy of super coiling is certainly enough to break several hydrogen bonds (about 4kcal/mol equiv. each) and expose some bases to solvent, although this is certainly not a major factor in the fairly large value of Gsc (see Section 4.4).

The behaviour of B in the temperature and PF experiments probably reflects two different effects. In the PF experiment, the negative value is found from $\sigma = -0.025$ to -0.0098; at lower values of $|\sigma|$ down to zero, B is zero, which is in accord with the hydrogen bond rupture hypothesis. The temperature experiment encompasses a smaller range of σ(-0.027 to -0.017)

where, according to the above interpretation, B should be negative. However, at 14.9^{o}C B is positive, becomes negative at 25^{o}C and positive again above 30^{o}C. This probably is an effect on B independent of any small tertiary structure transitions, and to do with the independent variation of the enthalpy and entropy contributions to the free energy, for the solvation of apolar bases in aqueous solution, with temperature. This type of behaviour has been found (to a greater degree) in poly A (Eisenberg & Felsenfeld, 1967) in which the bases are completely exposed to the solvent in single strands.

4.4

STRUCTURE TRANSITIONS

As noted in Section 3.1.2.3 at room temperature(σ = -0.025)ϕ X174-RFI is almost definitely some sort of Y shape, although exactly what is not clear as a really good fit for the experimental points was not found. It now seems possible that the reason for this is some breakdown in secondary structure; this could, in turn, alter the exact number of physical superhelical turns (Wang 1969a). However, it seems likely that this effect is small (e.g. the linear monotonic variation of τ with temperature) and wide error limits in τ have been allowed.

An interesting point about the Y structure is that all the Y's predictable from the r.m.s. radius have cylinder arm radii of 15 to 16nm, whereas the equivalent straight interwound model has a radius of 19.4nm and the toroid has a small radius of 19.8nm. Intuitively, one would imagine that the most thermodynamically likely conformation would be that which caused the least curvature of the duplex and a rough calculation seems to confirm. Gray & Hearst (1968) have derived an expression linking the free energy of bending of a DNA molecule with its curvature and persistence length by equating the continuous homogeneous thread model of Landau & Lifshitz (1958) with the Kratky & Porod (1949) worm-like coil model. This can be written

$$Gb = RTlzp^2/2 \qquad (27)$$

where Gb is the free energy/mole DNA required to bend a DNA molecule of contour length l and persistence length z to a curve with curvature p, which at any point is equal to the reciprocal of the radius at that point. For a curve wound as a helix round a cylinder of radius r at a pitch angle "a", $p = \cos^2 a/r$ (Fuller, 1971). R is the gas constant and T the absolute temperature; the expression does not apply to strongly bending molecules. Using this relationship and z = 41nm (see Section 3.2.2), Gb(Y) = 21 kcal/mole DNA, Gb (straight interwound) = 72 kcal/mole DNA and Gb (toroid) = 73 kcal/mole DNA. Thus, even from these simple considerations, the Y shape appears more likely, although the calculations are approximate since

constant curvature has been assumed, which is obviously not the case at the Y intersection, and perhaps not at the Y and interwound end-loops.

In Section 4.3 the total free energy of superhelix formation (Gsc) was found to be 78 kcal/mole at this point, $\tau = -12$. Thus there must be other components to Gsc. Davidson (1972) gives these as: (a) Gb; (b) torsional energy, Gt; (c) energy due to interactions between topologically distant segments in the characteristic contorted configurations of a supercoiled DNA, Gi. Davidson states that Gi is probably small.

At $\sigma = -0.018$, the PF experiment at the lowest value of bound PF, the toroid seems a fairly good model (Fig. 3.17) with the interwound model ruled out. Here ($\tau = -9$) Gsc = 43 kcal/mole DNA and Gb = 20 kcal/mole. For the interwound model Gb = 20 kcal/mole so the decisive factor here is probably Gt.

Fuller (1971), using an elastic rod as a model for the DNA duplex and, in effect, considering only Gb and Gt has derived an energy expression for the rod twisted into a supercoil. It can be written:

$$Gsc = \tfrac{1}{2}Alp^2 + 2\pi^2 C(\alpha - \tau)^2/l \qquad (28)$$

where A is the coefficient of flexural rigidity, C is the coefficient of torsional rigidity. The first expression on the right hand side is exactly equivalent to Gb, the second to Gt. Attempts to use eqn. (28), however, were hampered by the fact that the quantity $\alpha - \tau = \beta$ is not known, having been previously assumed a constant for the dye titration to evaluate τ. In addition C must alter with B, since when $\beta = 487$ (B structure of DNA) Gt $\simeq$ 0, and hence C must be zero.

One calculation was attempted; if $\beta = \beta 12$ at $\tau = -12$, $\beta = \beta 9$ at $\tau = -9$, Gi is assumed zero and C assumed constant over this range then, using eqn. (28) at $\tau = -12$ and -9, $\beta 12/\beta 9 = 1.55$. As this implies massive changes in the duplex winding, this seems impossible. Thus either C has changed or Gi is not negligible or both; the last seems most likely and this suggests that mathematical models of supercoiling will have to be even more complex to describe this phenomenon correctly.

At $|\sigma| < 0.018$ no models were very good (Figs. 3.11, 3.17) although the toroid error limits were always nearer the experimental points. It is likely that the structure here deviates from an exact toroid, e.g. flattens somewhat, and also the molecule will be becoming flexible, making the rigid models used inapplicable. As σ decreases to zero, the toroid turns can be expected to come out uniformly so that the molecule goes through a looped circle conformation to an open circle. There are no good models available for this state with which to construct $P\theta^{-1}$ curves for comparison with experimental values (Fig. 3.16), except at the open circular configuration which is considered later (Section 4.5).

The conformation changes deduced for moving from $\sigma = -0.027$ to 0 are shown in Fig. 4.1.

Upholt et al. (1971) have, as mentioned, obtained for SV40, PM2 and λb2b5c DNA curves of the type in Fig. 1.3. They then made electron micrographs of DNA molecules in region I, at the transitions of regions I and II, and II and III, and in region III. They concluded: (a) as supercoils were introduced in region IIIB to about $\sigma = -0.005$, there was little effect on the molecule and the hydrodynamic volume remained the same; (b) in region IIIA to the maximum at the boundary with region II the superhelical loops decreased the r.m.s. radius in a spherically coiled form thus increasing the sedimentation coefficient; (c) region II corresponded to a gradual change from a spherically coiled form to a tightly wound linear form; (d) the transition from region II to I represented a transition to branched Y forms.

The results obtained here disagree slightly with (a) in that some contraction of the dimensions of the molecule has been observed in this region. Proposition (b) seems very reasonable and coincides with the conclusions reached here. However, proposition (c) is in conflict with the results here; these suggest a direct and rapid transition from a spherically coiled toroidal form to a Y structure with further tightening of Y in region II and that this is masked in the ultracentrifuge by alteration of the free draining properties of the molecule. Thus the rigid straight interwound

form never seems to exist in solution. Although there is no information here it seems likely that the transition from regions II to I represents further branching to, say, H-shapes. Branching has also been invoked to explain the sedimentation behaviour of normal λ supercoiled DNA (Hinton & Bode, 1970), which is presumably in region II, as are almost all naturally occurring supercoiled DNA molecules (Wang, 1969b). Thus it seems that electron micrographs must be extrapolated with extreme caution to solution conditions. The use of included controls, such as normal PM2 DNA by Upholt et al. (1972) can monitor individual variations in electron micrographs but cannot help in interpretation of results with respect to solution structure. The almost universally used protein monolayer method of Kleinschmidt & Zahn (1959) for preparing electron micrographs subjects the molecules to strong spreading forces as part of the process to ensure clear visualisation of the molecules by eliminating three dimensional coiling due to thermal fluctuations. This process, however, obviously distorts molecules with respect to solution and could easily be imagined for example to pull out a Y structure into a linear form. These points are not new and have been discussed in some detail (Kleinschmidt et al., 1956; Vinograd et al., 1968). A particularly confusing situation has been found by Wang (1969a) where the effect of ionic strength on the number of superturns in closed cyclic λ DNA as examined by electron microscopy (Bode & MacHattie, 1968) seemed different in magnitude and sign from that found by Wang from hydrodynamic experiments.

The relevance of formaldehyde fixing experiments is questioned by these results also, in particular the temperature experiment. In formaldehyde fixing experiments, the DNA is incubated at a defined temperature (30° - $70^{\circ}C$) with formaldehyde, which is considered to "fix" the DNA duplex in the state it was in at that temperature, specifically by reacting with free groups which normally hydrogen bond (e.g. Inman, 1964); experiments are then performed at room temperature. Thus titrations of supercoiled DNA with temperature of fixing, examined by electron microscopy (Follet & Crawford, 1967) or sedimentation (Rhoades & Thomas, 1968) have been performed and show a transition to $\sigma = 0$ at about $50^{\circ}C$ and further superhelix winding

with positive turns at higher temperatures. However, the work reported here and also the temperature coefficients of Upholt et al. (1971) and Wang (1969a) for σ, imply no large unwinding of supercoiled DNA takes place at these temperatures. In fact formaldehyde fixing seems a somewhat arbitrary procedure, as the reaction is normally stopped after 10 min., before completion of the reaction; in addition it now seems that formaldehyde reaction at higher than room temperatures is more a reflection of the DNA duplex "breathing" (Utiyama & Doty, 1971) i.e. transient breaking and joining of the duplex hydrogen bonds, rather than permanent hydrogen bond rupture. Thus in the absence of really exact knowledge of what happens in the reaction, a kinetic approach with strict controls seems a better experiment (e.g. Dean & Lebowitz, 1971). The formaldehyde fixing experiments will be internally consistent but their relation to normal solution conditions is hard to ascertain.

4.5

PERSISTENCE LENGTHS

The correctness of the experimental $P\theta^{-1}$ against $\sin^2(\theta/2)$ curves is closely related to the correctness of extrapolation to 0^o; as discussed, this is believed to have been achieved with some precision. The anisotropy is also negligible.

The value of 41 ± 3.5nm for the persistence length of RFII seems to be reasonably accurate for further reasons: firstly, the result has been obtained from the shape of the whole scattering curve from 0^o to 150^o rather than from the initial slope and hence the r.m.s. radius (Eisenberg, 1969; Hays et al., 1969) which has a large error or from the high angle assymptote which has also a large error (Ptitsyn & Federov, 1965); secondly, as it is a small molecule, the curves of $P\theta^{-1}$ are insensitive to changes in the excluded volume factor (e.g. Figs. 3.21, 3.22) rendering an exact knowledge of this parameter unimportant; thirdly, the value is in good agreement with values from hydrodynamic techniques (Ptitsyn & Eizner, 1961; Gray et al., 1967; Hearst et al., 1968b; Triebel et al., 1971).

The Kuhn statistical element length (Kuhn, 1936, 1939) is equal to exactly twice the persistence length and is the equivalent bond length which allows the molecule to be treated as a freely jointed chain. Then (Tanford, 1961)

$$Rg^2 = mb^2/6 \qquad (29)$$

for a linear chain where Rg is the r.m.s. radius, b is the Kuhn statistical element length and m is the number of these in the molecule, if m is sufficiently large for statistical analysis. Cassassa (1965) has calculated that Rg for a linear freely jointed chain is just twice that for the equivalent circular molecule. Therefore

$$Rg^2 \text{ (circle)} = mb^2/12 \qquad (30)$$

Using b = 82nm and m = 20, which should be large enough to use eqns. (29) and (30), Rg for RFII is calculated as 106.1nm which is gratifyingly close to the experimental of 109.4nm. The persistence length found is, therefore, also compatible with the r.m.s. radius from the initial slope, providing a

good internal check on the experiment.

RFII DNA has at least one single stranded nick, which might be thought to affect its flexibility; however, Hays & Zimm (1969) have shown that single stranded nicks have no effect on the flexibility of DNA.

Finally there has been one previous report of light scattering on circular DNA (Dawson & Harpst, 1971) using a low angle instrument (down to 10^{o}) but λDNA, mol. wt. 30×10^{6} approx.; these experiments, therefore, encountered the difficulty in extrapolation to 0^{o} discussed previously, correspondingly giving a rather high mol. wt. ($34 \pm 3 \times 10^{6}$). No serious attempt was made to estimate the persistence length. Thus it would be interesting to apply the Pθ function calculated for circular DNA to these results; however, the results given did not include data extrapolated to zero concentration and the solution had a significant positive second virial coefficient so that the results actually given are not directly applicable to the calculated Pθ function. However, a rough fit indicates a persistence length of 60nm approx., which is higher than the value obtained here. However, it is known that DNA on being circularised contains a small amount of dimer and higher aggregates. The intercept in a Zimm plot is a weight average, the initial slope a Z-average and the rest of the curve higher averages (Geiduschek & Holtzer, 1958); thus any small contamination might hardly show in the intercept, but affect the shape of the curve significantly. That this may have happened is corroborated by the fact that the r.m.s. radii of the linear and circular forms are rather unexpectedly close. In considering the $P\theta^{-1}$ and persistence length of RFI titrated with PF to an open circular form there are a number of additional factors that must be considered. First, the titration may not be exact and some small torsion may remain in the DNA duplex; there is no real way of checking this and it might be expected to reduce by a small amount the dimensions of the molecule, thus apparently reducing the persistence length. Secondly, in calculating the $P\theta^{-1}$ function it was assumed that each dye molecule bound intercalated and lengthened the duplex by 0.335nm (Drummond et al., 1966); however, it has been suggested that not all the bound PF intercalates (Ramstein et al.,

1972). This would mean an overestimation of the molecular contour length in the theoretical $P\theta^{-1}$, and again an underestimation of the persistence length. This effect seems likely to be very small, especially in view of the clear cut spectrophotometric isobestic points obtained. In Fig. 3.18, the points for the titrated RFI are higher than those for RFII, indicating a more extended molecule, as do the relative r.m.s. radii. However, when the extension due to intercalation is allowed for the persistence length does seem to have fallen (to 36 $\pm$ 3nm) on the binding of dye. Although this is the effect the above errors would have, their effects seem unlikely to be as large as this (e.g. in Fig. 3.16 curve 4 (r = 0.052) is not far from curve 5 (r = 0.06)) and the qualitative conclusion is made that dye intercalation makes DNA more flexible. Bauer & Vinograd (1970a) have also suggested this on the basis of the asymmetry of the free energy of supercoiling with respect to the sign of τ, calculated from EB binding experiments and Lloyd et al. (1968) have found this also, from direct hydrodynamic experiments. Mauss et al. (1967) found that, at high values of bound dye ($>$ 0.13 moles dye/mol. equiv. monomer), the persistence length increased. However, their approach was not exact and there is some indication, anyway, from their results, that at low bound dye the persistence length drops.

4.6

APPLICATION OF RESULTS AND CONCLUSION

The value of this work in examining biological systems if fairly obvious and straight-forward.

Firstly, the conformation changes undergone by superhelical DNA as a function of σ have been mapped out; this allows visualisation of the problems implicit in the functions of transcription, replication etc., of circular DNA molecules as discussed in Section 1.3.5.2 (see also Dove et al., 1971). For example, the point at which replication stops until an untwisting enzyme acts could be the rapid transition from a spherically coiled form to a Y shape. Also, for example, the initial preference of the duplex under small twisting stresses to supercoil in a non-interwound fashion may have implications for supercoiled types of structure in eukaryotic chromosomes. Obviously in vivo, there are many protein binding effects on DNA conformation; as the free solution conformations now seem established, it would now be possible to examine and visualise protein effects on supercoiled DNA structure, e.g. the w protein of Wang (1971), RNA polymerase or deoxyribonuclease.

Secondly, a good value of the persistence length for the worm-like coil model for DNA has been found from light scattering, which agrees with values from hydrodynamic experiments; this resolves the difficulties caused by previous discrepancies and allays any suspicion that some unconsidered feature of the model was responsible for these. A good value for the persistence length is a quantitative measure of stiffness in the DNA duplex which is needed for even the simplest thermodynamic calculations with respect to DNA packaging, untwisting and rates of these, e.g. the simple calculations in Section 4.4 for the free energy of forcing DNA into superhelical forms.

Fig.4.1

PROJECTED STRUCTURE TRANSITIONS OF ϕX174-RFI DNA AS THE NUMBER OF SUPERCOILS DECREASES FROM 12 TO ZERO

1. $\tau = -12$, $\sigma = -0.025$; rigid interwound extended Y shape.
2. $\tau = -8$, $\sigma = -0.017$; fairly rigid very compact toroid-like structure.
3. $\tau = -4$, $\sigma = -0.086$; flexible looped circle.
4. $\tau = 0$, $\sigma = 0$; open circular form.

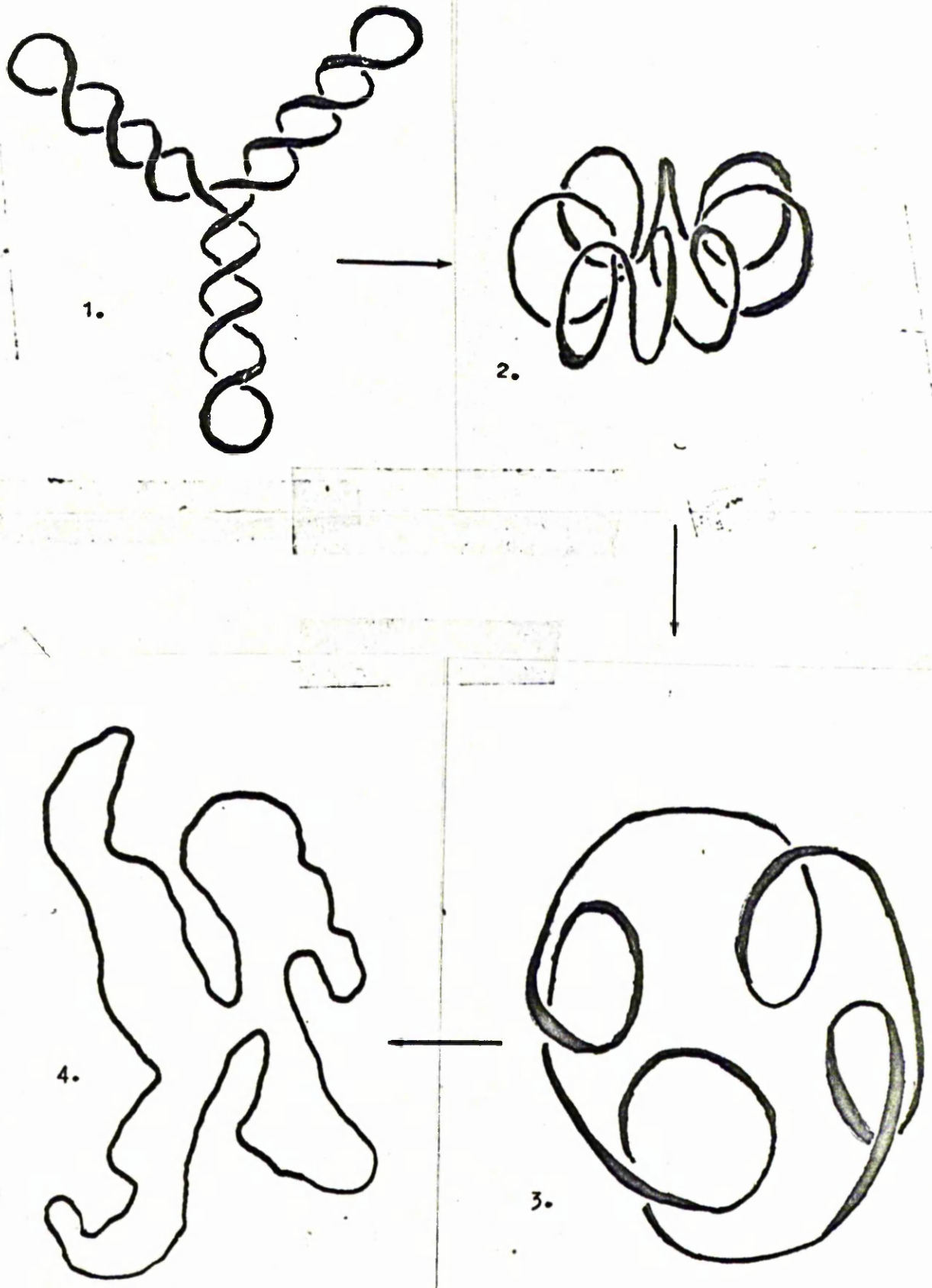
1.
2.
3.
4.

APPENDIX I

CALCULATION OF P_θ FOR A CIRCULAR WORM-LIKE COIL

For any macromolecule examined by light scattering the variation of scattered intensity with the scattering angle, θ, is expressed by a function $P(\theta)$ (Geiduschek & Holtzer, 1958)

Generally

$$P(\theta) = {}^{1}/_{N^2} \int_0^\infty f(r) \quad \sin \mu r/\mu r \quad dr \qquad \ldots\ldots(1)$$

Where $\mu = \frac{4\pi \quad \sin {}^{\theta}/_{2}}{\lambda}$ $\qquad P(\theta) = \frac{\text{scattered intensity at } \theta}{\text{scattered intensity at } 0}$

λ= wavelength of light in solution

N = number of segments in molecule

$f(r)$ = average number of pairs of elements separated by a distance r

$= N \int_0^N w(r,t)\, dt$ for a circular molecule

where $w(r,t)$ is the probability that elements separated by a distance t along the contour length of the molecule are separated by a distance r in space.

Hence $$P(\theta) = \frac{1}{N} \int_0^N \int_0^\infty w(r,t) \frac{\sin \mu r}{\mu r} \quad dr\, dt \qquad \ldots\ldots(2)$$

For $w(r,t)$ the Daniels distribution function (Daniels, 1952) has been used with the modification to include the excluded volume parameter (Gray et al., 1967; Sharp & Bloomfield, 1968)

This gives

$$w(r,t)dr = \left(\frac{3\lambda}{\pi t} \frac{1}{(\lambda t)^{\epsilon}}\right)^{\frac{3}{2}} \left(\frac{2}{\pi}\right)^{\frac{1}{2}} \exp\left[-\frac{3\lambda}{2t} \frac{1}{(\lambda t)^{\epsilon}} r^2\right]$$

$$\left(1 - \frac{5}{8\lambda t} + \frac{2}{t^2} \frac{1}{(\lambda t)^{\epsilon}} r^2 - \frac{33\lambda}{40t^3} \frac{1}{(\lambda t)^{2\epsilon}} r^4\right) r^2 \, dr \ldots(3)$$

where ϵ is the excluded volume factor

$\frac{1}{2\lambda}$ is the persistence length

and all distances are measured in terms of b, an arbitrary segment length.

This equation for the distribution function of a linear molecule is easily converted to that of a circular molecule following Zimm & Stockmayer(1949).

Hence for a circular molecule

$$w(r,t)dr = A \exp\left[\frac{-3\lambda}{2}\left(\frac{(N-t)^{(1+\epsilon)} + t^{(1+\epsilon)}}{(N-t)^{(1+\epsilon)}t^{(1+\epsilon)}\lambda^{\epsilon}}\right) r^2\right]$$

$$\times \left(1 - \frac{5}{8\lambda t} + \frac{2r^2}{t^{(2+\epsilon)}\lambda^{\epsilon}} - \frac{33r^4\lambda^{(1-2\epsilon)}}{40t^{(3-2\epsilon)}}\right)$$

$$\times \left(1 - \frac{5}{8\lambda(N-t)} + \frac{2r^2}{(N-t)^{(2+\epsilon)}\lambda^{\epsilon}} - \frac{33r^4\lambda^{(1-2\epsilon)}}{40(N-t)^{(3-2\epsilon)}}\right) r^2\,dr \quad \ldots\ldots(4)$$

Where A is the normalising constant, and $\frac{1}{A}$

$$= \int_0^{\infty} \exp(-kr^2)\,(a + br^2 + cr^4)\,(p + qr^2 + vr^4)\,r^2\,dr$$

Where $a = 1 - \frac{5}{8\lambda t}$ $\qquad b = \frac{2}{t^2}\,\frac{1}{(\lambda t)^{\epsilon}}$

$c = -\frac{33\lambda}{40t^3}\,\frac{1}{(\lambda t)^{2\epsilon}}$ $\qquad p = 1 - \frac{5}{8\lambda(N-t)}$

$q = \frac{2}{(N-t)^2}\,\frac{1}{[\lambda(N-t)]^{\epsilon}}$ $\qquad v = -\frac{33\lambda}{40(N-t)^3}\,\frac{1}{(\lambda(N-t))^{2\epsilon}}$

and $\quad k = \frac{3\lambda}{2}\left[\frac{(N-t)[\lambda(N-t)]^{\epsilon} + t(\lambda t)^{\epsilon}}{t(N-t)(\lambda t)^{\epsilon}(N-t)^{\epsilon}\lambda^{\epsilon}}\right]$

Thus $\int_0^{\infty} w(r,t)\,\frac{\sin\mu r}{\mu r}\,dr = Z$

$$= A\left(\frac{\pi}{k}\right)^{\frac{1}{2}}\,\frac{1}{4k}\,e^{\frac{-\mu^2}{4k}}\left[ap + (aq + pb)\left(3 - \frac{\mu^2}{2k}\right)/2k\right.$$

$$+ (av + bq + cp)\left(15 - \frac{5\mu^2}{k} + \frac{\mu^4}{4k^2}\right)/4k^2$$

$$+ (bv + cq)\left(105 - \frac{105\mu^2}{2k} + \frac{2\mu^4}{4k^2} - \frac{\mu^6}{8k^3}\right)/8k^3$$

$$\left. + cv\left(\frac{945}{2} - \frac{315\mu^2}{k} + \frac{189\mu^4}{4k^2} - \frac{9\mu^6}{4k^3} + \frac{\mu^8}{32k^4}\right)/8k^4\right] \quad \ldots\ldots\ldots\ldots\ldots(5)$$

Substitute in equation (2). When N is large

$$P(\theta) = \frac{1}{N}\int_0^N Z\,dt = \frac{1}{N} + \frac{1}{N}\sum_{t=1}^{N}(Z) \quad \ldots\ldots\ldots\ldots\ldots\ldots\ldots\ldots(6)$$

However at small values of t up to x, the Daniels distribution function is not correct for worm-like coils.and must be replaced

by the expression derived from the exact distribution function (Hearst & Stockmayer, 1962; Gray et al., 1967; Sharp & Bloomfield, 1968).

Hence a more accurate desription than equation 2 is

$$P(\theta) = \frac{1}{N} \int_0^x \int_0^\infty [W(r,t) - w(r,t)] \frac{\sin \mu r}{\mu r} \, dr \, dt + \frac{1}{N} \int_0^N \int_0^\infty w(r,t) \frac{\sin \mu r}{\mu r} \, dr \, dt \quad \ldots\ldots(7)$$

Where $w(r,t)$ is the Daniels type distribution function and $W(r,t)$ is the real distribution function.

Intersection between the two distributions occurs at values of $t \ll N$ so that the effect of circularity on the distribution should be negligible and straight chain expressions for $W(r,t)$ can be used (Gray et al., 1967)

Thus the model of Kratky & Porod (1949) without excluded volume can be used at small values of t since at these intersegment distances the excluded volume factor is negligible and can be ignored up to $t = x$, where intersection of the distributions occurs.

Thus

$$P(\theta) = \frac{1}{N} \sum_{t=1}^{x} \left(\int_0^\infty W(r,t) \frac{\sin \mu r}{\mu r} \, dr \right) - \frac{1}{N} \sum_{t=1}^{x} \left(\int_0^\infty w(r,t) \frac{\sin \mu r}{\mu r} \, dr \right) + \frac{1}{N} \sum_{t=1}^{N} \left(\int_0^\infty w(r,t) \frac{\sin \mu r}{\mu r} \, dr \right) + \frac{1}{N}$$

$$= \frac{1}{N} \sum_{t=1}^{x} \left(\int_0^\infty W(r,t) \frac{\sin \mu r}{\mu r} \, dr \right) + \frac{1}{N} \sum_{t=x+1}^{N} (Z) + \frac{1}{N} \quad \ldots\ldots(8)$$

$$\int_0^\infty W(r,t) \frac{\sin \mu r}{\mu r} \, dr = 1 - \frac{\mu^2 \langle r^2 \rangle}{3!} + \frac{\mu^4 \langle r^4 \rangle}{5!} \ldots\ldots(9)$$

Where $\langle r^n \rangle = \int_0^\infty r^n \, W(r,t) dr$

As we are dealing with small values of r, higher terms in equation (9) may be neglected.

Since $\langle r^2 \rangle$ and $\langle r^4 \rangle$ have been calculated (Hermans & Ullman, 1952) the first term in equation 8 can be evaluated. The intersection point at $t = x$ of the two distributions is taken as the point where $\langle r^2 \rangle$ is equal when calculated from both distributions. The validity of this procedure has been checked by evaluating $\langle r^2 \rangle$ at $t = x$ according to the equations of Sharp & Bloomfield (1968) and, to ensure similar values, comparing this with the value from our expression and that of Hermans & Ullman (1952). The two values should be and are similar (Table AI.1).

The total summation in equation 8 can therefore be carried out by computer since an analytical solution does not seem possible, for assigned values of $N, \lambda, \epsilon, \mu$, x and segment size.

Table AI.1

SEGMENT NUMBERS WHERE INTERSECTION OF THE TWO DISTRIBUTION FUNCTIONS OCCURS, ON VARYING THE PARAMETERS ϵ AND PERSISTENCE LENGTH

$\langle r^2 \rangle_x$ is the mean square separation of two segments x apart on the polymer chain. Values (a) are those which are the same for the Kratky-Porod distribution and the circular distribution calculated in this Appendix. Values (b) are computed from the distribution of Sharp & Bloomfield (1968b) for linear worm-like coils, for the same parameters as (a). At least for the lower values of the persistence length, values (a) and (b) are very similar, showing circularity has little effect at small intersegment numbers.

	$\epsilon = 0.141$			$\epsilon = 0.11$			
x	persistence length (nm)	$\langle r^2 \rangle_x$ $(nm)^2$(a)	$\langle r^2 \rangle_x$ $(nm)^2$(b)	x	persistence length (nm)	$\langle r^2 \rangle_x$ $(nm)^2$(a)	$\langle r^2 \rangle_x$ $(nm)^2$(b)
22	30	2.62	2.43	22	30	2.55	2.34
25	35	3.37	3.07	24	35	3.28	2.95
27	40	4.22	3.78	27	40	4.10	3.56
30	45	5.11	4.50	29	45	4.90	4.25
32	50	6.02	5.20	31	50	5.74	4.86
33	55	6.94	5.86	33	55	6.61	5.47
36	60	7.85	6.47	35	60	7.50	6.03
40	70	9.88	7.79	39	70	9.34	7.15
47	90	14.09	10.03	45	90	13.18	8.94
53	110	18.40	11.56	51	110	17.13	10.02

APPENDIX II

COMPUTER PROGRAMMES AND DIALOGUES

PROGRAMMES

Computer print-outs of six programmes are given; all are written in "Focal 1969" language for a PDP 8/L computer. The programmes are:

I to calculate $P\theta$ and $P\theta^{-1}$ for a straight interwound superhelix treated as a thin rod;

II to calculate $P\theta$ and $P\theta^{-1}$ for a toroidal superhelix;

III to calculate $P\theta$ and $P\theta^{-1}$ for a Y shaped superhelix;

IV to calculate $P\theta$ and $P\theta^{-1}$ for a straight interwound superhelix with diameter of size comparable with the length;

V to calculate $P\theta$ and $P\theta^{-1}$ for a circular worm-like coil;

VI to process instrument readings etc. in light scattering experiments to points for Zimm or Berry plots.

DIALOGUES

Full or initial dialogue sequences corresponding to the above programmes are given:

I full sequence for prog. I - the input-output is typical of those for computing $P\theta$ functions; all input dimensions must be in Angstroms; input, i) wavelengthof light in solution, ii) contour length of molecule, iii) Rg, iv) no. of superturns; output, i) radius of superhelix, ii) length of superhelix, iii) $\sin^2(\theta/2)$, $P\theta$, and $P\theta^{-1}$ at 10° intervals for θ, the scattering angle, from 1° to 151°;

II - V initial sequences for other programmes to calculate $P\theta$ functions; input-output is very similar to that in I, with the following additions: in II N1, N2 and N3 are the number of superturn in each of the three arms of the Y, and A12, A23 and A13 are the inter-arm angles; in II and IV the input specifies the superhelix radius rather than Rg which is included in the output; in V ($P\theta$ for the circular worm-like coil), N is the number of segments/molecule. D is the

PROG. I

```
C-FOCAL,1969

01.10 T "P THETA ROD UNITS ANGSTROMS"!
01.15 S PI=3.14159
01.16 A "WL IN SOLN"WL
01.20 A "CONT. LENGTH"CL
01.30 A "RAD. OF GYR."RG
01.35 A "NO. OF S/C."N
01.40 S L=FSQT(12*RG↑2)
01.46 T "CYLINDER RAD."FSQT(<CL/2*N>↑2-<L/N>↑2)/PI; T !
01.50 T %,"CYL LENGTH"L ; T !
01.51 S O=1
01.52 S H=4*PI*FSIN(O*PI/360)/WL
01.53 T "S↑2"<FSIN(O*PI/360)>↑2 ; T !
01.60 S J=1
01.70 S K=L*J/4*N
01.80 S T=T+2*(4*N-J)*FSIN(H*K)/H*K
01.90 S J=J+1

02.10 IF (4*N-J)1.1,2.2,1.7
02.20 T "P" T/(4*N)↑2+1/N*4
02.21 T "  1/P"(4*N)↑2/(T+4*N) ; T !!
02.22 S T=0
02.30 S O=O+10
02.40 IF (161-O)2.5,2.5,1.52
02.50 QUIT
*
```

PROG. II

```
AL,1969

  T "P TORROID ALL UNITS ANGSTROMS"!
  A "WL. IN SOLN."WL !
  A "CONI. LENGTH"L !
  S PI=3.14159
  A "NO. OF S/R TURNS"K !
  A "RAD GYR"RG
  S D=FSQT(<L↑2-(2*PI*K*RG)↑2>/4*PI↑2*(1-K↑2))
  T %,"LARGE RAD"D; T !
  S E=FSQT(L↑2-4*PI↑2*D↑2)/2*PI*K
  T "SMALL RAD"E; T !
  S N=15*K; S R=L/N
  S A=FSQT(PI/N*(1-<PI/N>↑2))

  S Z=2*FATN(PI*D/N*<D-E>*FSQT(1-(PI*D/N*<D-E>)↑2))
  S Z=Z-2*FATN(PI/N*A)
  S O=1
  T "S↑2"<FSIN(O*PI/360)>↑2; T !
  S I=0
  S H=4*PI*FSIN(O*PI/360)/WL
  S J=0
  S V1=Z*FCOS(J*R*2*PI*K/L)+2*J*FATN(PI/N*A)
  S U1=2*PI*K*J/N
  S I=0
  S V2=Z*FCOS(I*R*2*PI*K/L)+2*I*FATN(PI/N*A)
  S U2=2*PI*I*K/N
  DO 9
  S I=I+1

  IF (N-I)1.1,3.2,2.6
  S J=J+1
  IF (N/K-J)1.2,3.4,2.4
  T "P"I/N↑2; T "   1/P"N↑2/(I); T !!
  S O=O+10
  IF (161-O)3.8,1.1,2.2

  S Q=<1-FCOS(V1-V2)>*<2*L↑2+2*E*D*(FCOS(V1)+FCOS(V2))>
  S P=2*E↑2*<1-FCOS(V1-V2)*FCOS(V1)*FCOS(V2)-FSIN(V1)*FSIN(V2)>
  S X=FSQT(Q+P)
  IF (X)1.3,J.8,9.5
  S T=1+K*FSIN(H*X)/H*X
  S Q=0
```

PROG. III

```
C-FOCAL,1969

01.10 I "P(V) & ALL UNITS ANGSTROMS"!
01.11 A "WL IN SOLN"WL
01.12 S PI=3.14159
01.13 A "CON LGTH"L
01.20 A "N1"N1,"N2"N2,"N3"N3
01.25 S N=N1+N2+N3
01.30 A "A13"A1,"A12"A2,"A23"A3
01.40 A "CYL RAD"RC
01.50 S O=1
01.55 S B=FSQT(<L/N*2>↑2-<PI*RC>↑2)/4
01.56 I "SRG. LGTH."B; T !
01.57 T "S/R LGTH."4*B; I !
01.60 S H=4*PI*FSIN(O*PI/360)/WL
01.70 T "S↑2"<FSIN(O*PI/360)>↑2; T !
01.90 S K=2

02.10 S V=N1*4; S A=A1
02.30 S Y=4*N3
02.40 DO 9
02.50 S Y=Y-1
02.60 IF (Y)1.1,2.7,2.4
02.70 S V=V-1
02.75 IF (K)1.1,2.85,2.8
02.80 IF (V)1.1,2.9,2.3
02.85 IF (V)1.1,2.9,6.1
02.90 S K=K-1

03.10 IF (K)4.1,3.6,3.2
03.20 S V=N2*4; S A=A3
03.50 GOTO 2.3
03.60 S V=N1*4; S A=A2; S Y=N2
03.90 GOTO 2.4

04.10 S K=2; S X=N1*4
04.40 S J=1
04.45 DO 10
04.50 S J=J+1
04.60 IF (X-J)1.1,4.7,4.45
04.70 S K=K-1; IF (K)5.4,5.2,4.9
04.90 S X=N2*4

05.10 GOTO 4.4
05.20 S X=N3*4; GOTO 4.4
05.40 I %,"P"(I+N*4)/<4*N>↑2; T " I/P"<4*N>↑2/(I+N*4); T !
05.42 T "RG"FSQT(Z/2*(N*4)↑2); T !
05.44 S Z=0
05.45 S I=0
05.50 S O=O+10
05.55 IF (151-O)1.1,1.11,1.6

06.10 S Y=N2*4
06.20 GOTO 2.4

09.10 S P=J-1/2; S Q=Y-1/2
09.15 S R=B*FSQT(P↑2+Q↑2-2*P*Q*FCOS(A*PI/180))
09.20 S I=I+2*FSIN(H*R)/H*R
09.30 S Z=Z+2*R↑2

10.10 S R=J*B
10.20 S I=I+2*FSIN(H*R)*(X-J)/H*R
10.30 S Z=Z+(X-J)*R↑2
*
```

PROG. IV

```
FOCAL,1969

.10 T "P INTERMOUND UNITS ANGSTROMS"!
.20 A "WL IN SOLN"WL
.30 A "CONTOUR LENGTH"CL
.40 S PI=3.14159
.50 A "NO. OF S/H TURNS"K
.60 A "CYL RAD"R;S P=FSQT(CL↑2/K↑2-4*PI↑2*R↑2)
.70 T %,"PITCH"P;T "L"P*K/2;T !
.80 S N=16*K;S TB=2*FATN(PI/16*FSQT(1-PI↑2/256))
.84 S O=1
.87 T "S↑2"FSIN(O*PI/360)↑2;T !
.88 S T=0;S Y=0
.90 S H=4*PI*FSIN(O*PI/360)/WL

2.10 S I=0
2.15 S I=I+1
2.20 S J=0
2.25 S J=J+1
2.30 DO 9
2.40 IF (N/2-J)1.2,2.5,2.25
2.50 IF (N/2-I)1.3,2.6,2.15
2.60 S I=0
2.65 S I=I+1
2.70 S J=0
2.75 S J=J+1
2.80 DO 10
2.90 IF (N/2-J)1.1,2.95,2.75
2.95 IF (N/2-I)1.3,3.1,2.65

03.10 T "P"I*2/N↑2;T "  1/P"N↑2/2*I; I !
03.15 T "R"FSQT(Y/N↑2);T !!
03.20 S O=O+10
03.30 IF (161-O)3.6,1.1,1.87

09.10 S X=2*R↑2*(1-FCOS((I-J)*TB))+(P*(I-J)*TB/2*PI)↑2
09.20 S Y=Y+X
09.30 S X=FSQT(X); IF (X)9.4,9.5,9.4
09.40 S T=T+FSIN(H*X)/H*X
09.50 S X=0

10.10 S X=2*R↑2*(1-FCOS((I-J)*TB-PI))+(P*(I-J)*TB/2*PI)↑2
10.20 S Y=Y+X;S X=FSQT(X)
10.30 S T=T+FSIN(H*X)/H*X
*
```

```
 GO
-FOCAL,1969

1.30 A "N"N,"D"D,"PL"PL,"E"E,"X"X
1.50 S L=D/2*PI
1.52 S O=1
1.53 S U=4*D*3.14159/360/4.97
1.54 S T=0
1.55 S S=0
1.56 DO 5
1.57 S T=T+1
1.58 S G=EXP(T*LOG(L*1)); S H=EXP(T*LOG(L*(N-1)))
1.60 S A=1-5/8*L*T; S B=2/6*T↑2; S C=-33*L/6↑2*40*T↑3
1.65 S P=1-5/8*L*(N-1); S Q=2/H*(N-1)↑2; S V=-33*L/6↑2*40*(N-1)↑3
1.70 S K=3*L*(N-1)*H+1*G)/2*T*(N-T)*G*H
1.80 S Z=A*P+3*(A*Q+P*B)/K*2+105*(B*V+C*Q)/8*K↑3
1.90 S Z=Z+(A*V+C*P+B*Q)*15/4*K↑2+C*V*945/16*K↑4

2.10 S M=(945/2-315*U↑2/K+105*U↑4/4*M↑2-7*U↑6/4*K↑3+U↑8/32*K↑4)*C*V
2.40 S I=(105-105*U↑2/2*K+21*U↑4/4*A↑2-U↑6/8*K↑3)*(2*V+C*Q)/8*K↑3
2.60 S J=(15-5*U↑2/K+U↑4/4*A↑2)*(A*V+C*P+B*Q)/4*K↑2+A*P
2.80 S J=<J+(A*Q+P*B)*(3-U↑2/2*K)/2*K+M/8*A↑2+I>/Z*EXP(U↑2/4*A)

3.10 S S=S+J
3.20 IF (N-1-T)1.1,3.3,1.57
3.30 T %,"P" (S+1)/N; T "  1/P" N/(1+S); T " A(1/P)"PSI(N/<1+S>),!
3.35 T "S↑2"(PSIN(U*3.14159/360))↑2,!!
3.37 S O=O+10
3.40 IF (161-O)1.2,3.5,1.53
3.50 QUIT

5.05 S T=T+1
5.10 S A=5*T↑2/3*L↑3-26*T/9*L↑3+(EXP(-6*L*T)-1)/54*L↑4
5.20 S A=A+2*(1-EXP(-2*L*T))/L↑4-T*EXP(-2*L*T)/L↑3
5.30 S B=T/L-(1-EXP(-2*L*T))/2*L↑2
5.40 S S=S+1-U↑2*3/6+U↑4*A/120
5.50 IF (K-T)1.2,5.6,5.05
5.60
*
```

PROG. VI

```
AL,1969

 T "ZIMM PLOT,30-150,FLUOR COR IN,FOR ALPHA DATA"!
 A "CALIB. CONST. X 10↑6",Z
 A "GLASS STD. READING"IB
 S K9=47*Z/IB
 A "DN/DC IN ML/GM",NC
 A "REFR. INDEX OF SOLVENT",NE
 A "WL OF LIGHT IN NM",WL
 S PI=3.14159
 S K1=2*PI↑2*NE↑2*NC↑2*10↑11/WL↑4*6.023*K9

 T "FOR S↑2, GOTO 9.1"!
 A "SOLV 30-150"A3,A4,A5,A6,A7,A8,A9,B1,B2,B3,B4,!
 A "M"M,!
 A "CONC. IN MG/ML"C;T %,"LIST READINGS"!
 A R;S P=K1*C/(R-A3)*966;T "KC/R"P;T " R"FSQT(P),!
 A R;S P=K1*C/(R-A4)*977;T "KC/R"P;T " R"FSQT(P),!
 A R;S P=K1*C/(R-A5)*980;T "KC/R"P;T " R"FSQT(P),!

 A R;S P=K1*C/(R-A6)*988;T "KC/R"P;T " R"FSQT(P),!
 A R;S P=K1*C/(R-A7)*996;T "KC/R"P;T " R"FSQT(P),!
 A R;S P=K1*C/(R-A8)*1000;T "KC/R"P;T " R"FSQT(P),!
 A R;S P=K1*C/(R-A9)*1005;T "KC/R"P;T " R"FSQT(P),!
 A R;S P=K1*C/(R-B1)*1011;T "KC/R"P;T " R"FSQT(P),!
 A R;S P=K1*C/(R-B2)*1013;T "KC/R"P;T " R"FSQT(P),!
 A R;S P=K1*C/(R-B3)*1016;T "KC/R"P;T " R"FSQT(P),!
 A R;S P=K1*C/(R-B4)*1014;T "KC/R"P;T " R"FSQT(P),!

 T "S↑2+MC TERMS ARE"!
 T 0.06699+M*C,0.10332+M*C,!
 T 0.14645+M*C,0.25+M*C,0.37059+M*C,0.5+M*C,!
 T 0.62941+M*C,0.75+M*C,0.85355+M*C,0.89667+M*C,!
 T 0.93301+M*C;T "  M*C"M*C,!
 GOTO 2.5

 A "ANGLE",T,!
 T FSIN(T*3.14159/360)↑2,!
 GOTO 9.1
```

```
 GO
P THETA ROD UNITS ANGSTROMS
WL IN SOLN:4097
CONT. LENGTH:16440
RAD. OF GYR.:1035
NO. OF S/C.:12
CYLINDER RAD.= 0.196206E+03
CYL LENGTH= 0.356535E+04
S↑2= 0.761522E-04
P= 0.999740E+00   1/P= 0.100026E+01

S↑2= 0.918638E-02
P= 0.969826E+00   1/P= 0.103111E+01

S↑2= 0.332097E-01
P= 0.896994E+00   1/P= 0.111484E+01

S↑2= 0.714161E-01
P= 0.797356E+00   1/P= 0.125415E+01

S↑2= 0.122645E+00
P= 0.689887E+00   1/P= 0.144951E+01

S↑2= 0.185339E+00
P= 0.590302E+00   1/P= 0.169405E+01

S↑2= 0.257595E+00
P= 0.507641E+00   1/P= 0.196990E+01

S↑2= 0.337215E+00
P= 0.444216E+00   1/P= 0.225116E+01

S↑2= 0.421782E+00
P= 0.397790E+00   1/P= 0.251389E+01

S↑2= 0.508725E+00
P= 0.364267E+00   1/P= 0.274524E+01

S↑2= 0.595403E+00
P= 0.339655E+00   1/P= 0.294417E+01

S↑2= 0.679183E+00
P= 0.320975E+00   1/P= 0.311551E+01

S↑2= 0.757518E+00
P= 0.306363E+00   1/P= 0.326411E+01

S↑2= 0.828028E+00
P= 0.294787E+00   1/P= 0.339226E+01

S↑2= 0.888571E+00
P= 0.285722E+00   1/P= 0.349991E+01

S↑2= 0.937337E+00
P= 0.278899E+00   1/P= 0.358553E+01
```

DIAL. II - V

```
 GO
P(Ø) Y ALL UNITS ANGSTROMS
WL IN SOLN:4Ø97
CON LGTH:16440
N1:4,N2:4,N3:4
A13:12Ø,A12:12Ø,A23:12Ø
CYL RAD:157
SEG. LGTH.= Ø.116835E+Ø3
S/H LGTH.= Ø.475342E+Ø3
S↑2= Ø.761522E-Ø4
P= Ø.989277E+ØØ 1/P= Ø.1Ø1Ø84E+Ø1
RG= Ø.1Ø5666E+Ø4
S↑2= Ø.918636E-Ø2


 GO
P TORROID ALL UNITS ANGSTROMS
WL. IN SOLN.:4Ø97,
CONT. LENGTH:16440,
NO. OF S/H TURNS:12,
RAD GYR:1Ø35
LARGE RAD= Ø.1Ø153ØE+Ø4
SMALL RAD= Ø.2ØØ957E+Ø3
S↑2= Ø.761522E-Ø4


 GO
P INTERWOUND UNITS ANGSTROMS
WL IN SOLN:4Ø97,CONTOUR LENGTH:16440
NO. OF S/H TURNS:12
CYL RAD:157
PITCH= Ø.95Ø683E+Ø3L= Ø.57Ø41ØE+Ø4
S↑2= Ø.761522E-Ø4


 GO
N:547,D:3Ø,PL:45Ø,E:Ø.141,X:27
P= Ø.999599E+ØØ  1/P= Ø.1ØØØ4ØØE+Ø1 R(1/P)= Ø.1ØØØ2ØE+Ø1
S↑2= Ø.761522E-Ø4
```

DIAL. VI

```
M PLOT,30-150,FLUOR COR IN,FOR ALPHA DATA
IB. CONST. X 10↑6:0.282
SS STD. READING:470
DC IN ML/GM:0.166
R. INDEX OF SOLVENT:1.334
OF LIGHT IN NM:546.1
 S↑2, GOTO 9.1
V 30-150:80,:53,:47,:41,:35,:30,:30,:34,:42,:43,:45,
0

C. IN MG/ML:0.07898
T READINGS
75,KC/R= 0.350433E-06 R= 0.591974E-03
99,KC/R= 0.384643E-06 R= 0.620357E-03
41,KC/R= 0.432507E-06 R= 0.657652E-03
7,KC/R= 0.559205E-06 R= 0.747800E-03
1,KC/R= 0.719713E-06 R= 0.848359E-03
0,KC/R= 0.903723E-06 R= 0.950644E-03
4,KC/R= 0.108527E-05 R= 0.104177E-02
6,KC/R= 0.124522E-05 R= 0.111590E-02
3,KC/R= 0.138391E-05 R= 0.117640E-02
0,KC/R= 0.143549E-05 R= 0.119812E-02
2,KC/R= 0.148160E-05 R= 0.121696E-02
+MC TERMS ARE
.856790E+00= 0.893120E+00
.936250E+00= 0.103980E+01= 0.116039E+01= 0.128980E+01
.141921E+01= 0.153980E+01= 0.164335E+01= 0.168647E+01
.172281E+01  M*C= 0.789800E+00
C. IN MG/ML:
```

segment length, P_L is the persistence length, E is the excluded volume factor and X is the segment number where intersection of the two distributions used occurs (see Appendix I), in the input;.

VI full dialogue sequence for processing Zimm or Berry plot data; the first five inputs are self-explanatory except that the wavelength of light used, must be that in vacuo; inputs are then vi) solvent subtractions to be made at angles from 30°- 150° corresponding to the light scattering instrument's preset angles for integrated measurements, vii) constant by which to multiply the concentration to give a suitable scale on the abcissa of the Zimm plot, viii) concentration of DNA etc. in mg/ml; then alternate input of the instrument reading and output of $Kc/R\theta$ and $(Kc/R\theta)^{\frac{1}{2}}$ for the eleven readings, when the eleven corresponding values for the abcissa of the Zimm plot are printed out.

BIBLIOGRAPHY

Altman,S. & Lerman,L.S. (1970) J.Mol.Biol. 50, 263 - 267.

Arnott,S. (1970) Progr.Biophys.Mol.Biol. 21, 267 - 319.

Bancroft,C. & Freifelder,D. (1970) J.Mol.Biol. 54, 537 - 546.

Bauer,W. & Vinograd,J. (1968) J.Mol.Biol. 33, 141 - 171.

Bauer,W. & Vinograd,J. (1970a) J.Mol.Biol. 47, 419 - 435.

Bauer,W. & Viñograd,J. (1970b) J.Mol.Biol. 54, 281 - 298.

Bazaral,M. & Helinski,D.R. (1968) Biochemistry 7, 3513 - 3520.

Bendich,A. (1955) Methods Enzymol. 3, 715 - 723.

Benoit,H. & Doty,P. (1953) J.Phys.Chem. 57, 958 - 963.

Bernardi,G. (1964) Makromol.Chem. 72, 205 - 207.

Berry,G.C. (1966) J.Chem.Phys. 44, 4550 - 4564.

Billmeyer,F.W. (1945) Rubber Reserve Company, Technical Reports, Jan.15, Mar.1 (quoted in Hermans & Levinson (1951)).

Blake,A. & Peacocke,A.R. (1967) Biopolymers 5, 383 - 397.

Blake,A. & Peacocke,A.R. (1968) Biopolymers 6, 1225 - 1253.

Bloomfield,V.A. (1966) Proc.Nat.Acad.Sci.U.S. 55, 717 - 720.

Bloomfield,V.A. (1968) Macromol.Rev. 3, 255 - 316.

Bloomfield,V.A. & Zimm,B.H. (1966) J.Chem.Phys. 44, 315 - 323.

Bode,V.C. & Horowitz,H.J. (1967) J.Mol.Biol. 23, 191 - 199.

Bode,V.C. & MacHattie,L.A. (1968) J.Mol.Biol. 32, 673 - 679.

Bolstein,D. & Matz,M.J. (1970) J.Mol.Biol. 54, 417 - 440.

Bonnelycke,B.E. & Dandliker,W.B. (1959) J.Colloid Sci. 14, 567 - 571.

Borst,P. & Kroon,A.M. (1969) Int.Rev.Cytol. 26, 107 - 190.

Böttger,M. & Kuhn,W. (1971) Biochim.Biophys.Acta 254, 407 - 411.

Brahms,J. & Mommaerts,W.F.H.M. (1964) J.Mol.Biol. 10, 73 - 88.

Bram,S. (1971) Nature New Biol.(London) 232, 174 - 176.

Brice,B.A. & Halwer,M. (1951) J.Opt.Soc.Amer. 41, 1033 - 1037.

Brice,B.A., Halwer,M. & Speiser,R. (1950) J.Opt.Soc.Amer. 40, 768 - 778.

Britten,R.J. & Davidson,E.H. (1969) Science 165, 349 - 357.

Bujard,H. (1968) J.Mol.Biol. 33, 503 - 505.

Burton,A. & Sinsheimer,R.L. (1963) Science 142, 962 - 963.

Cairns,J. (1963) J.Mol.Biol. 6, 208 - 213.

Callis,P.R. & Davidson,N. (1969) Biopolymers 7, 335 - 352.

Campbell,A.M. & Lochhead,D.S. (1971) Biochem.J. 123, 661 - 663.

Carlton,B.C. & Helinski,D.R. (1969) Proc.Nat.Acad.Sci.U.S. 64, 592 - 599.

Carr,C.I. & Zimm,B.H. (1950) J.Chem.Phys. 18, 1616 - 1626.

Casassa,E.F. (1965) J.Polym.Sci.A 3, 605 - 614.

Casassa,E.F. & Eisenberg,H. (1964) Advan.Protein Chem. 19, 287 - 393.

Champoux,J.J. & Dulbecco,R. (1972) Proc.Nat.Acad.Sci.U.S. 69, 143 - 146.

Chandler,B., Hayashi,M., Hayashi,M.N. & Spiegelman,S. (1964) Science 143, 47 - 49.

Clayton,D.A. & Bramble,R.M. (1972) Biochem.Biophys.Res.Commun. 46, 1477 - 1482.

Clewell,D.B. & Helinski,D.R. (1970a) Biochemistry 9, 4428 - 4440.

Clewell,D.B. & Helinski,D.R. (1970b) Biochem.Biophys.Res.Commun. 41, 150 - 156.

Cohen,G. & Eisenberg,H. (1965) J.Chem.Phys. 43, 3881 3887.

Cohen,G. & Eisenberg,H. (1966) Biopolymers 4, 429 - 440.

Cohen,G. & Eisenberg,H. (1968) Biopolymers 6, 1077 - 1100.

Cohen,G. & Eisenberg,H. (1969) Biopolymers 8, 45 - 55.

Cohen,S.N. & Miller,C.A. (1969) Nature (London) 224, 1271 - 1273.

Coumou,D.J. (1960) J.Colloid Sci. 15, 408 - 417.

Coumou,D.J. & Mackor,E.L. (1964) Trans.Faraday Soc. 60, 1726 - 1735.

Coumou,D.J., Mackor,E.L. & Hijmans,J. (1964) Trans.Faraday Soc. 60, 1539 - 1547.

Cozzarelli,N.R., Kelly,R.B. & Kornberg,A. (1968) Proc.Nat.Acad.Sci. U.S. 60, 992 - 999.

Crawford,L.V. (1964) J.Mol.Biol. 8, 480 - 495.

Crawford,L.V. (1965) J.Mol.Biol. 13, 362 - 372.

Crawford,L.V. & Black,P.H. (1964) Virology 24, 388 - 392.

Crawford,L.V. & Waring,M.J. (1967) J.Mol.Biol. 25, 23 - 30.

Crick,F.H.C. (1971) Nature (London) 234, 25 - 27.

Daniels,H.E. (1952) Proc.Roy.Soc.,Edin. 63A, 290 - 294.

Davidson,N. (1972) J.Mol.Biol. 66, 307 - 309.

Dawson,J.R. & Harpst,J.A. (1971) Biopolymers 10, 2499 - 2508.

Dean,W.W, & Lebowitz,J. (1971) Nature New Biol.(London) 231, 5 - 8.

DeGennes,P.G. (1968) Biopolymers 6, 715 - 729.

Dezelic,Gj. & Kratohvil,J.P. (1960) Kolloid-Z. 171, 38 - 48.

Douthart,R.J. & Bloomfield,V,A. (1968) Biopolymers 6, 1297 - 1309.

Dove,W.F., Inokuchi,H. & Stevens,W.F. (1971) in The Bacteriophage Lambda Ed. Hershey,A.D. pp.747 - 771, Cold Spring Harbor Laboratory: New York.

Dressler,D. & Wolfson,J. (1970) Proc.Nat.Acad.Sci.U.S. 67, 456 - 463.

Drummond,D.S., Pritchard,N.J., Simpson-Gildenmeister,V,F.W. & Peacocke,A.R. (1966) Biopolymers 4, 971 - 987.

Dubin,S.B., Benedek,G.B., Bancroft,F.C. & Freifelder,D. (1970) J.Mol. Biol. 54, 547 - 556.

Dulbecco,R. & Vogt,M. (1963) Proc.Nat.Acad.Sci.U.S. 50, 236 - 243.

Edsall,J.T., Edeloch,H., Lontie,R. & Morrison,P.R. (1950) J.Amer.Chem. Soc. 72, 4641 - 4656.

Eisenberg,H. (1969) Biopolymers 8, 545 - 551.

Eisenberg,H. & Cohen,G. (1968) J.Mol.Biol. 37, 355 - 362.

Eisenberg,H. & Felsenfeld,G. (1967) J.Mol.Biol. 30, 17 -37.

Englander,J.J. & von Hippel,P.H. (1972) J.Mol.Biol. 63, 171 - 177.

Espejo,R.T., Canelo.E.S. & Sinsheimer,R.L. (1969) Proc.Nat.Acad.Sci.U.S. 63, 1164 - 1168.

Espejo,R.T., Espejo-Canelo,E.S. & Sinsheimer,R.L. (1971) J.Mol.Biol. 56, 597 - 621.

Felsenfeld,G. (1968) Methods Enzymol. 12B, 247 - 253.

Fica Introductory Manual (1970) Introduction on the new automatic digital light scattering photometer, Model 50000, 20th Jan., Société Fica: 78 - Le Mesnil St. Denis.

Fiers,W. & Sinsheimer,R.L. (1962) J.Mol.Biol. 5, 424 - 434.

Flory,P.J. (1953) Principles of Polymer Chemistry, Cornell University Press: Ithica.

Flory,P.J. (1969) Statistical Mechanics of Chain Molecules, Interscience: New York.

Follet,E.A.C. & Crawford,L.V. (1967) J.Mol.Biol. 28, 455 - 459.

Freifelder,D. (1968a) Cold Spring Harbor Symp.Quant.Biol. 33, 425 - 434.

Freifelder,D. (1968b) J.Mol.Biol. 34, 31 - 38.

Freifelder,D. (1968c) J.Mol.Biol. 35, 95 - 102.

Freifelder,D. (1970) J.Mol.Biol. 54, 567 - 577.

Froelich,D., Strazielle,C., Bernardi,G. & Benoit,H. (1963) Biophys.J. 3, 115 - 125.

Fukatsu,M. & Kurata,H. (1966) J.Chem.Phys. 44, 4539 - 4545.

Fuller,F.B. (1971) Proc.Nat.Acad.Sci.U.S. 68, 815 - 819.

Fuller,W. & Waring,M.J. (1964) Ber.Bunsenges.Physik.Chem. 68, 805 - 808.

Geiduschek,E.P. & Holtzer,A. (1958) Advan.Biol.Med.Physics 6, 431 - 551.

Gellert,M. (1967) Proc.Nat.Acad.Sci.U.S. 57, 148 - 155.

Gennis,R.B. & Cantor,C.R. (1972) J.Mol.Biol. 65, 381 - 399.

Gersch,N.F. & Jordan,D.O. (1965) J.Mol.Biol. 13, 138 - 156.

Gilbert,W. & Dressler,D (1968) Cold Spring Harbor Symp.Quant.Biol. 33, 473 - 484.

Gilham,P.T. (1970) Annu.Rev.Biochem. 39, 227 - 250.

Glaubiger,D. & HearstJ.E. (1967) Biopolymers 5, 691 - 696.

Goring,D.A.I. & Napier,P.G. (1954) J.Chem.Phys. 22, 147.

Goring,D.A.I., Senez,M., Melanson,B., & Huque,M.M. (1957) J.Colloid Sci. 12, 412 - 416.

Goulian,M. (1971) Annu.Rev.Biochem. 40, 855 - 898.

Gray,H.B.Jr. (1967) Biopolymers 5, 1009 - 1019.

Gray,H.B.Jr., Bloomfield,V.A. & Hearst,J.E. (1967) J.Chem.Phys. 46, 1493 - 1498.

Gray,H.B.Jr. & Hearst,J.E. (1968) J.Mol.Biol. 35, 111 - 129.

Gray,H.B.Jr., Upholt,W.B. & Vinograd,J. (1971) J.Mol.Biol. 62, 1 - 19.

Gross,J.D. (1972) personal communication.

Hamaguchi,K. & Geiduschek,E.P. (1962) J.Amer.Chem.Soc. 84, 1329 - 1338.

Hardy,A.C. & Perrin,F.H. (1932) Principles of Optics p.411, McGraw-Hill: New York.

Harpst,J.A., Krasna,A.I. & Zimm,B.H. (1968a) Biopolymers 6, 585 - 594.

Harpst,J.A., Krasna,A.I. & Zimm,B.H. (1968b) Biopolymers 6, 595 - 603.

Harrington,R.E. (1970) Biopolymers 9, 159 - 193.

Haugen,G.R. & Melhuish,W.H. (1964) Trans.Faraday Soc. 60, 386 - 394.

Hayashi,M., Hayashi,M.N. & Spiegelman,S. (1963) Proc.Nat.Acad.Sci.U.S. 50, 664 - 672.

Hayashi,M. Hayashi,M.N. & Spiegelman,S. (1964) Proc.Nat.Acad.Sci.U.S. 51, 351 - 359.

Hays,J.B. Magar,M.E. & Zimm,B.H. (1969) Biopolymers 8, 531 - 536.

Hays,J.B. & Zimm,B.H. (1970) J.Mol.Biol. 48, 297 - 317.

Hearst,J.E. & Stockmayer,W.H. (1962) J.Chem.Phys. 37, 1425 - 1433.

Hearst,J.E., Beals,E. & Harris,R.A. (1968a) J.Chem.Phys. 48, 5371 - 5377.

Hearst,J.E., Schmid,C.W. & Rinehart,F,P. (1968b) Macromolecules 1, 491 - 494.

Helinski,D.R. & Clewell,D.B. (1970) Biochem.Biophys.Res.Commun. 40, 608 - 613.

Helinski,D.R. & Clewell,D.B. (1971) Annu.Rev.Biochem. 40, 899 - 942.

Hermans,J.J. & Levinson,S. (1951) J.Opt.Soc.Amer. 41, 460 - 465.

Hermans,J.J. & Ullman,R. (1952) Physica 18, 951 - 971.

Hershey,A.D., Burgi,E. & Ingraham,L. (1963) Proc.Nat.Sci.U.S. 49, 748 - 755.

Herskowitz,I. & Signer,E.R. (1970) J.Mol.Biol. 47, 545 - 556.

Hinton,D.M. & Bode,V.C. (1971) Fed.Proc.Fed.Amer.Soc.Exp.Biol. 30, 1095.

Hirschman,S.Z. & Felsenfeld,G. (1966) J.Mol.Biol. 16, 347 - 358.

Hirt,B. (1969) J.Mol.Biol. 40, 141 - 144.

Hornick,C. & Weill,G. (1971) Biopolymers 10, 2345 - 2358.

Hotta,Y. & Bassel,A. (1965) Proc.Nat.Acad.Sci.U.S. 53, 356 - 362.

Houssier,C. (1968) J.Chim.Phys. 65, 36 - 39.

Hudson,B., Upholt,W.B., Devinny,J. & Vinograd,J. (1969) Proc.Nat.Acad. Sci.U.S. 62, 813 - 820.

Inman,R.B. (1964) J.Mol.Biol. 18, 464 - 476.

Inman,R.B. & Baldwin,R.L. (1962) J.Mol.Biol. 5, 172 - 184.

Inselburg,J. & Fuke,M. (1970) Science 169, 590 - 593.

International Critical Tables (1926a) Vol.I, p.83, McGraw-Hill: New York.

International Critical Tables (1926b) Vol.III, pp.25 - 26, McGraw-Hill: New York.

Jacob,F. & Wollman,E.L. (1957) Compt. Rend. 245, 1840 - ,1843.

Jacob,F. & Wollman,E.L. (1961) Sexuality and the Genetics of Bacteria, Academic Press: New York.

Janz,H.S. & Powels,P.H. (1965) Biochem.Biophys.Res.Commun. 18, 589 - 594.

Jennings,B.R. & Plummer,H. (1970) Biopolymers 9, 1361 - 1372.

Kasamatsu,H., Robberson,D.L., & Vinograd,J. (1971) Proc.Nat.Acad.Sci.U.S. 68, 2252 - 2257.

Kiger,J.A. & Sinsheimer,R.L. (1971) Proc.Nat.Acad.Sci.U.S. 68, 112 -115.

Kilkson,R. & Maestre,M.F. (1962) Nature (London) 195, 494 - 495.

Kirk,J.T.O. (1971) Annu.Rev.Biochem. 40, 161 - 196.

Kirkwood,J.G. (1954) J.Polym.Sci. 12, 1 - 14.

Kirschner,R.H., Wolstenholme,D.R. & Gross,N.J. (1968) Proc.Nat.Acad.Sci.U.S. 60, 1466 - 1472.

Kleinschmidt,A.K. & Zahn,R.K. (1959) Z.Naturforsch.B 14, 770 - 779.

Kleinschmidt,A.K., Burton,A. & Sinsheimer,R.L. (1963) Science 142, 961.

Kleinschmidt,A.K., Kass,S.J., Williams,R.C. & Knight,C.A. (1965) J.Mol. Biol. 13, 749 - 756.

Kline,B.C. & Helinski,D.R. (1971) Biochemistry 10, 4975 - 4980.

Krasna,A.I. (1970) Biopolymers 9, 1029 - 1038.

Krasna,A.I. & Harpst,J.A. (1964) Proc.Nat.Acad.Sci.U.S. 51, 36 - 40.

Krasna,A.I., Dawson,J.R. & Harpst,J.A. (1970) Biopolymers 9, 1017 -1028.

Kratky,O. & Porod,G. (1949) Rec.Trav.Chim.Pays-Bas, 68, 1106 - 1122.

Kratohvil,J.P., Dezelic,Gj., Kerker,M. & Matijevic,E. (1962) J.Polym.Sci. 57, 59 - 78.

Kraut,J. & Dandliker,W.B. (1955) J.Chem.Phys. 23, 1544 - 1545.

Kuhn,W. (1936) Kolloid-Z. 76, 258 - 271.

Kuhn,W. (1939) Kolloid-Z. 87, 3 - 12.

Landau,L. & Lifshitz,E. (1958) Statistical Physics, pp.478 - 482, Pergamon Press: London.

Lang,D. (1970) J.Mol.Biol. 54, 557 - 565.

Lang,D., Kleinschmidt,A.K. & Zahn,R.K. (1964) Biochim.Biophys.Acta 88, 142 - 154.

Lang,D., Bujard,H., Wolfe,B. & Russel,D. (1967) J.Mol.Biol. 23, 163 - 181.

Lark,K.G. (1969) Annu.Rev.Biochem. 38, 569 - 604.

Lee,C.S. & Davidson,N. (1968) Biochem.Biophys.Res.Commun. 32, 757 - 762.

Lee,C.S. & Davidson,N. (1970) Biochim.Biophys.Acta 204, 285 - 295.

Lerman,L.S. (1961) J.Mol.Biol. 3, 18 - 30.

Lerman,L.S. (1964) J.Mol.Biol. 10, 367 - 380.

Levine,A.J., Kang,H.S. & Billheimer,F.E. (1970) J.Mol.Biol. 50, 549 - 568.

Litzler,R., Cerf,R. & Sadron,Ch. (1964) Compt.Rend. 259, 473 - 475.

Lloyd,P.H., Prutton,R.N. & Peacocke,A.R. (1968) Biochem.J. 107, 353 - 359.

Londos-Gagliardi,D., Serros,G. & Aubel-Sadron,G. (1971) J.Chim.Phys. 68, 666 - 669.

Lubas,B. & Wilczok,T. (1970) Biochim.Biophys.Acta 224, 1 - 9.

Lubas,B. & Wilczok,T. (1971) Biopolymers 10, 1267 - 1276.

Luzzati,V. & Nicolaieff,A. (1963) J.Mol.Biol. 7, 142 - 163.

Luzzati,V., Mathis,A., Masson,F. & Witz,J. (1964) J.Mol.Biol. 10, 28 - 41.

Luzzati,V., Masson,F., Mathis,F & Saludjian,K. (1967) Biopolymers 5, 491 - 508.

MacConnel,B. & von Hippel,P.H. (1970) J.Mol.Biol. 50, 297 - 316.

MacDonald,C.C., Philips,W.D., & Penman,S. (1964) Science 144, 1234 - 1237.

McIntyre,D. (1964) J.Res.Nat.Bur.Std.A 68, 87 - 96.

Maestre,M.F. & Kilkson,R. (1965) Biophys.J. 5, 275 - 287.

Maestre,M.F. & Wang,J.C. (1971) Biopolymers 10, 1021 - 1030.

Marmur,J. & Doty,P. (1962) J.Mol.Biol. 5, 109 - 118.

Maron,S.H. & Lou,R.L.H. (1954) J.Polym.Sci. 14, 29 - 36.

Matsubara,K. & Kaiser,A.D. (1968) Cold Spring Harbor Symp.Quant.Biol. 33, 769 - 775.

Mauss,Y., Chambron,J., Daune,M. & Benoit,H. (1967) J.Mol.Biol. 27, 579 - 589.

Mekshenkov,M.I. (1964) Biofizika 9, 128 - 131.

Nass,M.M.K. (1969) Science 165, 25 - 35.

Padmanabhan,R. & Wu,R. (1972) J.Mol.Biol. 65, 447 - 467.

Paoletti,C. & LePecq,J.-B. (1971a) J.Mol.Biol. 59, 43 - 62.

Paoletti,C. & LePecq,J.-B. (1971b) Biochimie 53, 969 - 972.

Pardon,J.F., Wilkins,M.F.H. & Richards,B.M. (1969) Nature (London) 215, 508 - 509.

Peacocke,A.R. & Skerret,J.N.H. (1956) Trans.Faraday Soc. 52, 261 - 279.

Peterlin,A. (1955) J.Chem.Phys. 23, 2464 - 2465.

Pilarski,L.M. & Egan,J.B. (1972) Nature New Biol. (London) 237, 102 - 104, 128.

Powels,P.H. & Janz,H.S. (1964) Biochim.Biophys.Acta 91, 177 - 179.

Powels,P.H., Knijnenburg,C.M., van Rotterdam,J., Cohen,J.A. & Janz,H.S. (1968) J.Mol.Biol. 32, 169 - 182.

Ptitsyn,O.B. & Eizner,Yu.E. (1961) Vysokomolekul.Soedin. 3, 1863 - 1869.

Ptitsyn,O.B. & Federov,B.A. (1965) Chem.Abstr. 62, 1887d.

Radloff,R., Bauer,W. & Vinograd,J. (1967) Proc.Nat.Acad.Sci.U.S. 57, 1514 - 1521.

Rajbhandary,U.L. & Stuart,A. (1966) Annu.Rev.Biochem. 35, 759 - 788.

Ramstein,J., Dourlent,M. & Leng,M. (1972) Biochem.Biophys.Res.Commun. 47, 874 - 882.

Ray,D. (1969) J.Mol.Biol. 43, 631 - 647.

Reichmann,M.E., Bunce,B.H. & Doty,P. (1953) J.Polym.Sci. 10, 109 - 119.

Reichmann,M.E., Rice,S.A., Thomas,C.A. & Doty,P. (1954) J.Amer.Chem. Soc. 76, 3047 - 3053.

Revet,B.M.J., Schmir,M. & Vinograd,J. (1971) Nature New Biol.(London) 229, 10 - 13.

Rhoades,M & Thomas,C.A.Jr. (1968) J.Mol.Biol. 37, 41 - 61.

Riou,G. & Paoletti,C. (1967) J.Mol.Biol. 28, 377 - 382.

Riou,G. & Delain,E.H. (1969) Proc.Nat.Acad.Sci.U.S. 62, 210 - 217.

Rosenblum,J. & Cox,E.C. (1966) Biopolymers 4, 747 - 757.

Roth,T.H. & Helinski,D.R. (1967) Proc.Nat.Acad.Sci.U.S. 58, 650 - 657.

Rubinstein,I., Thomas,C.A.Jr. & Hershey,A.D. (1961) Proc.Nat.Acad.Sci. U.S. 47, 1113 - 1122.

Rush,M.G., Kleinschmidt,A.K., Hellmann,W. & Warner,R.C. (1967) Proc. Nat.Acad.Sci.U.S. 58, 1676 - 1683.

Rush,M.G., Gordon,C.N., Novick,B.P. & Warren,R.C. (1969) Proc.Nat.Acad. Sci.U.S. 63, 1304 - 1310.

Ruttenberg,C.J.C.M., Smit,E.M., Borst,P. & van Bruggen,E.F.J. (1968) Biochim.Biophys.Acta 157, 429 - 432.

Samejima,T. & Yang,J.T. (1965) J.Biol.Chem. 240, 2094 - 2100.

Saucier,J.M., Festy,B. & LePecq,J.-B. (1971) Biochimie 53, 973 - 980.

Schmid,C.W. & Hearst,J.E. (1969) J.Mol.Biol. 44, 143 - 160.

Schmid,C.W., Reinhart,F.P. & Hearst,J.E. (1971) Biopolymers 10, 883 - 893.

Schnös,M. & Inman,R.B. (1970) J.Mol.Biol. 51, 61 - 73.

Schnös,M. & Inman,R.B. (1971) J.Mol.Biol. 55, 31 - 38.

Sharp,P. & Bloomfield,V.A. (1968a) J.Chem.Phys. 48, 2149 -, 2155.

Sharp,P. & Bloomfield,V.A. (1968b) Biopolymers 6, 1201 - 1211.

Sinanoglu,O. & Abdulnur,S. (1964) Photochem.Photobiol. 3, 333 - 342.

Sinsheimer,R.L. (1959) J.Mol.Biol. 1, 43 - 53.

Sinsheimer,R.L., Starman,B., Nagler,C. & Guthrie,S. (1962) J.Mol.Biol. 4, 142 - 160.

Smith,K.O. (1965) Science 148, 100 - 102.

Sponar,J., Boublik,M. & Votavova,H. (1965) Collection Czech.Chem.Commun. 30, 2920 - 2927.

Stacey,K.A. (1956) Light Scattering in Physical Chemistry Butterworths Scientific Publications: London.

Stacy,C.J. & Arnett,R.L. (1964) J.Polym.Sci.A,2, 167 - 179.

Stahl,F.W. (1962) Proc.Ann.Reunion Soc.Chim.Phys. 11, 194 - 199.

Studier,F.W (1965) J.Mol.Biol 11, 373 - 390.

Subake-Sharpe,J.H., Burk,R.R., Crawford,L.V., Morrison,J.M., Hay,J. & Keir,H.M. (1966) Cold Spring Harbor Symp.Quant.Biol. 31, 737 - 748.

Sugiara,M., Okamoto,T. & Takanami,M. (1969) J.Mol.Biol. 43, 299 - 315.

Sutton,W.D. (1972) Nature New Biol.(london) 237, 70 - 71.

Tanford,C. (1961) Physical Chemistry of Macromolecules Wiley: New York.

Ter Schegget,J. & Borst,P. (1971a) Biochim.Biophys.Acta 246, 239 - 248.

Ter Schegget,J. & Borst,P. (1971b) Biochim.Biophys.Acta 246, 249 - 257.

Ter Schegget,J., Flavell,R.A. & Borst,P. (1971) 254, 1 - 14.

Thomas,C.A.Jr. & MacHattie,L.A. (1964) Proc.Nat.Acad.Sci.U.S. 52, 1297 - 1301.

Thomas,C.A.Jr. & MacHattie,L.A. (1967) Annu,Rev.Biochem. 36, 485 - 518.

Thomas,C.A.Jr., Kelly,T.J.Jr. & Rhoades,M. (1968) Cold Spring Harbor Symp.Quant.Biol. 33, 417 - 424.

Thomas,C.A.Jr., Hamalko,B.A., Misra,D.N. & Lee,C.S. (1970) J.Mol.Biol. 51, 621 - 632.

Tomizawa,J. & Ogawa,T. (1968) Cold Spring Harbor Symp.Quant.Biol. 33, 533 - 551.

Triebel,H., Reinert,K.E. & Strassburger,J. (1971) Biopolymers 12, 2619 - 2621.

Tunis,M.J.B. & Hearst,J.E. (1968) Biopolymers 6, 1218 - 1223.

Tunis-Schneider,M.J.B. & Maestre,M.F. (1970) J.Mol.Biol. 52, 521 - 541.

Ullman,R. (1968) J.Chem.Phys. 49, 5486 - 5497.

Upholt,W.B., Gray,H.B.Jr., Vinograd,J. (1971) J.Mol.Biol. 62, 21 - 38.

Utiyama,H. & Doty,P (1971) Biochemistry 10, 1254 - 1264.

Vinograd,J. & Lebowitz,J. (1966) J.Gen.Physiol. 49, 103 - 125.

Vinograd,J., Lebowitz,J., Radloff,R., Watson,R. & Laipis,P. (1965) Proc.Nat.Acad.Sci.U.S. 53, 1104 - 1111.

Vinograd,J., Lebowitz,J. & Watson,R. (1968) J.Mol.Biol. 33, 173 - 197.

Wada,A. (1964) Biopolymers 2, 361 - 380.

Wallace,T.P., Volosin,M.T., Delumyea,R.G. & Gingello,A.D. (1972) J. Polym.Sci.A2 10, 193 - 200.

Wang,J.C. (1969a) J.Mol.Biol. 43, 25 - 39.

Wang,J.C. (1969b) J.Mol.Biol. 43, 263 - 272.

Wang,J.C. (1971) J.Mol.Biol. 55, 523 - 533.

Wang,J.C., Baumgarten,D. & Olivera,B.M. (1967) Proc.Nat.Acad.Sci.U.S. 58, 1852 - 1858.

Waring,M.J. (1965) J.Mol.Biol. 13, 269 - 282.

Waring,M.J. (1970) J.Mol.Biol. 54, 247 - 279.

Warnaar,S.O., Mulder,G., van den Sigtenhorst-van der Sluis,I., van Kesteren,L.W. & Cohen,J.A. (1969) Biochim.Biophys.Acta 174, 239 - 245.

Wasserman,E. (1960) J.Amer.Chem.Soc. 82, 4433 - 4434.

Watson,J.D. & Crick,F.H.C. (1953a) Nature (London) 171, 737 - 738.

Watson,J.D. & Crick,F.H.C. (1953b) Cold Spring Harbor Symp.Quant.Biol. 18, 123 - 131.

Weil,R. & Vinograd,J. (1963) Proc.Nat.Acad.Sci.U.S. 50, 730 - 738.

Weill,G., Hornick,C. & Toylov,S. (1968) J.Chim.Phys. 65, 182 - 187.

Westphal,H. (1970) J.Mol.Biol. 50, 407 - 420.

Wu,R. & Taylor,E. (1971) J.Mol.Biol. 57, 491 - 511.

Yang,J.T. & Samejima,T. (1969) Progr.Nucl.Acid Res.Mol.Biol. 9, 223 - 300.

Young,E.T.II & Sinsheimer,R.L. (1964) J.Mol.Biol. 10, 562 - 564.

Zimm,B.H. (1948) J.Chem.Phys. 16, 1093 - 1116.

Zimm,B.H. & Stockmayer,W.H. (1949) J.Chem.Phys. 17, 1301 - 1314.

CONFORMATIONS AND STRUCTURE TRANSITIONS OF ϕX174 BACTERIOPHAGE CIRCULAR DOUBLE-STRANDED DNA

by

Douglas.J. Jolly B.Sc.

SUMMARY

July, 1972

Institute of Biochemistry,

University of Glasgow,

Glasgow,

Scotland.

Initially general aspects of DNA structure, particularly tertiary, and its investigation are discussed together with the difficulties encountered; this leads to the choice of ϕX174-RF DNA, investigated mainly by light scattering as the experimental system for investigating DNA structure. As ϕX174-RF DNA is circular and exists in two forms, RFI which is supercoiled and RFII which is an open circle, the implication of this and the significance of the experimental work undertaken are discussed in the light of previous workers' findings.

The following experiments were performed: (1) light scattering on ϕX174-RFI at 25°C; (2) light scattering on ϕX174-RFI at temperatures from 14.9°C - 74.5°C; (3) light scattering on ϕX174-RFI at different mol bound proflavine/mol equiv. nucleutide from 0 to 0.06; (4) light scattering on ϕX174-RFII at 25°C. All experiments were in buffer pH 6.8 and I = 0.2.

From all experiments the value of the mol.wt. was $3.22 \pm 0.05 \times 10^6$ (S.D. of 20 experiments), which is somewhat less than the accepted value of 3.4×10^6. This downward re-evaluation of the mol. wt. is in line with the recent re-evaluation for a number of widely-used phage DNA molecules. In experiment (1), the experimental r.m.s. radius, contour length and number of superhelical turns determined by ethidium bromide titration, were used to define exactly the dimensions of various models for a superhelix; the straight interwound, the Y interwound and the toroidal models. The $P\theta$ for these was calculated from the formula $P\theta = \frac{1}{N^2} \sum_{N} \sum_{N} \frac{\sin hr_{nm}}{hr_{nm}}$ where N is the no. of scattering segments, r_{nm} the distance between the nth and mth segments and h is aconstant dependent on the scattering angle, θ, by computer summation. These results indicated that at $\tau = -12$ a.Y shape was the best model, though no exact fit was found.

In experiments (2) and (3) the superhelix density (σ) was varied by temperature variation and by proflavine intercalation. These experiments indicated, both from thr r.m.s. radius and general appearance

of the $P\theta^{-1}$ curves, that from $\sigma = -0.027$ ($\tau = -12.5$) to $\sigma = -0.021$ ($\tau = -10$) the molecular configuration was as in experiment (1), a Y shape; as σ decreased further to 0.017 approx., the molecule became very compact (r.m.s. radius = 60 - 70nm) before expanding slowly to an open circular conformation at $\sigma = 0$ (r.m.s. radius = 120nm with 0.06 mol dye bound/mol equiv. nucleotide). From experiments (1) - (3) the r.m.s. radius of the Y type structure of ϕX174-RF1 at 25°C was 97.4 ± 8nm (S.D. of 5 experiments). Predicting $P\theta^{-1}$ curves on the lines of experiment (1) indicated the compact conformation was a toroid-type structure.

Some small variation of the seconnd virial coefficient from zero, was found, which was tentatively attributed to increased exposure of hydrophobic bases due to torsional strain ih the superhelix. Simple thermodynamic calculations on the energy requirements of the various models indicated that the above structures and transitions were quite reasonable and possible.

In experiment (4), RFII was found to have a second virial coefficient of zero and a r.m.s. radius of 109.4 ± 15nm. A theoretical $P\theta$ function was calculated for a circular worm-like coil at different values of the persistence length from the above formula for $P\theta$, using polymer distribution functions. One summation was performed analytically, the other by computer summation. From this experiment the persistence length was found to be 41 ± 3.5nm for DNA which is in good agreement with the values from hydrodynamic experiments, in contrast to almost all other light scattering results; this is attributed to the correctness of the interpretation of the results by conventional methods, due to the small size and optical isotropy of ϕX174-RFII.

The persistence of RFI titrated to an open circle with proflavine was also found; this was 36 ± 3.0nm which indicates a drop in the persistence length on binding proflavine.